REPORT DOCUMENTATION PAGE		READ INSTRUCTIONS BEFORE COMPLETING FORM
1. REPORT NUMBER AFIT/CI/NR 86- 77D	2. GOVT ACCESSION NO.	3. RECIPIENT'S CATALOG NUMBER
4. TITLE *(and Subtitle)* Ion Assisted Deposition of Optical Coatings		5. TYPE OF REPORT & PERIOD COVERED THESIS/DISSERTATION
		6. PERFORMING ORG. REPORT NUMBER
7. AUTHOR(*s*) James J. McNally		8. CONTRACT OR GRANT NUMBER(*s*)
9. PERFORMING ORGANIZATION NAME AND ADDRESS AFIT STUDENT AT: University of New Mexico		10. PROGRAM ELEMENT, PROJECT, TASK AREA & WORK UNIT NUMBERS
11. CONTROLLING OFFICE NAME AND ADDRESS AFIT/NR WPAFB OH 45433-6583		12. REPORT DATE 1986
		13. NUMBER OF PAGES 164
14. MONITORING AGENCY NAME & ADDRESS(*if different from Controlling Office*)		15. SECURITY CLASS. *(of this report)* UNCLAS
		15a. DECLASSIFICATION/DOWNGRADING SCHEDULE

16. DISTRIBUTION STATEMENT *(of this Report)*

APPROVED FOR PUBLIC RELEASE; DISTRIBUTION UNLIMITED

DTIC
ELECTE
AUG 1 2 1986
E

17. DISTRIBUTION STATEMENT *(of the abstract entered in Block 20, if different from Report)*

18. SUPPLEMENTARY NOTES

APPROVED FOR PUBLIC RELEASE: IAW AFR 190-1

LYNN E. WOLAVER   6 AUG 86
Dean for Research and
Professional Development
AFIT/NR

19. KEY WORDS *(Continue on reverse side if necessary and identify by block number)*

20. ABSTRACT *(Continue on reverse side if necessary and identify by block number)*

ATTACHED.

DD FORM 1 JAN 73 1473   EDITION OF 1 NOV 65 IS OBSOLETE

AD-A170 672

DTIC FILE COPY

James Joseph McNally
_____
Candidate

Electrical and Computer Engineering
_____
Department

This dissertation is approved, and it is acceptable in quality
and form for publication on microfilm:

Approved by the Dissertation Committee:

_____ , Chairperson

_____

_____

_____

_____

_____

_____

_____

Accepted:

_____
Dean, Graduate School

_____
Date

ION ASSISTED DEPOSITION

OF OPTICAL COATINGS

BY

JAMES JOSEPH McNALLY

BEE, Manhattan College, 1975

M.S., Univ. of Calif., Santa Barbara, 1976

DISSERTATION

Submitted in Partial Fulfillment of the
Requirements for the Degree of

Doctor of Philosophy in Electrical Engineering

The University of New Mexico
Albuquerque, New Mexico

August, 1986

To my parents, Catherine and Bill McNally, my wife, Mary Ann,

our sons, James and Sean, and our soon-to-be-born child, I

dedicate this work to them for their love, support and guidance.

Accession For	
NTIS CRA&I	X
DTIC TAB	☐
Unannounced	☐
Justification	
By	
Distribution/	
Availability Codes	
Dist	Avail and/or Special
A-1	

QUALITY
INSPECTED
4

ACKNOWLEDGEMENTS

ION ASSISTED DEPOSITION

OF OPTICAL COATINGS

BY

JAMES JOSEPH McNALLY

ABSTRACT OF DISSERTATION

Submitted in Partial Fulfillment of the
Requirements for the Degree of

Doctor of Philosophy in Electrical Engineering

The University of New Mexico
Albuquerque, New Mexico

August, 1986

ION ASSISTED DEPOSITON

OF OPTICAL COATINGS

James J. McNally

B.E.E., Manhattan College, 1975

M.S., University of California, Santa Barbara, 1976

Ph.D., University of New Mexico, 1986

The effects on the properties of Ta_2O_5, Al_2O_3, SiO_2 and HfO_2 single- and multi-layer optical coatings deposited using ion assisted deposition (IAD) were investigated. IAD is a novel deposition technique which utilizes a separate ion source to direct a beam of ions at the growing film. A Kaufman ion source was used to provide a monoenergetic, neutralized beam of oxygen ions independent of the material evaporation process. The optical and physical properties, as well as laser-induced damage threshold (LIDT) values, were studied for coatings bombarded with 200, 300, 500 and 1000 eV oxygen ions at values of current density from 0 to 200 μA cm^{-2}.

Oxygen ion bombardment during deposition produced Ta_2O_5 and Al_2O_3 coatings with increased values of refractive index. No increase in refractive index was observed for IAD SiO_2. An increase in optical absorption was observed for IAD Ta_2O_5 coatings. The increase in optical absorption was attributed to preferential sputtering of oxygen in the Ta_2O_5 molecule. No increase in optical absorption was observed for Al_2O_3 and SiO_2 coatings. The optical scatter characteristics for IAD

coatings were measured. The optical scatter for IAD coatings was lower than the scatter for unbombarded coatings. The coatings were subjected to humidity tests. Improved environmental stability was obtained for IAD coatings. Ion-induced crystalline phase transitions were observed using Raman spectroscopy in IAD Ta_2O_5 coatings.

A number of coatings were exposed to fluorine gas tests. It appears that IAD did not improve the resistance of single-layer Al_2O_3 and SiO_2 coatings to fluorine gas attack. A small improvement was observed in IAD Ta_2O_5 coatings.

A limited number of Al_2O_3/SiO_2 and Ta_2O_5/SiO_2 anti-reflection (AR) coatings were laser damage tested. It appears that the IAD coatings did not have higher LIDT values than the coatings deposited with no ion bombardment.

IAD was successfully applied to deposit coatings at low temperature on heavy metal fluoride (HMF) glass substrates. The coatings deposited using IAD were hard and dense. The IAD coatings improved the durability and abrasion resistance of the HMF glass substrates.

The results of this investigation show that IAD can be used to improve the optical and physical properties of optical coatings. Further investigation of the effects of IAD on LIDT values is warranted.

TABLE OF CONTENTS

LIST OF FIGURES

LIST OF TABLES

CHAPTER I

INTRODUCTION

Coated optical components have been performance and output power-limiting elements in optical and laser systems since their introduction. The optical, physical and chemical properties of materials in thin film form vary significantly from their bulk properties. The refractive index (n), extinction coefficient (k) and stoichiometry of a thin film deviate from the corresponding material in bulk form. This creates problems for the optical designer. Multi-layer device designs can be extremely complex, and assumptions regarding each individual layer must be made. Each layer is modeled as a uniform slab, and values for n and k are usually assumed constant throughout the coating. Unfortunately, these assumptions are frequently not valid.

These differences in properties are directly related to film microstructure which is predominantly columnar, containing voids and material inhomogeneities. This is illustrated in cross-sectional electron micrographs of coatings which reveal a columnar microstructure leading to porosity and rough interfaces.[1,2] Packing density, defined as the ratio of the solid volume to the total volume (solid plus voids) of a film, is one parameter used to characterize film microstructure. It is used in models to calculate film refractive index from knowledge of the indices of the bulk material and the film voids.[3] Changes in packing density with thickness are used to explain index inhomogeneities in coatings. It is also used to evaluate the spectral shift observed when a coating is exposed to a humid environment. The shift is most likely due

to water adsorption into the microvoids in the film microstructure.

Microstructure-related effects on coating performance can be observed in the following properties: optical scatter, environmental durability, optical stability and laser damage threshold. Coatings can cause high optical scatter due both to volume defects (e.g. voids, nodules) and surface roughness. Minimization of scatter is crucial in low-gain laser systems and in devices such as laser gryoscopes. The environmental durablility of coatings is critical, particularly for components used in severe environments. Diffusion of gaseous or liquid reagents along dislocations or void boundaries in a protective coating can cause chemical attack to the underlying mirror or substrate. The optical stability of coatings is generally limited due to the porosity of the film microstructure. It is essential for optical components to perform at their design wavelengths for extended periods of time. However, coatings are prone to adsorb moisture along their voids through capillary action. This results in an increased film refractive index and a shift in spectral characteristics to longer wavelengths. Lower laser-induced damage threshold (LIDT) values are obtained for thin film coatings than for most any other optical component in high-energy laser systems. The LIDT values for materials in thin film form are frequently up to a factor of 10 times less than for materials in bulk.[4]

The morphology of damage to dielectric coatings suggests that damage is due to localized absorption of laser energy which heats a small region to melting or stress fracture leading to pitting. An extensive laser damage experiment was performed by Walker et.al.[5] on nine coating materials as a function of pulse length, wavelength and thickness. The conclusion from their investigation is that laser damage in thin film

coatings results from absorbing defects included during the deposition process. It was found that the only damage process which consistently modeled the experimental results was impurity-induced damage. Thus, it is essential to identify and control the critical deposition process parameters that affect film growth dynamics and defect incorporation.

A number of simulation models have been developed to aid in the understanding of the growth dynamics of thin films. Recent studies by Macleod[6] and Messier,[7] based on the two-dimensional model of Dirks and Leamy,[8] used computer simulated models to study resultant film morphology. Dirks and Leamy developed a purely kinematic, two-dimensional model in which hard disks serially impinge on a flat surface at oblique angles. The disks would come to rest upon contact or upon two-point contact simulating adatoms with zero or very low surface mobility. The simulated packing densities were below values for real films. Macleod's modification to this model was to include a relaxation parameter which allows variations in adatom surface mobility to be examined. More realistic packing densities are obtained with this improved model. Messier's modification includes an allowance for the redistribution of adatoms (sputtering) after their first contact with a growing column. All of these models illustrate that film morphology is a mobility-related property inherent in the nature of materials. Two other models, Movchan and Demchishin's Temperature Zone Model (TZM)[9] and Thornton's Structural Zone Model (SZM),[10] examine film morphology as a function of deposition parameters. The TZM relates microstructure to the temperature ratio T_s/T_m where T_s is the substrate temperature and T_m is the material melting point. Thornton modified the TZM to include the effects of pressure on magnetron sputtered films. The modification accounted for

apparent Ar^+ bombardment effects on film morphology. The results relate film microstructure to deposition parameters through thermal-induced mobility and bombardment-induced mobility. A general conclusion from all these models is that increased packing densities are obtained by supplying additional energy to the growing film.

A number of novel deposition techniques have been developed as methods to overcome the weaknesses of thin films relative to bulk materials. In these techniques, energetic processes are employed to supply sufficient activation energies to increase adatom mobility and eliminate the formation of columnar microstructure. Some examples of novel deposition techniques are ion-plating,[11] reactive sputtering,[12,13] ion-beam sputtering,[14,15] plasma-assisted chemical vapor deposition (PA-CVD),[16,17] nozzle-beam deposition[18] and ion-assisted deposition.[19-22] These techniques can provide improved film properties due to enhanced surface reaction rates and increased adatom surface mobility.[23-25]

Mattox and Kominiak[11] used a planar dc plasma diode configuration to investigate the effects of ion bombardment on the properties of tantalum deposits. The columnar structure was disrupted, density increased and stress modified with increasing negative substrate bias. Pawlewicz et.al.[12] demonstrated that crystal grain size and phase composition for TiO_2 films could be controlled by varying the deposition parameters in a rf-reactive sputtering configuration. Their results showed that film refractive index, optical scatter and LIDT values were directly related to these material properties. Sites et.al.[14] used a dual ion-beam sputtering configuration to study the effects of various Ar/O_2 mixtures on TiO_2 and Ta_2O_5 film absorption and LIDT values. Williams and Hess[16] deposited TiO_2 films using a PA-CVD arrangement. The effects of rf power

density and substrate temperature on the structural properties of TiO_2 were investigated. Conventional CVD requires very high temperatures to obtain reasonable reaction rates. With the introduction of a plasma discharge, useful deposition rates were obtained at reduced substrate temperatures. Wong et.al.[18] reported on the deposition of SiO_2 films using a nozzle-beam technique (very similiar to the ionized cluster beam (ICB) process[26]). Evaporated SiO_2 is ejected through a nozzle and partially ionized prior to deposition. Film refractive index and stoichiometry were strongly dependent on the acceleration voltage and ionization current applied to the material.

All of the above examples of energetic deposition techniques demonstrate that dramatic changes in film microstructure and composition may be realized. However, a shortcoming of these techniques is the lack of versatility in controlling the energetic/reactive process parameters independent of the film deposition parameters. For example, in conventional plasma diode configurations, the deposition rate is a direct function of the discharge current which also determines the bombarding flux of ions. This process requires high pressures (>1 mTorr) which makes accurate control of bombardment energy, flux and arrival direction impossible. These problems can be overcome by using a separate, well-controlled ion source to direct a beam of ions at the film surface during deposition. A separate ion source allows control of the ion energy, current density, direction and species independent of the material deposition process. This technique is called ion assisted deposition (IAD).

Early work utilizing a separate ion source to bombard evaporated SiO with 5 keV oxygen ions during deposition was done by Dudonis and

Pranevicius.[19] They investigated the effects of current density on film stoichiometry, and found that for increasing current densities the O/Si ratio approached two. In another early study using 1-5 keV argon ions from a separate source, Marinov[20] demonstrated enhanced surface mobility of silver adatoms due to ion bombardment during deposition. Cuomo et.al.[27] used IAD to modify stress in Nb films bombarded with 100 eV Ar ions. Allen[28] applied IAD to obtain increased packing densities in TiO_2 films. Martin and Netterfield have studied the modifications of ZrO_2[21,29] and CeO_2[30] films deposited using IAD. They obtained increased packing densities, improvements in optical stability and changes in film crystal structure. McNeil et.al.[31,32] have studied the effects of 30-500 eV oxygen ion bombardment on the properties of TiO_2 and SiO_2 films deposited using TiO and SiO source material. Al-Jumaily, McNally and McNeil[33-35] have examined the effects of ion energy and current density on optical scatter and crystalline phase in metal and dielectric films. They reported ion-induced phase transitions and reductions in optical scatter for bombarded films.

In this research program, the film material was evaporated using an electron gun. A Kaufman ion source[36] was used to bombard the growing film with low energy (200-1000 eV) ions during deposition. Use of a Kaufman ion source allows the ion energy, current density and angle of arrival to be independently controlled and accurately measured. The purpose of this work was to systematically investigate the effects of IAD parameters on the properties of Ta_2O_5, Al_2O_3, HfO_2 and SiO_2 thin films. Single- and multi-layer coatings were produced, and the following film properties analyzed:

> refractive index
>
> absorption
>
> optical scatter
>
> stability
>
> stress
>
> stoichiometry
>
> durability.

Low energy ion-induced phase transitions in films have not been extensively explored. Control of film crystalline phase is important in determining coating performance. In this study, Raman spectroscopy was used to investigate the crystal structure of IAD Ta_2O_5 films.

This work was the first study of IAD effects on the properties of Ta_2O_5, Al_2O_3 and HfO_2 films.[37-39] It was the first attempt to systematically examine laser damage thresholds for anti-reflection coatings produced using IAD.[40] A number of unique modifications to the ion source were made due to concern about contamination levels in IAD coatings.[41]

The material in the remainder of this dissertation is organized as follows. In Chapter II, the facilities and equipment to deposit and analyze the coatings are described. The results for single-layer IAD films are presented in Chapter III. Protective and anti-reflection coatings were deposited on heavy metal fluoride substrates using IAD. The results for film and substrate environmental durability, abrasion resistance and adhesion are presented in Chapter IV. In Chapter V the laser damage experiment and results are described. A discussion of results obtained in this study is given in Chapter VI. Chapter VII contains conclusions and recommendations for further investigations.

CHAPTER II

EXPERIMENTAL EQUIPMENT

In this chapter, the equipment and facilities to deposit and analyze the optical coatings are described. The chapter is organized as follows: the coating facility is described; the operation of the Kaufman ion source is reviewed; the procedures for substrate preparation and materials deposition are listed; the equipment and techniques to analyze the film properties are presented; and the facilities for Raman spectroscopy, Rutherford backscattering spectroscopy (RBS) and high energy laser damage testing are described.

II.1 Coating Facility

The coatings were deposited in a 90-cm diameter stainless-steel bell jar vacuum system. A schematic of the chamber is shown in Figure II-1. The system employs a dual-stage mechanical roughing pump to evacuate the chamber to a vacuum of 150 mTorr. An anti-backstreaming gas injection port was attached to the rough g line to prevent molecular back-streaming of pump oil into the chamber. The high vacuum pump for the system was a CTI Model CT-8 cryogenic pump with a pump speed of 2000 liters/sec. The system was capable of routinely achieving a base pressure of 2.0×10^{-8} Torr. High vacuum pressure was measured by a KEY G-75 ionization gauge, and a Varian cold cathode gauge monitored pressures during deposition. A type EAI 250A quadrupole mass spectrometer was attached to the chamber to characterize the chamber residual background constituents, to help characterize the ion source output, and
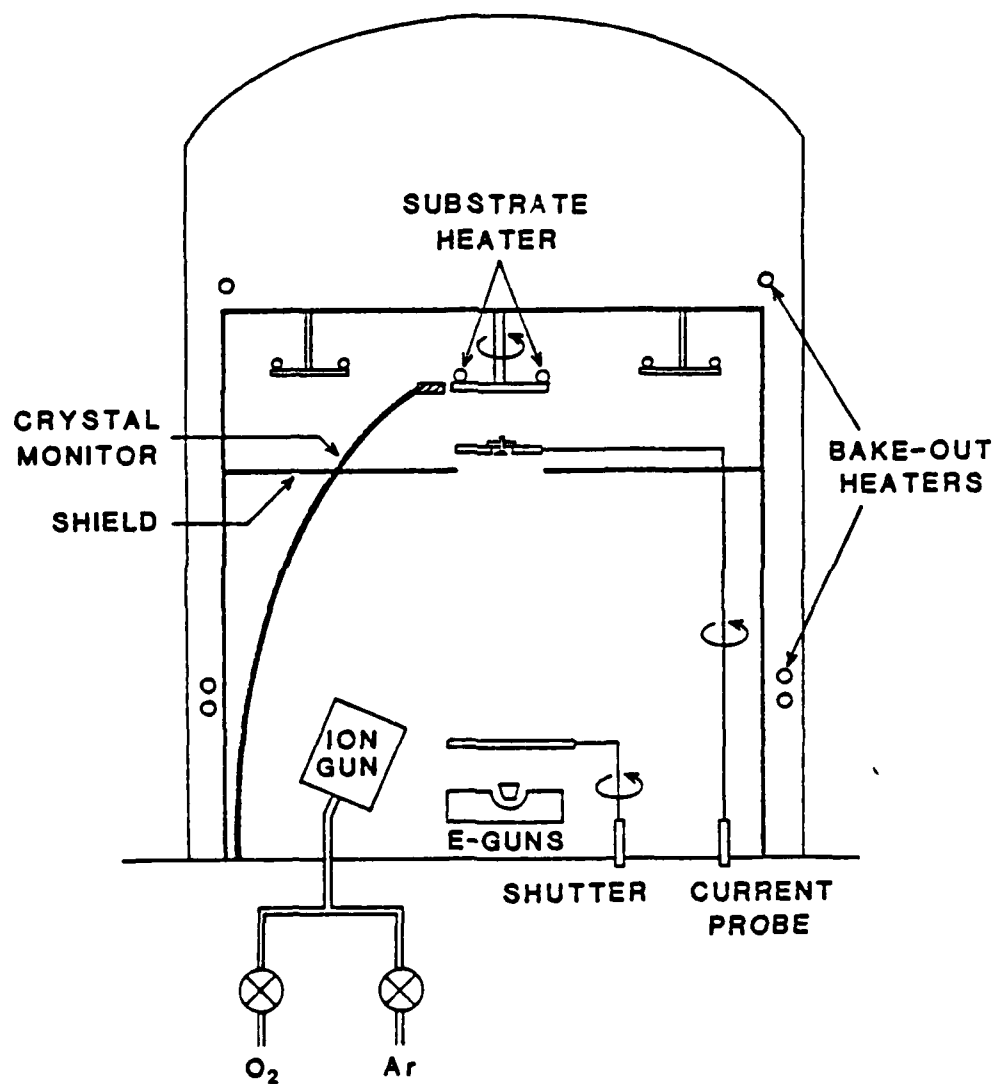
Figure II-1. Schematic of the deposition system.

was essential for leak detection during chamber construction.

The source materials were evaporated using two Airco Temescal water-cooled electron guns. The surface of the source materials was heated by a focused electron beam, and higher evaporation temperatures were obtained than by using resistively heated boats. There was limited interaction between source material and crucible, because the material in contact with the crucible was at a lower temperature than the surface of the source material. This lowered the risk of the crucible as a source of contaminants in the coatings. The source-to-substrate separation was 35 cm. Each electron gun had a shutter associated with it. This allowed the source material to be pre-heated prior to coating without exposing the rest of the chamber to the material. Also, for multi-layer coatings, this protected each material from contaminating the other during deposition. The deposition rate and film thickness were monitored by Inficon water-cooled quartz crystal monitors located adjacent to the substrate holder. The monitors were calibrated for each material and for each electron gun.

The chamber contained eight 500 W quartz lamps used to bake-out the system. The substrates were heated from the backside by a 500 W quartz lamp located within the substrate holder cannister. There were three substrate holders which could be indexed into coating position, one at a time. Therefore, three different sets of deposition conditions were examined in one vacuum pump-down.

The gases used in the vacuum system were "Ultra High Purity" grade supplied by Big Three Industries. The oxygen was 99.995+% pure with a total hydrocarbon content (THC) less than 0.5 ppm; the argon was 99.9995+% pure with a THC less than 0.5 ppm.

II.2 Ion Source

A 10-cm Kaufman ion source[36] provided a monoenergetic, neutralized

ion beam directed at the substrates. This source has a number of

advantages over conventional plasma configurations as described in the

Introduction. These advantages are derived from the basic operating

principle of the ion source. This principle is the isolation of ion

production and acceleration from the substrates. Briefly, the ion

source operates as follows. Gas is introduced into the discharge

chamber; electrons emitted from the cathode impact-ionize the gas

molecules. The discharge-chamber contains a conducting plasma composed

of approximately equal numbers of ions and electrons. The plasma

potential is essentially equal to the anode potential, therefore the

ions originate at approximately the anode potential. The screen grid

aligns the ions that are accelerated from the source by the electric

field established in the region between the screen and accelerator

grids. The ions travel from the source to the substrates which are held

at ground potential.

Two collisional processes that could occur for the ions traveling to

the substrates are resonant charge exchange and elastic collisions. The

mean-free paths, at the standard operating pressures used (10^{-4} Torr),

are greater than 100 cm for resonant charge exchange collisions. The

ion source-to-substrate distance was ~35 cm. The mean free paths for

elastic collisions are about ten times larger than for resonant charge

exchange collisions. Therefore, the ions reach the substrates with

negligible scattering.

An attractive feature of a Kaufman ion source is the monoenergetic

ion beam it produces. The ion beam energy distribution was measured for

the ion source used in this study.[32] The energy distribution was characterized using a retarding grid arrangement in front of a Faraday probe. The energy spread was measured to be approximately 10 eV over the range of ion energies examined in this study. A Faraday probe was used to measure the ion current density at the substrates. The probe was negatively biased (-27 V) in order to repel electrons and extract positive ions from the plasma sheath formed in front of the probe. It was mounted on a movable platform that also served as a shutter at approximately the substrate height. The ion current density was stabilized and measured before deposition commenced, and it was re-measured after deposition was completed. During deposition the ion source discharge current and beam current were monitored to maintain a fixed ion flux at the substrates.

One part of this research program involved the laser damage testing of a number of IAD coatings. A contamination analysis of IAD TiO_2 films indicated the ion source was a contributor to impurities in the coatings.[41] These results led to a number of modifications to the ion source. The first was the replacement of the graphite grids with a material that was more compatible with the coating materials. A number of grids were fabricated from 0.032-inch thick high purity Al. The second modification involved replacement of tungsten (W) wire with tantalum (Ta) wire for the filaments.

II.3 Procedures

The coatings produced in this study were deposited onto a number of different substrates. One inch diameter, 1/4" thick UV-grade fused silica substrates were used for single-layer coatings of high index

materials; 1" dia., 1/4" thick high-index substrates (SF-11) were used for SiO_2 coatings; and 1" dia., 0.5 mm thick fused silica substrates were used for stress characterization. The substrates used for the laser damage coatings were provided by Los Alamos National Laboratory (LANL) and were 2" dia., 3/8" thick fused silica. The substrates were cleaned as follows. Lint and dust particles were removed using dry nitrogen gas. A horse hair brush was used in a circular motion to scrub the substrate surface with a 50-50 mixture of Liquinox soap and de-ionized water (18 MΩ-cm). The substrate was rinsed with de-ionized water (DI), and the scrubbing/rinsing process repeated. The substrate was dried with nitrogen. Kodak lens tissue with ethyl alcohol (200 proof) was used to drag wipe each substrate surface.

Two inch diameter polished silicon wafers were coated for optical scatter measurements, RBS and ellipsometry. The wafers were cleaned using a standard semiconductor industry technique as follows. The wafers were rinsed in DI and degreased in a 3:2 solution of H_2SO_4/H_2O_2 for 10 minutes. A DI rinse was repeated, followed by a 10 minute etch in a 5% HF solution. After a final DI rinse the wafers were blown-dry with nitrogen.

After the substrates were loaded in the chamber a vacuum bake-out procedure was followed. The substrates were heated to ~350°C for approximately two hours. The chamber heaters were then turned on and the total vacuum chamber heated to ~275°C for approximately four hours. With the heaters off the chamber would achieve a pressure of approximately 4.0×10^{-8} Torr after an additional 12 hours. As a final cleaning step the substrates were ion bombarded with 500 eV Ar^+ prior to depositon.

Three high index materials were deposited for this research program. The Ta_2O_5 (99.99% pure), Al_2O_3 (99.999% pure) and HfO_2 (99.999% pure) were purchased from E. Merck Chemicals in the form of 3-5 gram tablets. The SiO_2 (99.999% pure) was purchased from CERAC in 10 mesh granules.

II.4 Methods of Analysis

The coatings transmittance and reflectance spectra were measured over the wavelength range 0.185 - 1.2 μm using a Perkin Elmer 330 dual-beam spectrophotometer. A 3600 Data Station was used to store the spectra, analyze the results, and replot the spectra in different formats. Before measuring the spectra of a series of coatings, an instrument background correction was performed, and a 100% line established for reference.

The transmittance and reflectance spectra were used to calculate the refractive index (n), the extinction coefficient (k) and the thickness (t) for each coating. They were also used to determine the possible presence of index inhomogeneity in the coatings. One technique to determine the optical constants of a thin film is referred to as the ΔT method. The analysis is from Turner[42] and assumes non-absorbing films (k=0). Although limited, the technique is straightforward and allows for a quick determination of n and t. For high index films on fused silica substrates, the required inputs are (1) the transmittance values at wavelengths for which the film is multiple half-waves (T_{max}) and odd-multiple quarter-waves (T_{min}) in optical thickness; (2) the wavelength values at which T_{max} and T_{min} occur; and (3) the refractive index of the substrate. (The incident medium is assumed to be air, n = 1.) Another technique due to Manifacier, et.al.[43] allows the determination

of n, k and t for weakly absorbing thin films. In this technique, T_{max} and T_{min} are each considered continuous functions of wavelength (i.e. the envelopes of the transmittance spectra are examined). The values of n and k are determined from these functions. The value of t is calculated from two successive values of T_{max} (or T_{min}). A computer program for this technique was written to analyze the film transmittance spectra. The inputs are T_{max} and T_{min} values, the respective wavelengths for these values, and the refractive index of the substrate. The outputs are n, k and t for the film. Minor changes in inputs allow the same calculations to be performed for SiO_2 films on high index substrates.

The optical scatter characteristics of the coatings were examined using an angle-resolved scatterometer which is described in detail in Reference 44. When evaluating the scatter characteristics of a dielectric coating it is important to know the optical thickness of the film. For a film which is an integral number of half-waves in optical thickness, scatter is primarily due to volume effects in the film. The films were deposited onto polished silicon wafers and were multiple half-wave optical thickness at 633 nm. A He-Ne laser illuminated the coated Si wafers; scattered light was collected by a photo-multiplier detector. The detector rotated about the scatter point on the sample in the plane of incidence at a radius of ~40 cm. System background noise was measured as a function of angle before the samples were characterized and was incorporated in the calculations.

Humidity cycle tests were conducted in a Vapor-Temp controlled humidity chamber to examine film stability properties. The spectral characteristics of conventional coatings are unstable, primarily due to porosity and their tendency to adsorb moisture. The coatings were

exposed to 97% relative humidity at 35°C for extended periods of time. The humidity was determined from temperature readings of both the dry and wet bulb thermometers. The film transmittance spectra were examined before and after the humidity exposure to determine the amount of spectral shift.

The stress characteristics of a number of the coatings were measured using a ZYGO Mark III Interferometer System. The coatings were deposited onto Hibshman 0.5 mm thick fused silica substrates. The interferometer uses a phase measurement technique to perform optical wavefront measurements. The system modulates the interference pattern piezoelectrically and detects the varying light intensity with a diode array camera. The information is automatically evaluated by the processor module which performs a least-squares fit to calculate the fractional deviation of the interference pattern from a flat plane. The deviation (or deflection) from flatness is then analyzed following a technique given by Ennos.[45] All the stress substrates were characterized before and after coating.

A Rudolph Research ellipsometer with a photoelectric detector was used to examine a number of coatings. The ellipsometer is a recent addition to the laboratory's capabilities, and a number of difficulties have been encountered in its use. The primary difficulty was a design flaw in the detector section. The "front end" of this section was not equipped with a variable aperature which could be partially closed to block the extraordinary ray produced by the analyzer. This and a number of software problems have recently been corrected.

II.5 Raman Spectroscopy

A number of Ta_2O_5 coatings were examined using Raman spectroscopy by Dr. Gregory Exarhos, Battelle Pacific Northwest Laboratory.[46] Raman scattering is the shift in the frequency of radiation when transmitted through optically transparent solids, liquids or gases. The shift of the radiation frequency by the molecular frequency is associated with transitions between rotational, vibrational and electronic levels of the molecule being probed. Vibrational spectroscopic probes can provide localized bonding information and unambiguously characterize particular crystalline phases having identical composition. This technique has the major advantage of being non-destructive, and is well suited to thin film characterization where optical interference phenomena can considerably enhance signal strengths. The appropriate choice of scattering geometry can suppress interference from the substrate allowing direct measurement of a deposited film.

The Raman experimental arrangement is illustrated in Figure II-2. The Raman spectra were measured at normal incidence with a 100 mW CW Ar^+ laser (488 nm) focused to a 50 μm diameter spot size. The perpendicular component of the scattered light was analyzed in order to suppress Raman scattering from the silica substrate. Scattered radiation was collected and imaged onto the slits of a double monochromator. A notch filter centered at the probe laser wavelength was used which rejected the first 350 cm^{-1} of the Raman spectrum.

II.6 Rutherford Backscattering Spectroscopy

A number of Ta_2O_5 coatings were examined using Rutherford back-scattering spectroscopy (RBS) by Dr. J. Beery, Los Alamos National
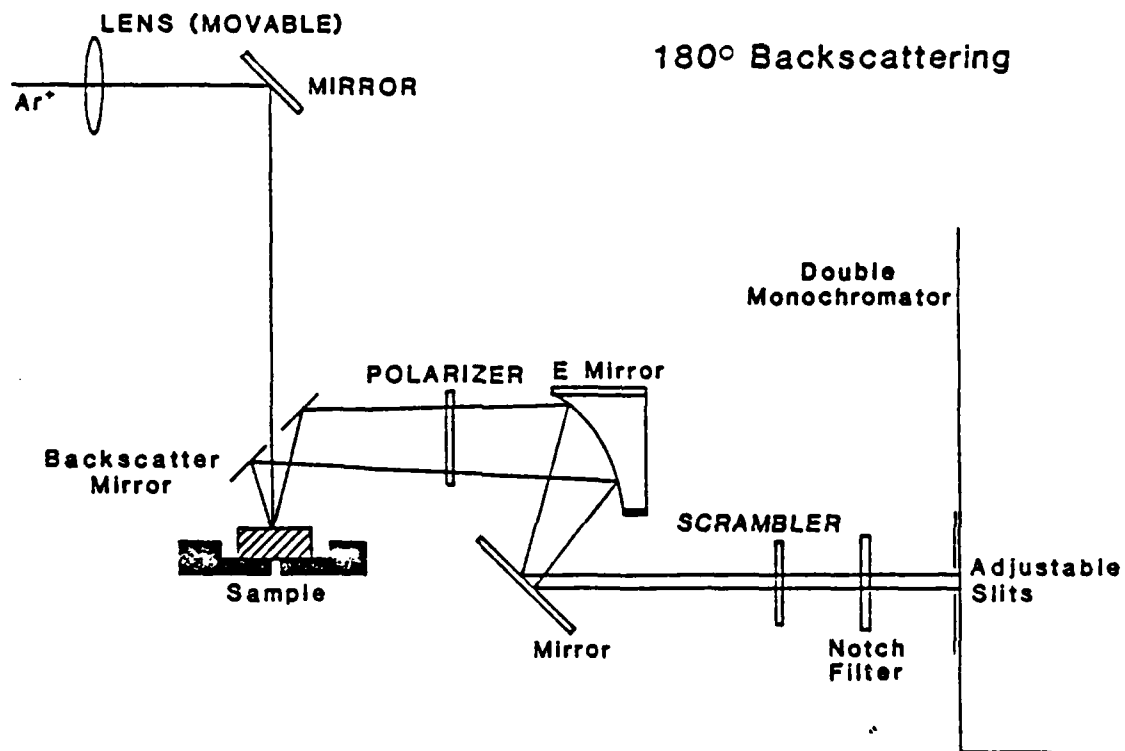
Figure II-2. Backscattering geometry for Raman measurement.

Laboratory.[47] RBS is a well-established quantitative technique for interface and thin film analysis. It is an analytical technique based on known kinematics and energy loss that can determine the composition and structure in materials to a depth of a few microns. A basic RBS measurement utilizes a beam of high-energy light ions incident on a target. The scattered particles are detected at a fixed angle. The measured energy of the backscattered particles is determined by the kinematics of the elastic scattering and the depth of the scattering below the surface. The technique favors high Z elements because the Rutherford backscattering cross section is proportional to Z^2.

Figure II-3 is a schematic of the geometry of the Rutherford backscattering experiment. A 5 mm x 5 mm beam of 2.3 or 2.5 MeV α-particles from a Van de Graaff accelerator was incident on single-layer Ta_2O_5 coatings coated on Si wafers. The scattered particles were detected with a surface barrier detector at an angle of 20°.

II.7 Laser Damage Facility

A number of anti-reflecting (AR) coatings were laser damage tested at Los Alamos National Laboratory by Stephen Foltyn and L. John Jolin. The damage thresholds were measured with 8 nsec 351 nm pulses. The pulse repetition frequency was 35 pps. The laser beam was focused to give a beam with a mean spot diameter ($1/e^2$) of 0.46 mm at the sample surface. All the testing was n-on-m, where m sites were irradiated at each fluence for a maximum of n pulses. Details on the testing and results are presented in Chapter V.
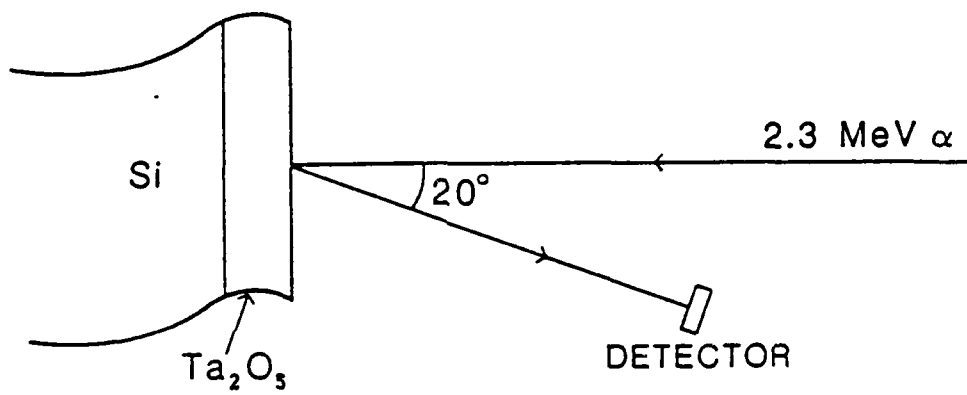
Figure II-3. Schematic of RBS experimental geometry.

II.8 Fluorine Gas Environmental Testing

A number of single-layer and AR coatings were tested at Los Alamos National Laboratory for their resistance to fluorine gas attack. The testing was performed by Glen Lindholm. The coated substrates were used as windows on one end of a gas filled cannister. The transmittance at 351 nm was monitored at various time intervals to examine the durability of the coatings in a fluorine gas environment similar to that for an excimer laser system. The gas content was 0.5% F_2 in He at 3 atm.

CHAPTER III

RESULTS

The analytical results for the single-layer coatings are discussed in this chapter. The chapter is divided in sections by coating material (Ta_2O_5, Al_2O_3, SiO_2 and HfO_2).

III.1 Tantalum Pentoxide

Tantalum pentoxide (Ta_2O_5) thin films have been produced by a variety of techniques: thermal oxidation,[48] electron-beam evaporation,[49] reactive magnetron sputtering,[50] reactive rf diode sputtering,[12,51] reactive dc diode sputtering,[52-54] and ion-beam sputtering.[15] Thin films of Ta_2O_5 have been used as anti-reflection coatings on silicon solar cells,[50] optical waveguides,[48,51] transducers for surface acoustic wave devices,[54] and optical coatings for high energy laser systems.[12,15] The values of refractive index (n) for the films deposited by these techniques varied from 2.10 to 2.20 (at $\lambda=400$ nm). The value of n for bulk Ta_2O_5 is 2.28.[55]

In this study, the Ta_2O_5 coatings were electron-beam evaporated at a rate of 0.30 nm sec^{-1} with oxygen backfill pressure of 1.0×10^{-4} Torr. The coatings were deposited onto heated substrates (~275°C), and were bombarded with oxygen ions during deposition. The values of refractive index and extinction coefficient presented in this section were determined from transmittance and reflectance spectra as described in Chapter II.

The transmittance spectra for two Ta_2O_5 coatings are given in Figure
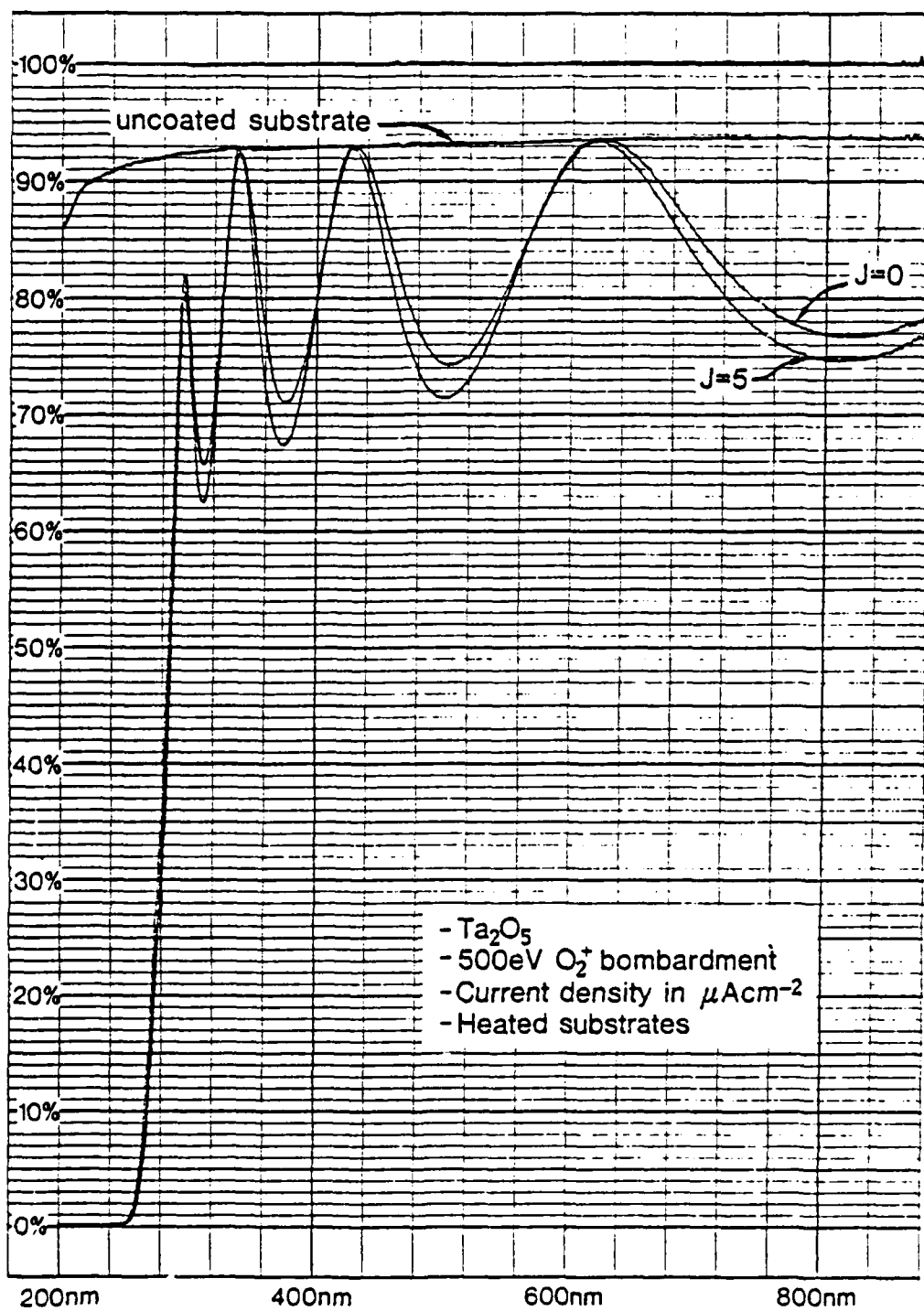
Figure III-1. Transmittance spectra for two Ta_2O_5 coatings.

III-1. The curve labeled J=0 is for a coating deposited with no ion bombardment; the curve labeled J=5 is for a coating bombarded during deposition with 500 eV O_2^+ at a current density of 5 µA cm^{-2}. The curve for the ion assisted coating contains larger differences in transmittance extrema than the curve for the conventional e-beam evaporated coating. These larger differences indicate a larger value of refractive index for the ion assisted coating. Good film stoichiometry was obtained for the ion bombardment conditions employed as indicated by an absence of measurable absorption at wavelengths for which the film is multiple half-wave in optical thickness down to 340 nm. Examination of the reflectance spectra for these coatings indicated the absence of any refractive index inhomogeneity. All IAD Ta_2O_5 coatings examined except those bombarded with O_2^+ current densities greater than 100 µA cm^{-2} contained no index inhomogeneity. As illustrated in the figure, the absorption band edge for Ta_2O_5 coatings was approximately 290 nm. (The absorption band edge was defined as the wavelength at which the transmittance was ~ 50%.)

The values of n (λ=400 nm) for Ta_2O_5 coatings bombarded with 200, 300 and 500 eV oxygen ions are plotted in Figure III-2 as a function of O_2^+ current density. The error bars indicate the uncertainty in the calculations introduced by the precision of the spectrophotometer. (See Appendix I for sample calculation.) The values increase from 2.16 for coatings deposited without bombardment to maximum values of 2.25, 2.28 and 2.19 for films bombarded with 500, 300 and 200 eV O_2^+, respectively. The value of 2.16 (J=0) is comparable to the value of 2.15 for e-beam evaporated Ta_2O_5 reported by Herrmann.[49] Demiryont, Sites and Geib reported a value of 2.18 for ion-beam sputtered Ta_2O_5.[15]
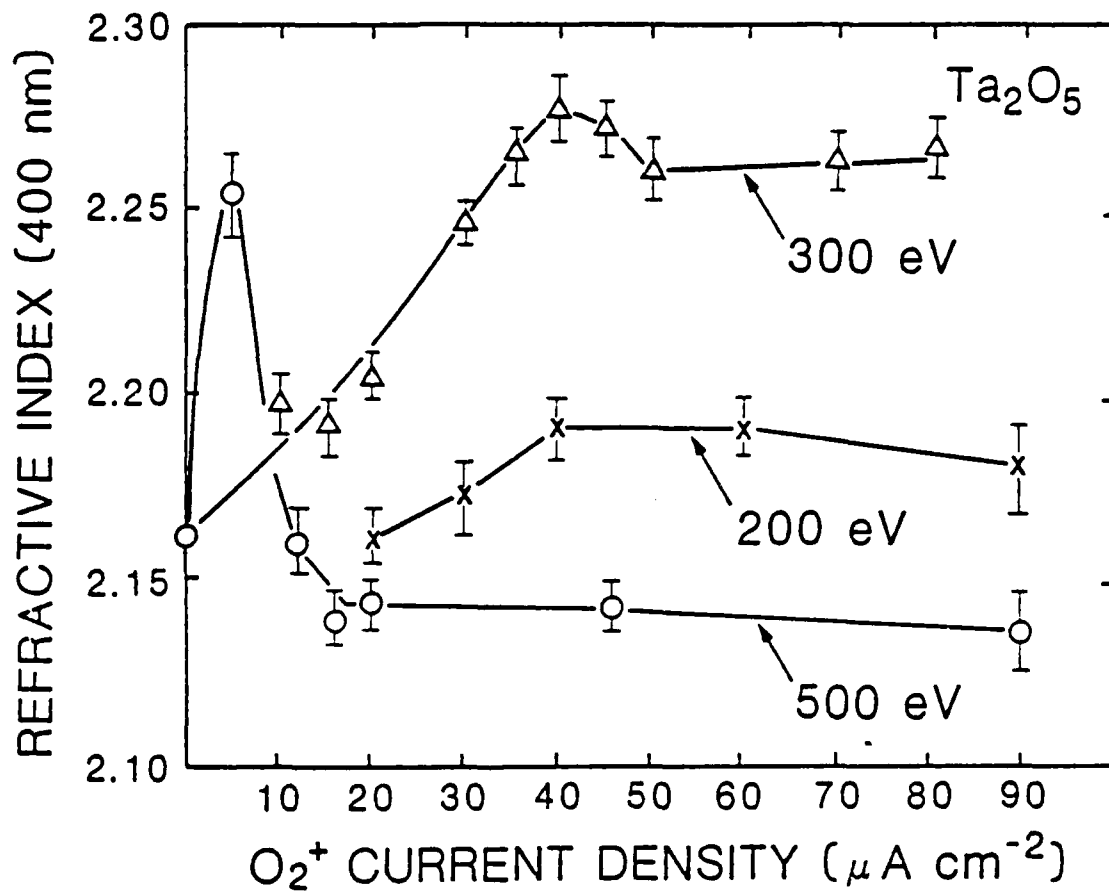
Figure III-2. Values of refractive index for Ta_2O_5 coatings plotted as a function of O_2^+ current density.

The increase in the values of n for increasing levels of O_2^+ current density indicates that ion bombardment during deposition modifies the growth of film columnar microstructure resulting in film densification. The results indicated that the coatings bombarded with 300 eV O_2^+ had larger values of n than those bombarded with 500 eV O_2^+. The difference in film densification may be due to the differences in the average ion penetration depths. A similar dependence of refractive index on bombarding ion energy has been reported for ion assisted CeO_2 films.[30] Further discussions regarding ion-induced densification are given in Chapter VI.

The results in Figure III-2 indicate that only minor densification occurred for coatings bombarded with 200 eV oxygen ions during deposition. A possible explanation is that at this ion energy only a few surface adatoms can be displaced into the bulk which results in minor densification. Also, it may be that the 200 eV ions do not transfer sufficient energy to the surface adatoms for them to sufficiently increase their surface mobility and overcome the tendency for film columnar growth. Further discussion is given in Chapter VI.

The current density value (for a fixed ion energy) at which the maximum n occurs is termed the critical value. The results in Figure III-2 illustrate that film index values decreased for ion current densities greater than the critical values. The decrease in index may be explained as a result of degradation in film stoichiometry, creation of closed isolated voids or oxygen incorporation into the films. The decrease was greatest for bombardment with 500 eV ions and least for 200 eV ions. This energy dependent decrease is consistent with the dependence of the average ion penetration depth and preferential sputtering

yield on ion energy. Similar results for which the values of refractive index decreased for current densities greater than the critical values have been reported for ion assisted ZrO_2 films[29] and CeO_2 films.[30]

The coatings bombarded during deposition at oxygen ion current densities up to approximately the critical values exhibited good optical characteristics. For higher levels of bombardment, the optical absorption of the coatings increased. In Figure III-3, values of extinction coefficient (k) for Ta_2O_5 coatings (~300 nm thick) bombarded with 500, 300 and 200 eV oxygen ions are plotted as a function of O_2^+ current density. The values of k were calculated at λ = 400 nm. The error bars indicate the uncertainty in the calculations due to the precision of the spectrophotometer. The dashed line across the bottom at $k = 2.0 \times 10^{-4}$ indicates the level below which the values of k were too small to be regarded as reliable because of the minimum absorption values measurable by the spectrophotometer (~0.2%).

As illustrated in Figure III-3, film optical absorption increased with higher levels of oxygen ion bombardment. The most probable mechanism for this is the preferential sputtering of oxygen in the Ta_2O_5 molecule. Preferential sputtering would result in oxygen-deficient layers continuously integrated into the coatings as deposition occurs. Values of k for coatings bombarded at a fixed current density were the lowest for 200 eV O_2^+, higher for 300 eV and highest for 500 eV O_2^+. This result is consistent with increasing preferential sputtering yields for higher energy ions. This damage mechanism has been observed in other IAD films.[29]

Auger electron spectroscopy (AES) and x-ray photoelectron spectroscopy (XPS) studies of the effects of ion bombardment on the composition
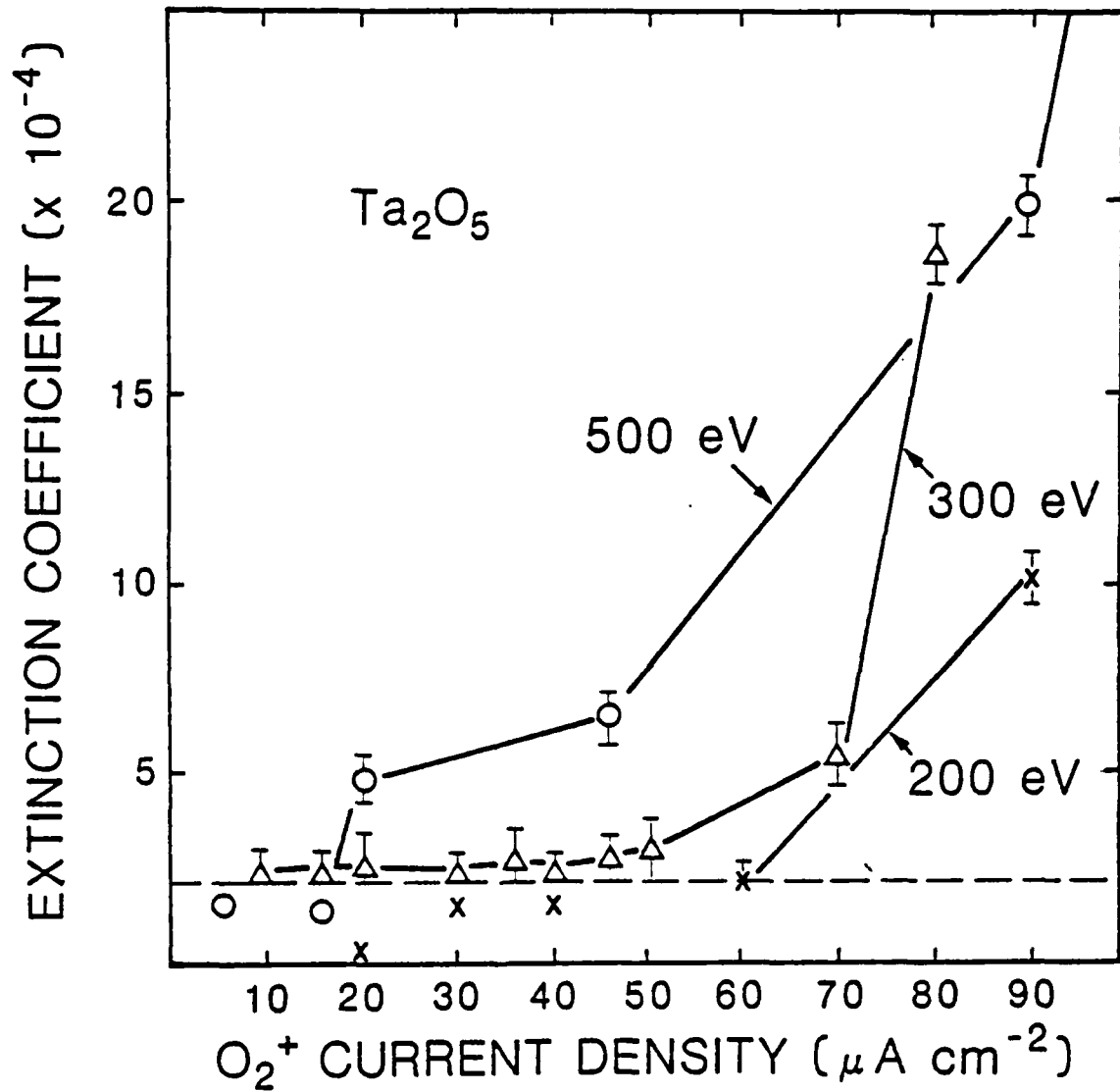
Figure III-3. Values of extinction coefficient for Ta_2O_5 coatings plotted as a function of O_2^+ current density.

of oxide materials indicated that preferential sputtering of the more

volatile species, oxygen, occurred producing an oxygen-deficient

sample.[56,57] These studies involved the low energy (400 - 2000 eV) ion

bombardment of samples and indicated that the reduction was localized in

the near surface region. Extending these results to continuous ion

bombardment during deposition supports the supposition that the coatings

were reduced due to preferential sputtering. The effects of preferential

sputtering are further discussed in Chapter VI.

Measurement of the optical scatter characteristics of coatings is a

method used to determine the effects of O_2^+ bombardment on film micro-

structure. The optical scatter characteristics of the coatings were

examined using an angle-resolved scatterometer as described in Chapter

II. The coatings were deposited onto polished silicon wafers and were

multiple half-wave optical thickness at 633 nm so that scatter was

primarily due to volume effects in the coatings.

Figure III-4 illustrates the scatter characteristics of two Ta_2O_5

coatings; one deposited without ion bombardment (J=0), and the other

bombarded during deposition with 200 eV O_2^+ at a current density of 40 µA

cm^{-2}. The vertical axis is the bidirectional reflectance distribution

function (BRDF) of the coating, in units of inverse steradians. The BRDF

is proportional to the normalized intensity of scattered light (logarith-

mic scale). The horizontal axis is the angle from the normal to the

sample, in degrees, at which the scattered light is collected. The

scatter characteristic for an uncoated silicon wafer is illustrated for

comparison.

As illustrated in Figure III-4, the optical scatter from the IAD

coating (J=40) was less than that from the coating deposited without

Figure III-4. BRDF vs scatter angle for two Ta_2O_5 coatings. One deposited with no ion bombardment (J=0); the other bombarded during deposition with 200 eV O_2^+ at J=40 μA cm^{-2}.

bombardment. Figures III-5 and -6 illustrate the scatter characteristics for Ta_2O_5 coatings bombarded during deposition with 300 eV and 500 eV ions at current densities of 20 and 12 μA cm^{-2}, respectively. The IAD coatings were compared with coatings deposited without ion bombardment (J=0), and a reduction in optical scatter was observed. Comparable reduction in scatter was observed for other IAD Ta_2O_5 coatings relative to unbombarded coatings except for coatings bombarded with very high levels of current density. For coatings bombarded during deposition with 500 eV O_2^+ at current densities greater than 90 μA cm^{-2}, the optical scatter increased by a factor of 2-5 times that for a coating deposited without bombardment.

These results are similar to the reductions in scatter reported for IAD TiO_2 coatings.[33] Total integrated scatter (TIS) measurements reported for IAD CeO_2 coatings also indicated less optical scatter in coatings deposited under certain conditions of ion bombardment.[30] A possible explanation for this reduction in scatter is that ion bombardment modifies film columnar growth producing a more homogeneous film morphology. This explanation is supported by micrographs of IAD TiO_2 coatings showing an absence of columnar microstructure and smoother interfaces in multi-layer IAD film structures.[58]

The environmental stability of optical coatings is in a large part limited by the porosity of the film microstructure as discussed in Chapter I. A number of Ta_2O_5 coatings were exposed to humidity testing as described in Chapter II to examine the effects of ion bombardment on film stability. Figures III-7 and -8 are the transmittance curves for two Ta_2O_5 coatings exposed to humidity testing. The spectra in Figure III-7 are for a coating deposited onto a heated fused silica substrate

Figure III-5. BRDF vs scatter angle for two Ta_2O_5 coatings. One deposited with no ion bombardment (J=0); the other bombarded during deposition with 300 eV O_2^+ at J=20 μA cm^{-2}.

Figure III-6. BRDF vs scatter angle for two Ta_2O_5 coatings. One deposited with no ion bombardment (J=0); the other bombarded during deposition with 500 eV O_2^+ at J=12 $\mu A\ cm^{-2}$.

100%

90% — POST HUMIDITY

80% — AIR

70%

Ta₂O₃ deposited onto
heated substrates with
no ion bombardment.
(J≈0)

60%

50%

300nm   400nm   500nm   600nm

Figure III-7. Transmittance spectra for a Ta₂C₅ coating deposited
with no ion bombardment subjected to humidity test.

Figure III-8. Transmittance spectra for a Ta_2O_5 coating bombarded during deposition with 300 eV O_2^+ at J=20 $\mu A\ cm^{-2}$ subjected to humidity test.
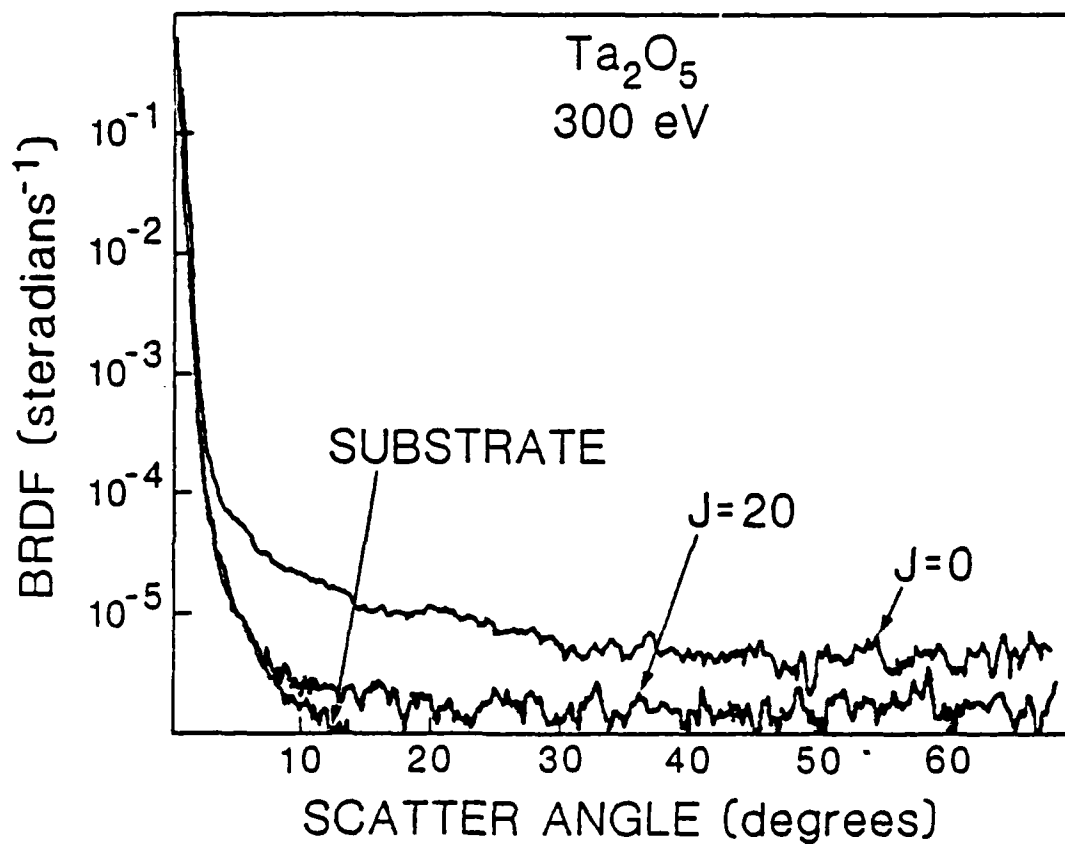
Figure III-5. BRDF vs scatter angle for two Ta_2O_5 coatings. One deposited with no ion bombardment (J=0); the other bombarded during deposition with 300 eV O_2^+ at J=20 μA cm^{-2}.
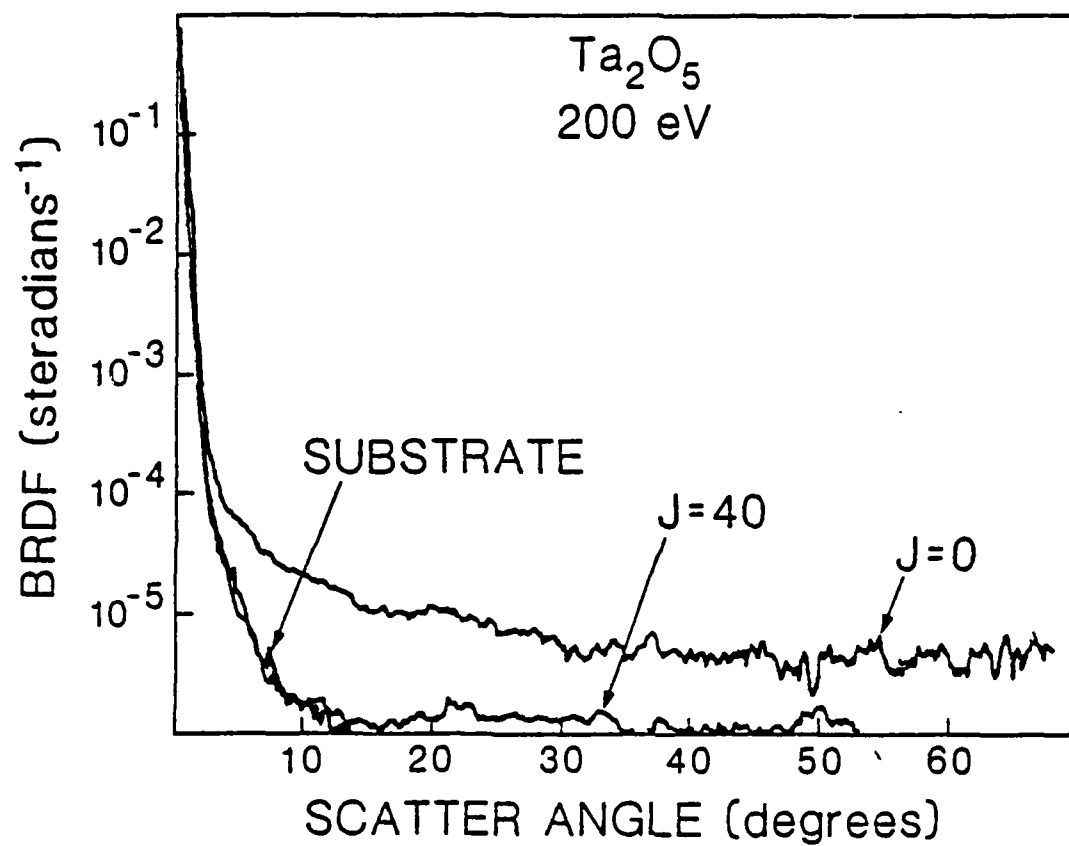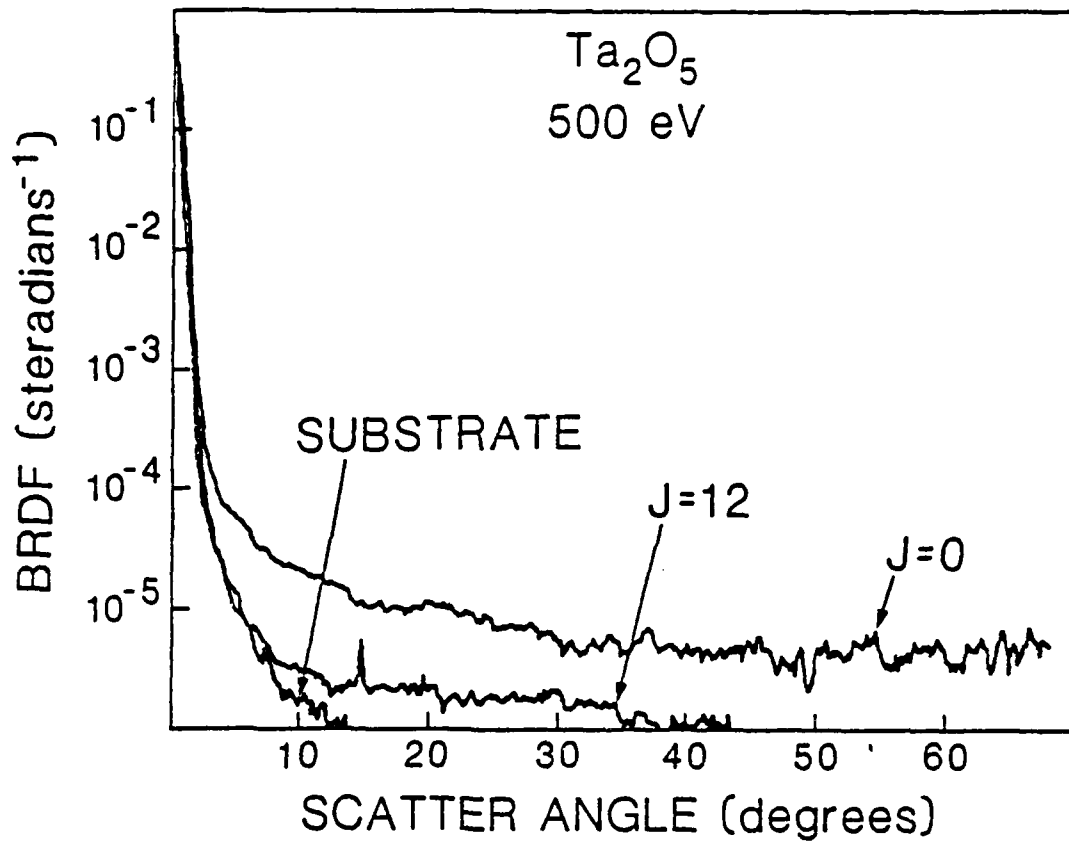
Figure III-6. BRDF vs scatter angle for two Ta_2O_5 coatings. One deposited with no ion bombardment (J=0); the other bombarded during deposition with 500 eV O_2^+ at J=12 μA cm^{-2}.
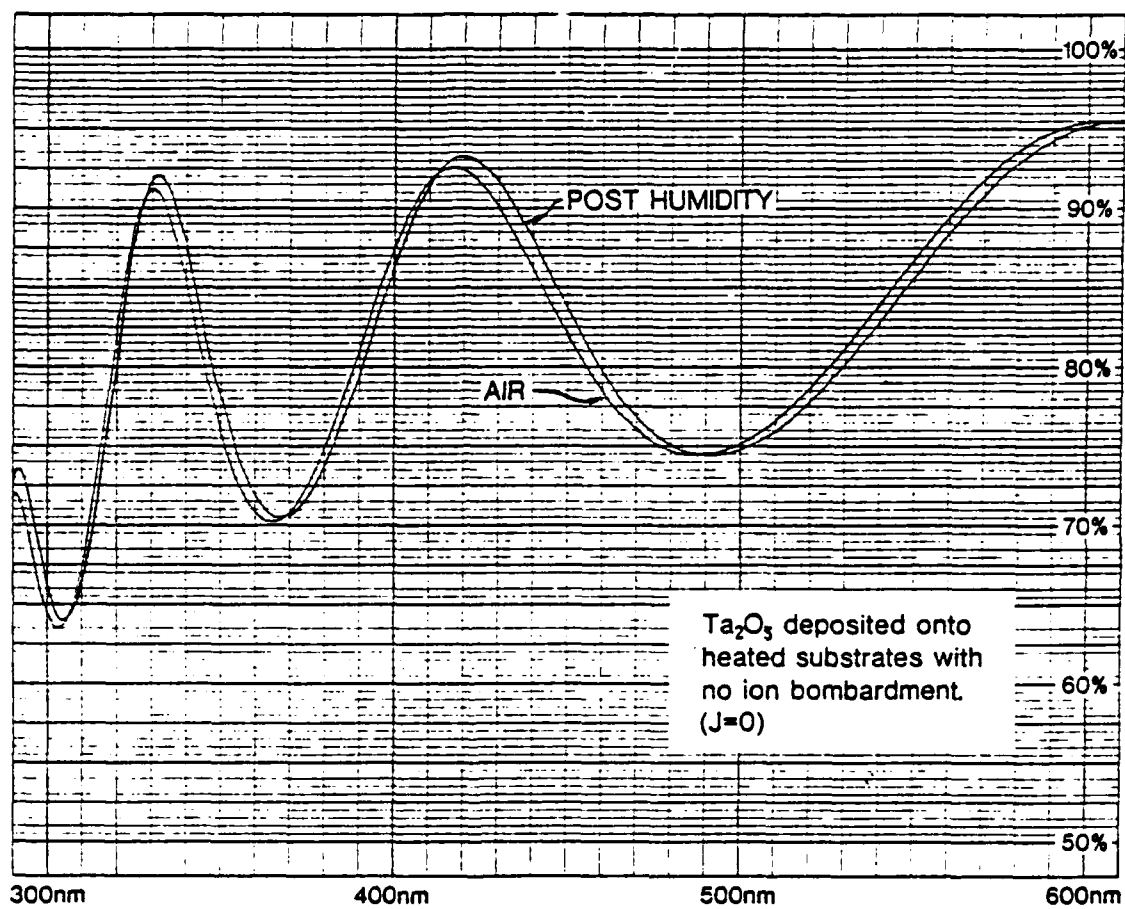
Figure III-7. Transmittance spectra for a Ta_2O_5 coating deposited with no ion bombardment subjected to humidity test.

with no ion bombardment (J=0). The spectra in Figure III-8 are for a coating bombarded during deposition with 300 eV O_2^+ at a current density of 20 µA cm^{-2}. The curve labeled AIR is the spectrum measured after the coating has been removed from the vacuum chamber and exposed to the ambient atmosphere. This procedure to establish the spectral character- istics of the control sample was not ideal due to day-to-day variations in the ambient atmosphere. However, care was taken to immediately measure the transmittance spectra of the coatings within fifteen minutes of exposure to atmosphere. Also, weather conditions in Albuquerque are extremely stable and only minor variations in conditions occurred for the coatings examined. The curve labeled POST HUMIDITY is the spectrum for the same coating remeasured after exposure to 97% relative humidity at 35°C for six hours.

The curves in Figure III-7 illustrate a spectral shift to longer wavelengths of 1% for the coating deposited without bombardment. The shift was most likely due to water adsorption into the microvoids in the film microstructure. This increased the effective refractive index value of the coating and, in turn, increased the optical thickness (nt). Figure III-8 is typical of the results obtained for all IAD coatings examined except one. No spectral shifts within the measurement precision (± 0.5 nm) of the spectrophotometer were observed. The coating bombarded with 300 eV O_2^+ at a current density below the critical value exhibited a spectral shift of 0.3%. Similar results have been reported for IAD ZrO_2 and TiO_2 coatings.[29,21] The Ta_2O_5 results are summarized in Table III-1.

The spectral shift for the J=0 coating indicated the likely exist- ence of columnar microstructure. The shift for the coating bombarded with 300 eV O_2^+ at a current density of 10 µA cm^{-2} indicated some

TABLE III-1

Spectral shifts for Ta_2O_5 coatings after humidity exposure

E (eV)	$J(\mu A\ cm^{-2})$	Spectral Shift (%)
0	0	1.0%
300	10	0.3%
300	20	0.0%
300	40	0.0%
500	10	0.0%
500	20	0.0%

columnar microstructure existed although the coating was more stable and had a larger value of n (see Figure III-2) than the J=0 coating. These humidity test results, as well as the observation of reduced optical scatter and increased refractive index, are consistent with IAD Ta_2O_5 coatings having an increased packing density and being less susceptible to water adsorption.

A number of Ta_2O_5 coatings were examined using Raman spectroscopy to study ion-induced crystallization effects as a function of IAD conditions. A number of studies on bombardment-induced crystallization in materials have been published, mostly for high energy (> 20 keV) particle bombardment.[59-61] The induced phase transition effect for low energy ion bombardment of thin films has not been extensively explored.[16,21,33] Control of thin film crystalline phase can be very important in determining coating properties.[12]

Figure III-9 illustrates the Raman spectra for three Ta_2O_5 coatings deposited onto heated fused silica substrates. The curve labeled J=0 is the spectrum for a coating deposited with no bombardment.' The curves labeled J=8 and J=90 are spectra for coatings bombarded during deposition with 500 eV O_2^+ at current densities of 8 and 90 μA cm^{-2}, respectively. The J=0 coating exhibited vibrational features at 520, 627, 881, 976 and 1064 cm^{-1}. These frequencies were identified as those for crystalline Ta_2O_5.[62] The J=8 coating exhibited some very weak features at 627 and 1064 cm^{-1} indicating that ion-induced amorphization had occurred in the coating. The spectrum for the J=90 coating contained features at 520, 627, 881, 976, and 1064 cm^{-1} although these were not as sharp as those for the J=0 coating. Two other Ta_2O_5 coatings were examined using Raman
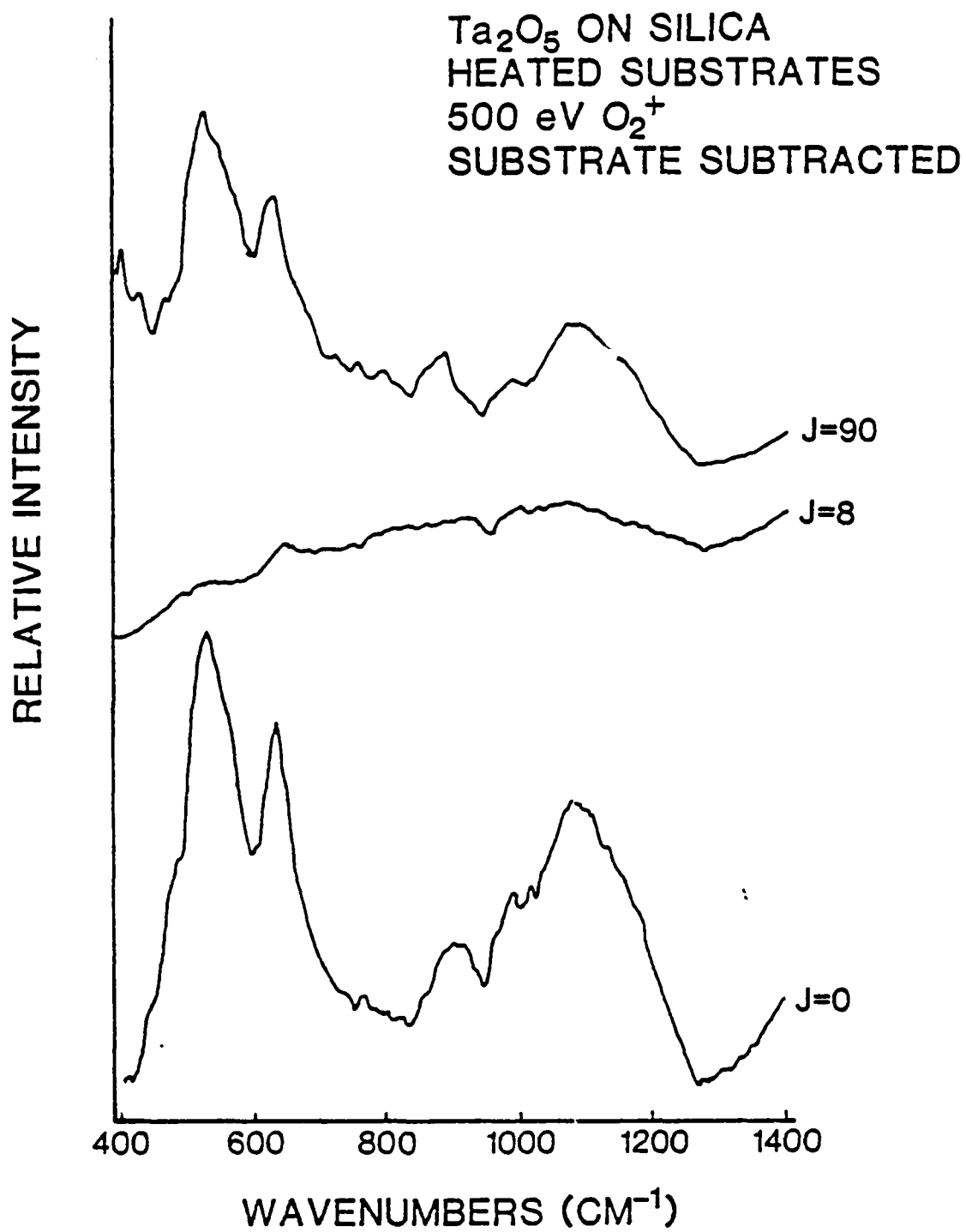
Figure III-9. Raman spectra for three Ta_2O_5 coatings.

spectroscopy. One coating was bombarded during deposition with 500 eV O_2^+ at a current density of 15 μA cm^{-2}. The spectrum for this coating exhibited no structure indicating that complete ion-induced amorphization occurred in the coating. The other coating was bombarded during deposition with 500 eV O_2^+ at a current density of 45 μA cm^{-2}. The spectrum for this coating exhibited weak features at 520, 627, 881, 976 and 1064 cm^{-1}. The features were not as sharp as those contained in the J=0 spectrum. However, they were stronger than those in the J=8 spectrum. The results obtained for all the Ta_2O_5 coatings examined using Raman spectroscopy are summarized in Table III-2.

There is a lack of quantitative information concerning the effects of ion bombardment on material properties for the low energy range (<2 keV). However, Murti et. al.[60] conducted experimental work to study the structural and compositional effects due to 35 keV O_2^+ bombardment of Ta_2O_5. Their results indicated that crystalline Ta_2O_5 readily amorphized for moderate bombardment doses. With continued bombardment at higher doses the material re-crystallized as a reduced oxide. Rutherford backscattering spectroscopy (RBS) measurements revealed the reduced phase to be Ta_2O_x, where x was between 4.7 and 4.8. The results illustrated in Figure III-9 follow the trends reported for the high energy ion bombardment of Ta_2O_5. The coatings were amorphous for bombardment at low current densities. As the bombarding current density increased the coatings exhibited crystalline structure again. The coatings bombarded at higher current densities exhibited increased optical absorption. The increase in absorption is indicative of oxygen-deficient coatings. Thus the results for IAD Ta_2O_5 qualitatively match both the structural and compositional changes observed for ion bombarded Ta_2O_5. Further dis-

Table III-2

Raman results for Ta_2O_5 coatings

E (eV)	J ($\mu A\ cm^{-2}$)	Comments
0	0	Crystalline
500	8	Very weak lines; disorder induced
500	15	Amorphous
500	45	Weak lines; structure present
500	90	Crystalline

cussion on ion-induced crystalline structure effects is given in Chapter VI.

A limited number of Ta_2O_5 coatings were examined using Rutherford backscattering spectroscopy (RBS). The purpose of this study was to examine stoichiometry as a function of ion bombardment conditions and to attempt to measure the contamination levels in the coatings. A short-coming of RBS to examine stoichiometry is that the output is only the relative ratio of oxygen to tantalum (O:Ta). There is no information about the oxidation state of the materials in the output spectra. It is unclear whether the oxygen is stoichiometric with the tantalum or is free oxygen incorporated into the coatings. A shortcoming of using RBS to measure the contaminant levels in Ta_2O_5 coatings is related to the resolution and sensitivity of the technique. Two contaminants from the ion source expected in IAD coatings are tungsten (W) and carbon (C). The problems with identifying trace amounts of W is that its atomic mass is too close to Ta. For the heavier mass elements like Ta and W, they can only be distinguished if their mass difference is approximately 10 atomic units.[63] The difference between Ta and W is only 4. The problem with identifying trace amounts of C is that RBS has very poor sensitivity for detecting light elements (also true for identifying H content). There-fore, the RBS results could not be used to measure contaminant levels in Ta_2O_5 coatings.

In applying RBS to the Ta_2O_5 coatings, an interesting fact was revealed. It was discovered that to obtain any reasonable results significant deviations from published stopping powers for oxygen had to be applied in the data analysis. This problem was initially discovered when preliminary O:Ta ratios showed all films to be super-stoichiometric

(O:Ta > 2.5). The RBS data has been analyzed as a function of oxygen stopping power, and the results presented in this section were obtained by applying a 27% scaling factor to the published stopping power value. A word of caution is given regarding the accuracy of the results due to the uncertainty introduced by the oxygen stopping power. The normal accuracy for these RBS measurements is 10%, however it is unclear how accurate the results are without more study. The run-to-run precision of these RBS measurements is 5%. Therefore, the data is analyzed for relative trends to help understand IAD effects on film content. In collaboration with scientists at Los Alamos National Laboratory this problem is being further examined and is discussed in more detail in Chapter VI.

Figure III-10 is a typical RBS spectrum for a 2.5 MeV beam of α-particles incident on a 0.3 μm Ta_2O_5 film coated on a silicon substrate. The scattered energies for Ta atoms range from ~2.35 to 2.05 MeV; the scattered energies for Si atoms range from ~1.2 to 0.0 MeV; and the scattered energies for O atoms range from ~0.8 to 0.3 MeV.

In Figure III-11, the O:Ta ratios for coatings bombarded with 300 eV O_2^+ are plotted versus O_2^+ current density. The coating deposited without bombardment had an O:Ta ratio of 2.70. A possible source for some of the excess oxygen is water adsorbed in the film voids. As illustrated in Figure III-7, the J=0 coating was subject to water adsorption. The coating bombarded at a current density of 15 μA cm^{-2} had a ratio of 2.40. It is unclear why this coating would be sub-stoichiometric when examined in conjunction with the optical absorption data in Figure III-3. The value of k for the J=15 coating is at the lower limit of the measurement sensitivity, indicating good film stoichiometry. It
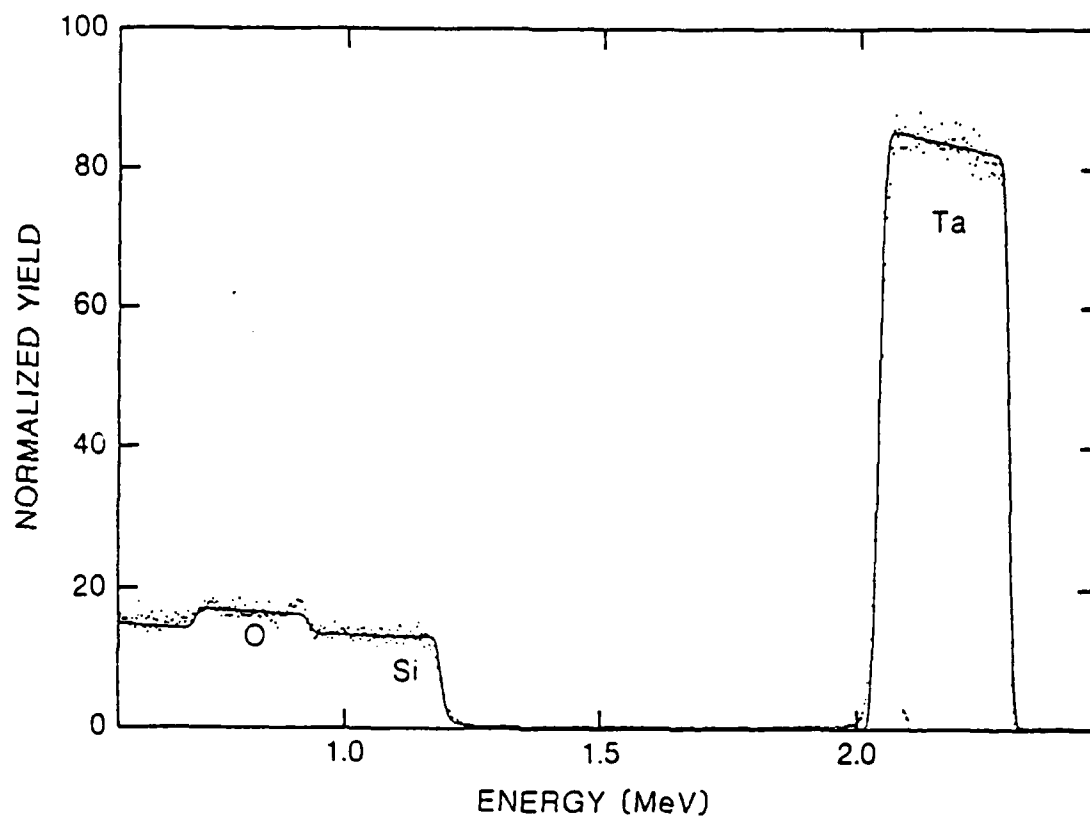
Figure III-10. RBS spectrum for a 0.3 µm Ta_2O_5 coating.
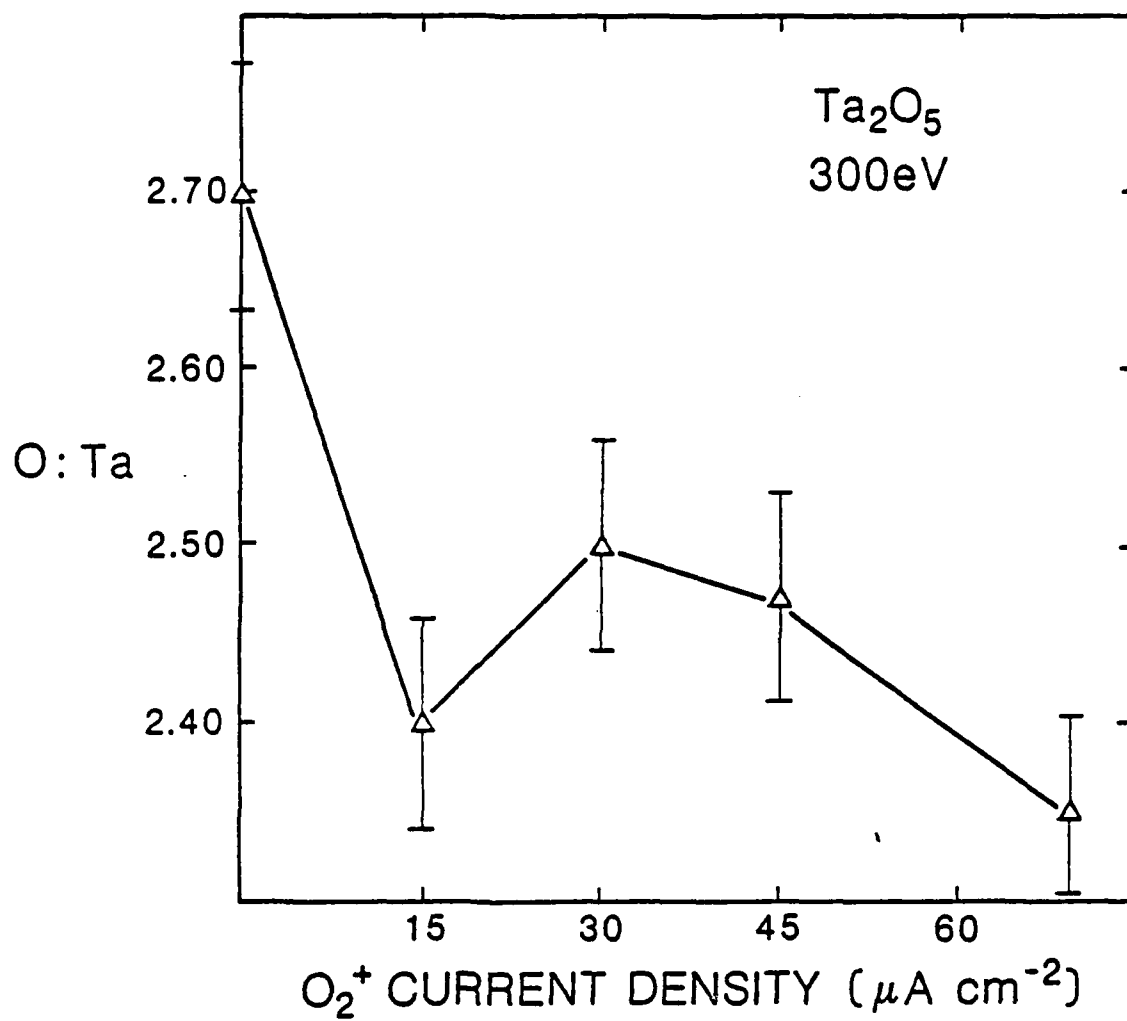
Figure III-11. O:Ta ratio for Ta_2O_5 coatings vs O_2^+ current density.

is possible that the coating was 4% oxygen deficient and possessed a value of extinction coefficient less than 2.0×10^{-4}. This possibility is supported by k values reported by Sites et.al.[14] for ion beam sputtered Ta_2O_5 coatings. For a coating that was 6% oxygen deficient they reported an extinction coefficient of 1×10^{-4}. The coatings bombarded at current densities of 30 and 45 μA cm^{-2} had ratios of 2.50 and 2.47, respectively. These results are consistent with the good optical properties measured for these coatings. The coating bombarded at a current density of 70 μA cm^{-2} had a ratio of 2.35. This indication of an oxygen-deficient coating is consistent with the slight increase in optical absorption measured for this coating.

Three other IAD Ta_2O_5 coatings were examined using RBS. These coatings were bombarded during deposition with 500 eV O_2^+ at current densities of 45, 90 and 120 μA cm^{-2}, respectively. The O:Ta ratios for these coatings were 2.06, 2.06 and 2.26 (± 0.05), respectively. These results are consistent with the measured optical absorption values (Figure III-3) which indicated that the coatings were highly oxygen deficient.

A number of Ta_2O_5 coatings were examined for intrinsic stress. The stress was measured interferometrically as described in Chapter II. The stress was computed from measured substrate bending, and because film thickness was much less (factor of 1000) than substrate thickness the elastic constants of the coating were not required. The stress was assumed uniform and isotropic in the coating. The stress induced a deflection of the substrate from an ideal optical flat. The deflection from flatness was defined as Δ in units of μm. The stress was computed using equation (III-1)[45]:

$$S = \frac{4}{3} \frac{Y}{(1-\nu)} \frac{d^2}{D^2} \frac{\Delta}{t} . \tag{III-1}$$

The values of Young's Modulus (Y) and Poisson's ratio (ν) for the fused silica stress substrates were 7.31×10^{10} N m^{-2} and 0.16, respectively.[64] The substrate diameter (D) and thickness (d) were 25.4 mm and 0.51 mm, respectively. The film thickness (t), in units of μm, was calculate· from transmittance spectra for each coating. Because the uncoated substrates deviated from ideal flats, each substrate was characterized before and after coating.

Figure III-12 illustrates the values of film stress plotted versus oxygen ion current density. The triangles (Δ) and circles (o) represent stress values for coatings bombarded during deposition with 300 and 500 eV O_2^+, respectively. The results indicate that film stress was compressive and increased for increasing levels of ion bombardment. The values of stress obtained are consistent with results reported by Pawlewicz[65] for rf reactive sputtered Ta_2O_5 coatings. The average stress reported was 3×10^7 N m^{-2} and values as high as 9.5×10^7 N m^{-2} were obtained. The highest value was for a coating produced with the highest rf power. Sites et.al.[15] also reported compressive stress in ion-beam sputtered Ta_2O_5 coatings.

There have been a number of studies which examined the effects of ion bombardment on stress in metal films. Cuomo et.al.[27] reported a change in stress from tensile to compressive for evaporated Nb films bombarded with 100-800 eV Ar^+ during deposition. They attributed the changes in stress to modifications in film microstructure and incorpor-
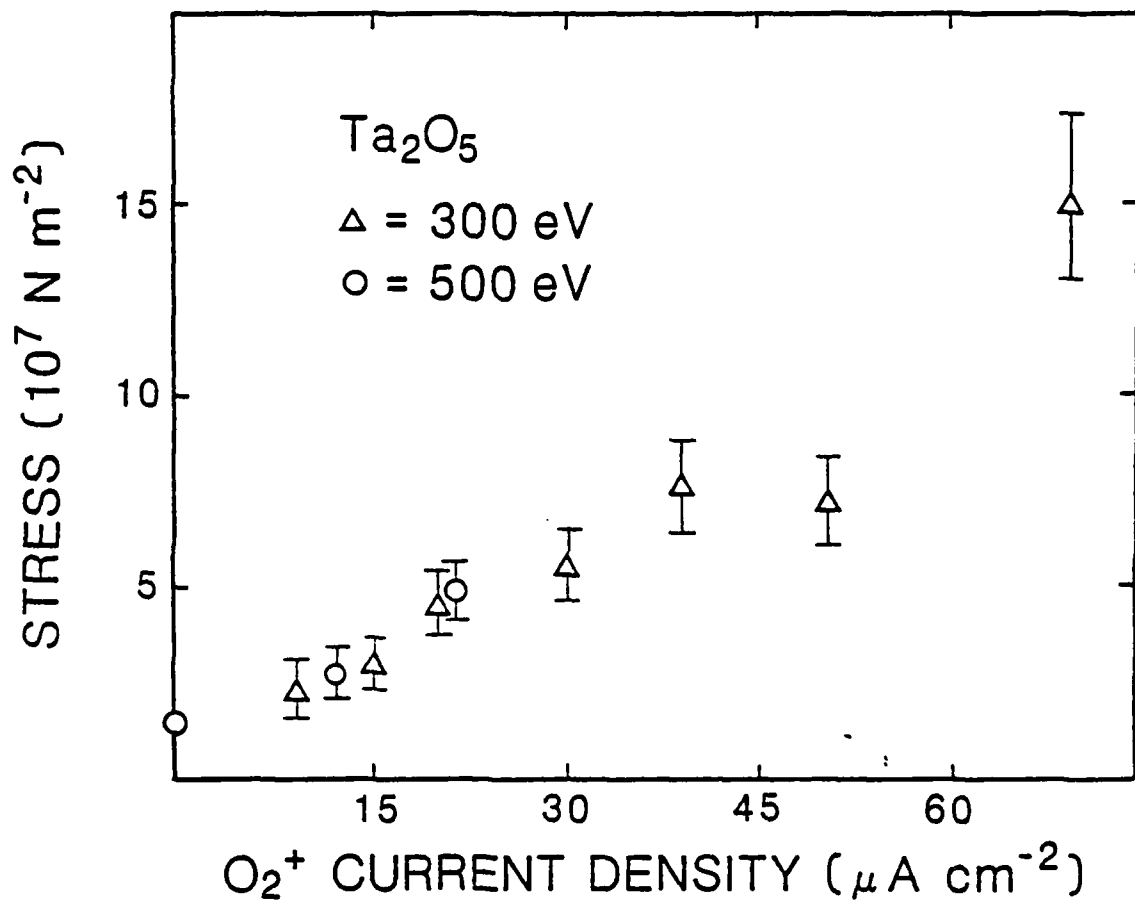
Figure III-12. Values of stress for Ta_2O_5 coatings vs O_2^+ current density.

ation of argon. Hirsh and Varga[66] measured stress relief in evaporated Ge films bombarded with 100-3000 eV Ar^+ during deposition. The stress changed towarded compressive values. Hoffman and Gaerttner[24] bombarded evaporated Cr films during deposition with 11.5 keV Ar^+. They reported changes in stress from tensile to compressive and attributed the results to modification in film microstructure. Thornton and Hoffman[67] examined the stress properties of magnetron sputtered Si films. They reported that increasing compressive stress correlated with the amount of trapped Ar gas. Thus, the results illustrated in Figure III-12 are consistent with the trend toward increasing compressive stress for increasing levels of ion bombardment.

A limited number of Ta_2O_5 coatings were exposed to static fluorine (F_2) gas testing at Los Alamos National Laboratory (LANL). The purpose of the tests was to examine the durability of coatings in a simulated excimer laser environment. The tests at LANL were specifically designed to examine AR and HR coatings at 351 nm. The performance criteria were chosen to examine the decrease in transmittance of the coating at 351 nm. Therefore, the results for the single-layer coatings were sometimes ambiguous. The single-layer coatings were not designed to have a multiple half-wave optical thickness (maximum transmittance) at 351 nm. The coatings tested were secondary samples in depositions designed for other tests (calibration, RBS, Raman, scatter, etc.). In particular, two of the Ta_2O_5 coatings exhibited an increase in transmittance at 351 nm. The coatings were odd-multiple quarter-wave optical thickness at ~351 nm. Figure III-13 illustrates the transmittance spectra for one of these coatings before and after exposure to fluorine gas.

Figure III-14 illustrates the results for 4 Ta_2O_5 coatings. The
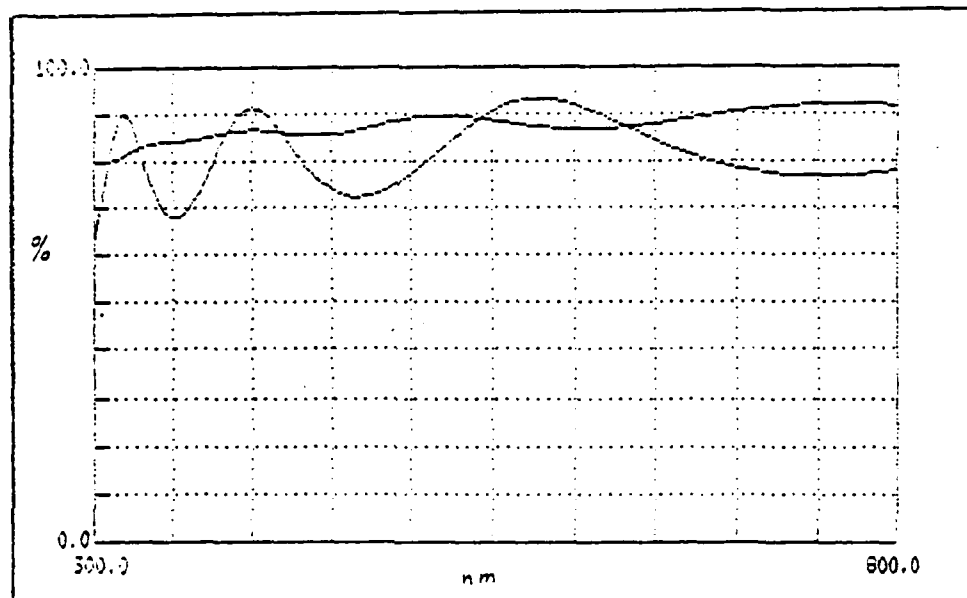
Figure III-13. Transmittance spectra for a Ta_2O_5 coating before and after fluorine gas exposure.
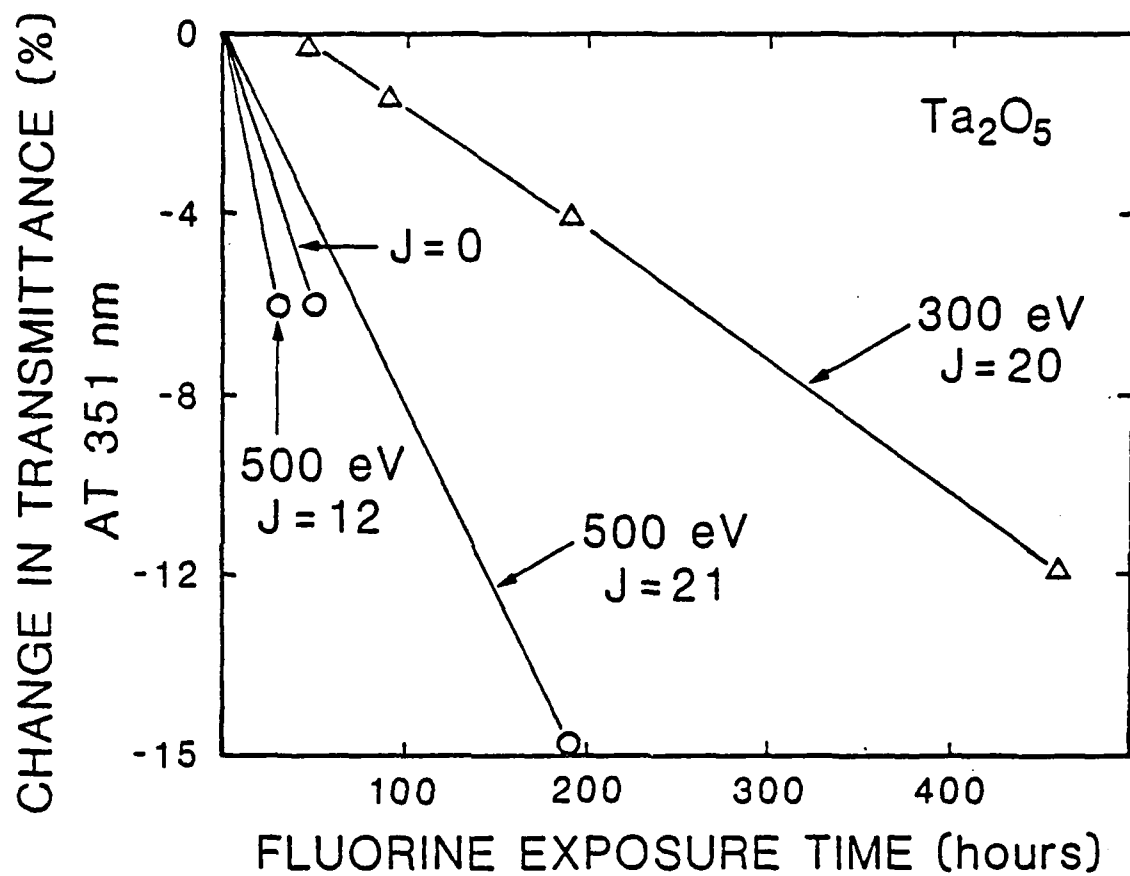
Figure III-14. Decrease in transmittance at 351 nm for Ta_2O_5 coatings vs fluorine gas exposure time.

vertical axis is the decrease in transmittance at 351 nm relative to the pretest value, in percent. The horizontal axis is the length of time the coating was exposed to 0.5% dry F_2 in He gas mixture. As illustrated in Figure III-14, the coating bombarded with 300 eV O_2^+ at a current density of 20 μA cm^{-2} had the best resistance to optical degradation. However, the performance of even this coating was poor relative to required performance criteria.

The dynamics of fluorine attack are not well understood. To date, static exposure to F_2 has reduced the optical performance of almost all materials examined. In addition, the laser damage resistance of coatings diminish substantially after F_2 exposure. One exception has been the performance of rf sputtered AlN/Al_2O_3 AR coatings. These coatings exhibited no degradation after over 1000 hours exposure to 0.5% F_2.[68] Unfortunately, the laser damage threshold value for this coating is very low (< 1 J cm^{-2}). Further discussion relative to the combined results of other IAD coatings (Al_2O_3, SiO_2 and Al_2O_3/SiO_2 AR) is given in Chapter VI.

III.2 Aluminum Oxide

Aluminum oxide (Al_2O_3) thin films have been produced by a variety of techniques: electron-beam evaporation,[69,70] reactive magnetron sputtering,[71] reactive rf diode sputtering,[72] laser evaporation,[73] laser chemical vapor deposition[74,75] and anodic oxidation.[76] Thin films of Al_2O_3 have been used for microelectronic applications,[74-76] adhesive underlayers for metal mirrors[70] and optical coatings for high energy laser systems.[77,78] The values of refractive index (n) for the films deposited by these techniques varied from 1.62 to 1.66 (at λ=350 nm).

The value of n for bulk Al_2O_3 is 1.77.[55] Despite its relatively low value of n, Al_2O_3 is a promising material as the high index component in multi-layer coatings for high energy laser systems.[77,79]

In this study, the Al_2O_3 coatings were electron-beam evaporated at a rate 0.40 nm sec^{-1} with oxygen backfill pressure of 1.0 x 10^{-4} Torr. The coatings were deposited onto heated substrates (~275°C), and were bombarded with oxygen ions during deposition. The values of refractive index and extinction coefficient presented in this section were determined from transmittance and reflectance spectra as described in Chapter II.

The transmittance spectra for two Al_2O_3 coatings are given in Figure III-15. The curve labeled J=0 is for a coating deposited with no ion bombardment; the curve labeled J=25 is for a coating bombarded during deposition with 500 eV O_2^+ at a current density of 25 μA cm^{-2}. The curve for the ion assisted coating contains larger differences in transmittance extrema than the curve for the J=0 coating. These larger differences indicate a larger value of refractive index for the ion assisted coating. Good film stoichiometry was obtained for the ion bombardment conditions employed as indicated by an absence of measurable absorption at wavelengths for which the film is multiple half-wave in optical thickness down to 250 nm. Examination of the reflectance spectra for these coatings indicated the absence of any refractive index inhomogeneity. As illustrated in Figure III-15, the absorption band edge for Al_2O_3 coatings was less than 200 nm.

The values of n (λ=350 nm) for Al_2O_3 coatings bombarded with 300, 500 and 1000 eV oxygen ions are plotted in Figure III-16 as a function of O_2^+ current density. The values increase from 1.64 for coatings deposit-
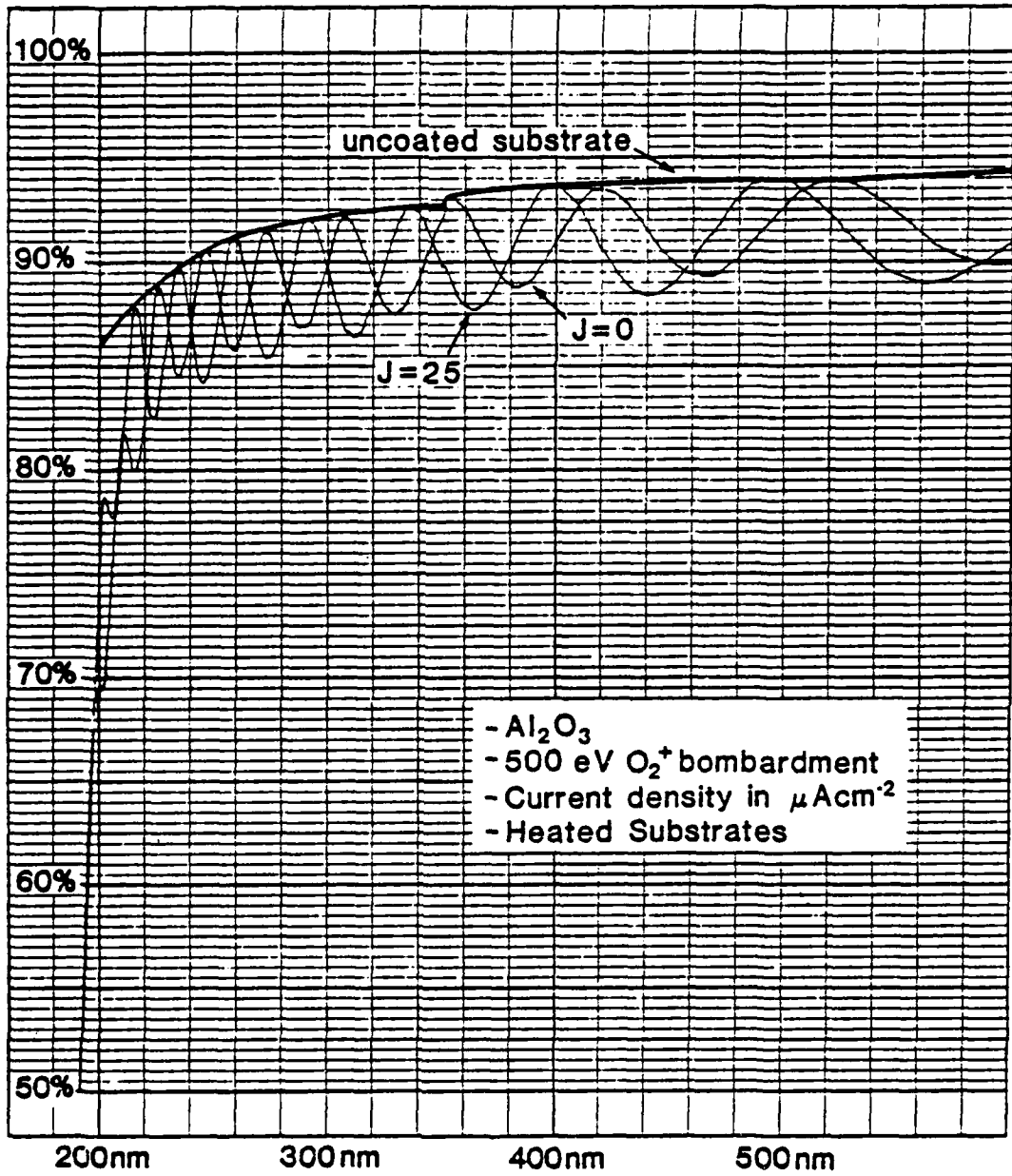
Figure III-15. Transmittance spectra for two Al₂O₃ coatings.
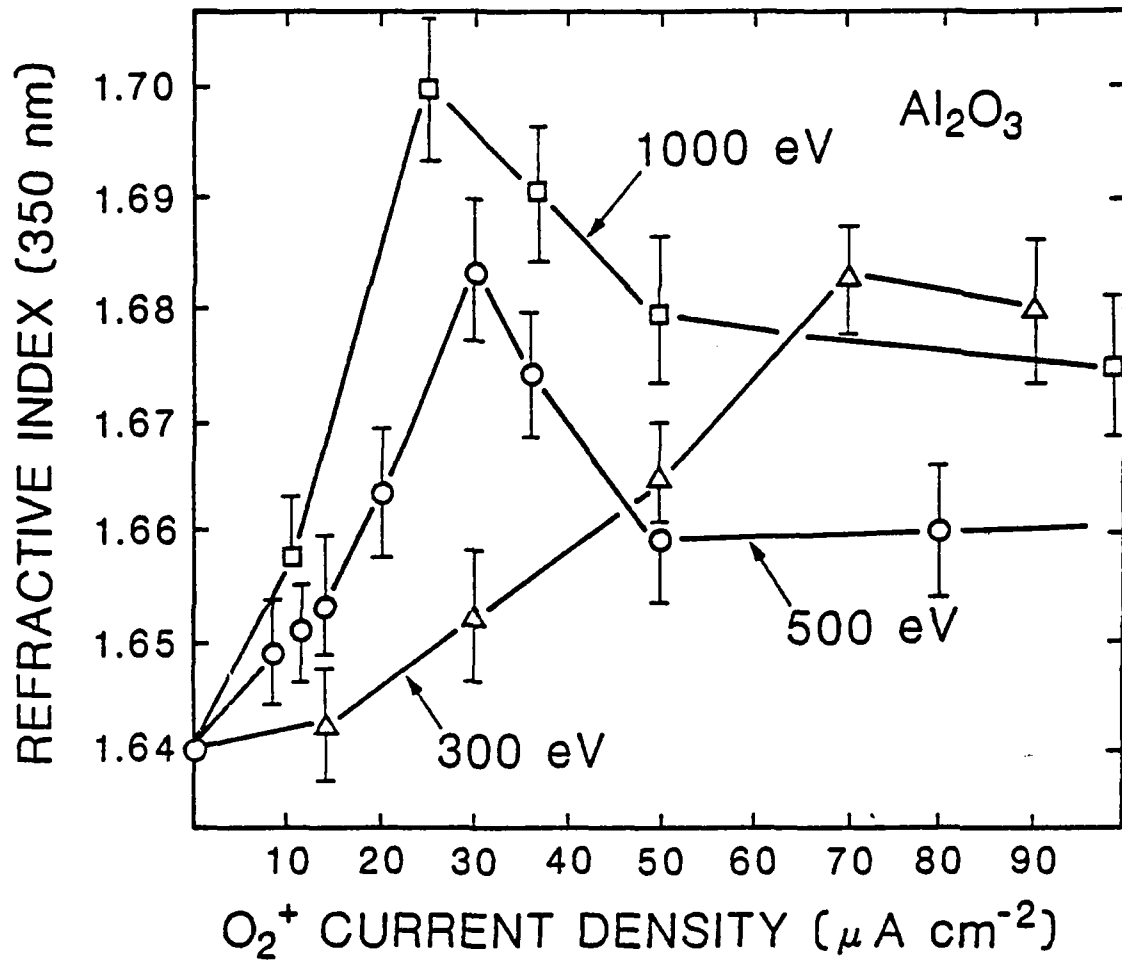
Figure III-15. Values of refractive index for Al_2O_3 coatings plotted as a function of O_2^+ current density.

ed without bombardment to maximum values of 1.70, 1.68 and 1.68 for films bombarded with 1000, 500 and 300 eV O_2^+, respectively. The value of 1.64 (J=0) is comparable to the value of 1.65 (at λ=355 nm) for e-beam evaporated Al_2O_3 reported by other investigators.[69,78]

The increase in the values of n for increasing levels of O_2^+ current density is similar to Ta_2O_5 results (Figure III-2) and indicates that ion bombardment during deposition results in film densification. The results indicated that the Al_2O_3 coatings bombarded with 1000 eV O_2^+ had larger values of n than those bombarded with 500 and 300 eV O_2^+. These results illustrate that the effects of ion bombardment on the values of n are material dependent. The ion energy at which the largest value of n occurred for Ta_2O_5 was 300 eV, yet, for Al_2O_3 it was 1000 eV.

The results in Figure III-16 illustrate that values of n decreased for ion current densities greater than the critical values. The decrease in index might be explained as a result of the creation of closed isolated voids and oxygen incorporation in the films. The decrease was greatest for bombardment with 1000 eV ions and least for 300 eV ions. This energy dependent decrease is consistent with the results for Ta_2O_5 coatings (Figure III-2) and results reported for ion assisted ZrO_2 film[29] and CeO_2 films.[30]

Attempts to measure the values of extinction coefficient for the Al_2O_3 coatings (400 nm thick) were limited due to the minimum sensitivity of the measurement equipment. All computed values of k were less than 2.0×10^{-4}. The only exceptions were coatings bombarded during deposition at current densities greater than 100 μA cm^{-2}. These coatings exhibited a small amount of optical absorption and slight index inhomo-geneity. The low values of k calculated for all the other Al_2O_3 coatings

indicate that for the conditions examined, preferential oxygen sputtering is not a dominant mechanism for Al_2O_3 as was the case for Ta_2O_5 (Figure III-3). Further discussion on preferential sputtering is given in Chapter VI.

Measurement of the optical scatter characteristics of coatings is a method used to determine the effects of O_2^+ bombardment on film microstructure. The optical scatter characteristics of the coatings were examined using an angle-resolved scatterometer as described in Chapter II. The coatings were deposited onto polished silicon wafers and were multiple half-wave optical thickness at 633 nm so that scatter was primarily due to volume effects in the coatings.

Figure III-17 illustrates the scatter characteristics of two Al_2O_3 coatings; one deposited without ion bombardment (J=0), and the other bombarded during deposition with 300 eV O_2^+ at a current density of 50 $\mu A\ cm^{-2}$. The scatter characteristic for an uncoated silicon wafer is illustrated for comparison.

As illustrated in Figure III-17, the optical scatter from the IAD coating (J=50) was less than that from the coating deposited without bombardment. Figures III-18 and -19 illustrate the scatter characteristics for Al_2O_3 coatings bombarded during deposition with 500 and 1000 eV ions at current densities of 35 and 25 $\mu A\ cm^{-2}$, respectively. The IAD coatings were compared against coatings deposited without ion bombardment (J=0), and a reduction in optical scatter was observed. Comparable reduction in scatter was observed for other IAD Al_2O_3 coatings relative to unbombarded coatings except for coatings bombarded with very high levels of current density. For coatings bombarded during deposition with 500 eV O_2^+ at current densities greater than 90 $\mu A\ cm^{-2}$, the optical

Figure III-17. BRDF vs scatter angle for two Al_2O_3 coatings. One deposited with no ion bombardment (J=0); the other bombarded during deposition with 300 eV O_2^+ at J=50 μA cm^{-2}.
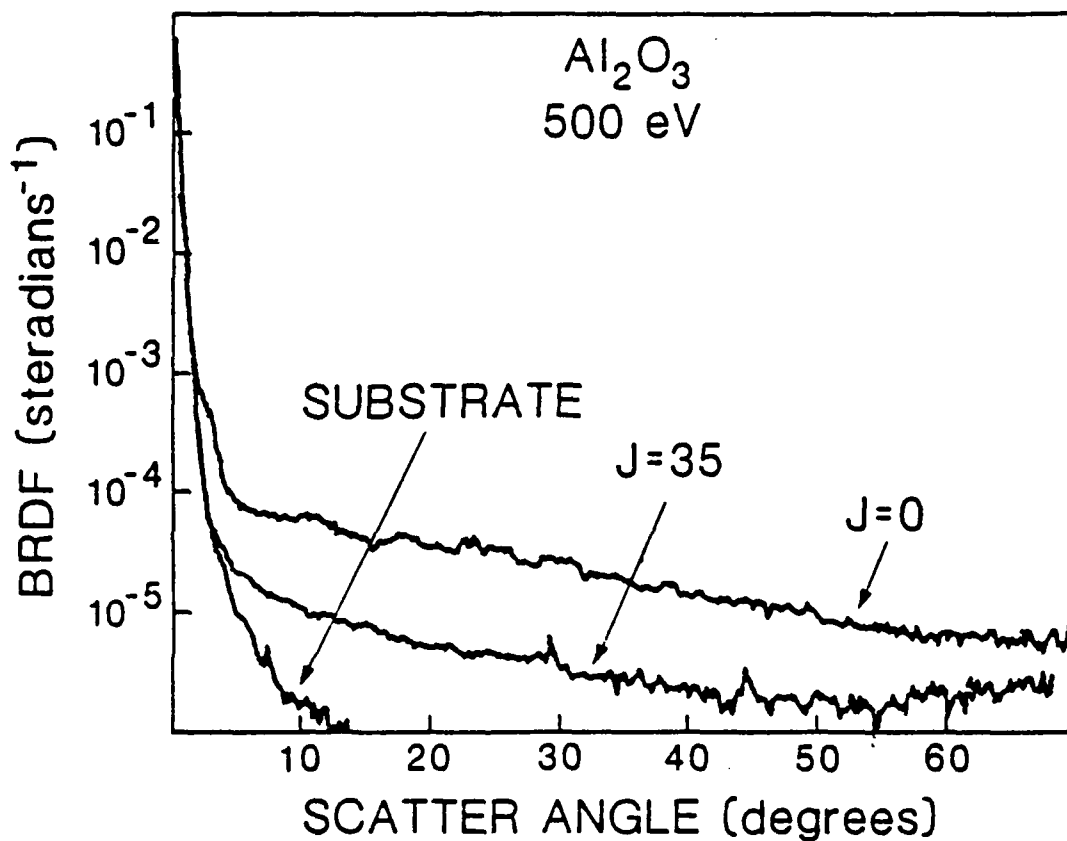
Figure III-18. BRDF vs scatter angle for two Al_2O_3 coatings. One deposited with no ion bombardment (J=0); the other bombarded during deposition with 500 eV O_2^+ at J=35 μA cm^{-2}.
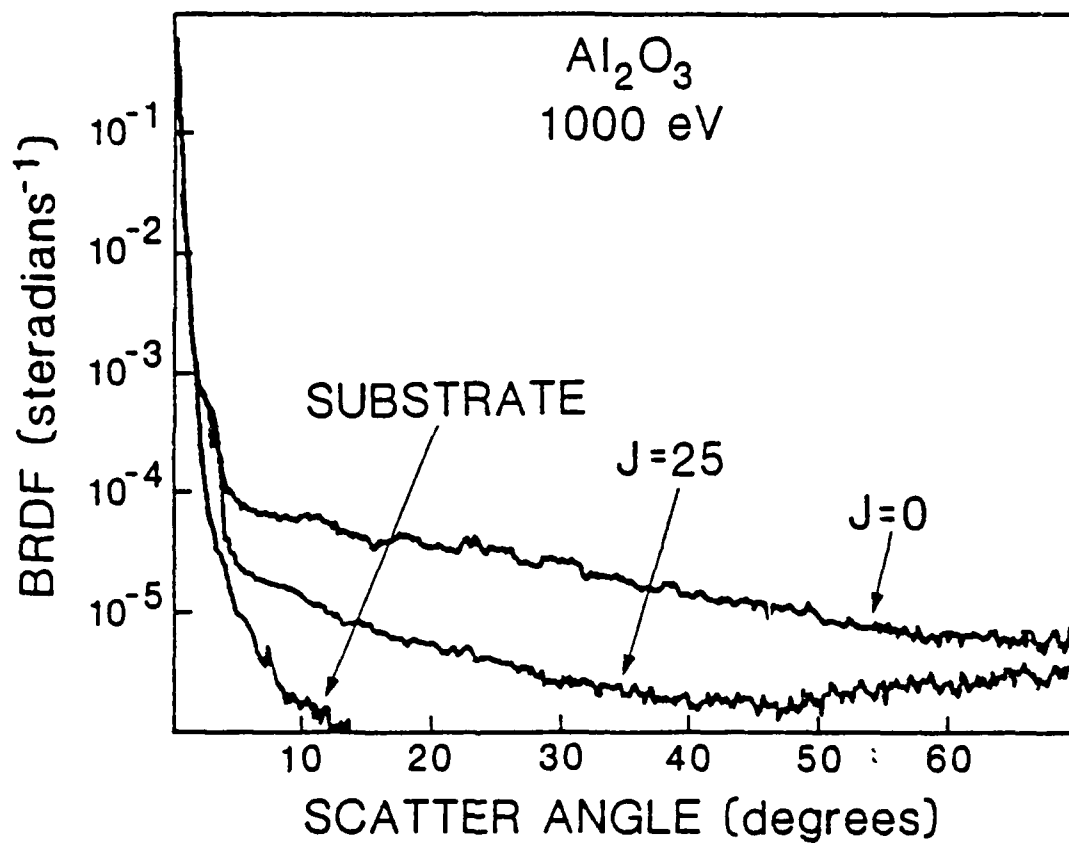
Figure III-19. BRDF vs scatter angle for two Al_2O_3 coatings. One deposited with no ion bombardment (J=0); the other bombarded during deposition with 1000 eV O_2^+ at J=25 μA cm^{-2}.

scatter increased by a factor of 2-3 times that for a coating deposited without bombardment (see Figure III-20). The reduction in optical scatter is similar to the reduction in scatter observed for IAD Ta_2O_5 coatings (Figures III-4,-5 and -6). This reduction in optical scatter indicates that ion bombardment during deposition modifies the growth of film columnar microstructure producing a more homogeneous film morphology.

The Al_2O_3 coatings were not examined using Rutherford backscattering spectroscopy (RBS). The technique is unable to measure the quantity of Al in Al_2O_3 films coated on silicon substrates due to the lack of mass resolution between Al and Si (their difference is only 1). Therefore, no data is available to examine stoichiometry nor oxygen incorporation in the coatings.

Three Al_2O_3 coatings were exposed to fluorine gas tests at LANL. The coatings were exposed to a 0.5% dry F_2 in He gas mixture and their optical transmittance at 351 nm was measured at various time intervals. The three coatings were multiple half-wave in optical thickness at approximately 351 nm. Figure III-21 illustrates the results of the F_2 testing. The Al_2O_3 coating deposited with no ion bombardment has suffered no degradation in optical transmittance after 670 hours of exposure. This coating is still undergoing F_2 exposure. The Al_2O_3 coating bombarded during deposition with 500 eV O_2^+ at a current density of 50 μA cm^{-2} suffered approximately 4.5% loss in optical transmittance after 470 hours of exposure. The coating bombarded with 500 eV O_2^+ at a current density of 25 μA cm^{-2} suffered approximately 10% loss in optical transmittance after only 28 hours of exposure. It is unclear why the results for the IAD coatings are much worse than the coating deposited
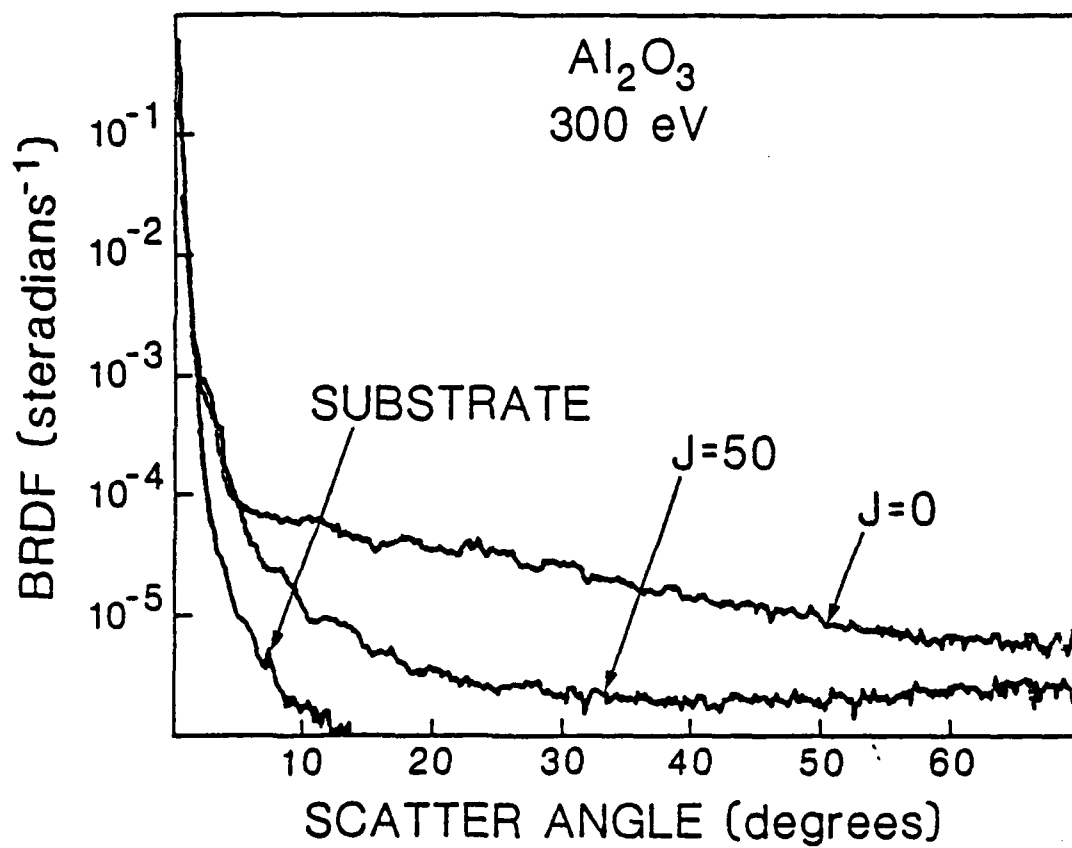
Figure III-20. BRDF vs scatter angle for two Al_2O_3 coatings. One deposited with no ion bombardment (J=0); the other bombarded during deposition with 500 eV O_2^+ at J=195 $\mu A\ cm^{-2}$.
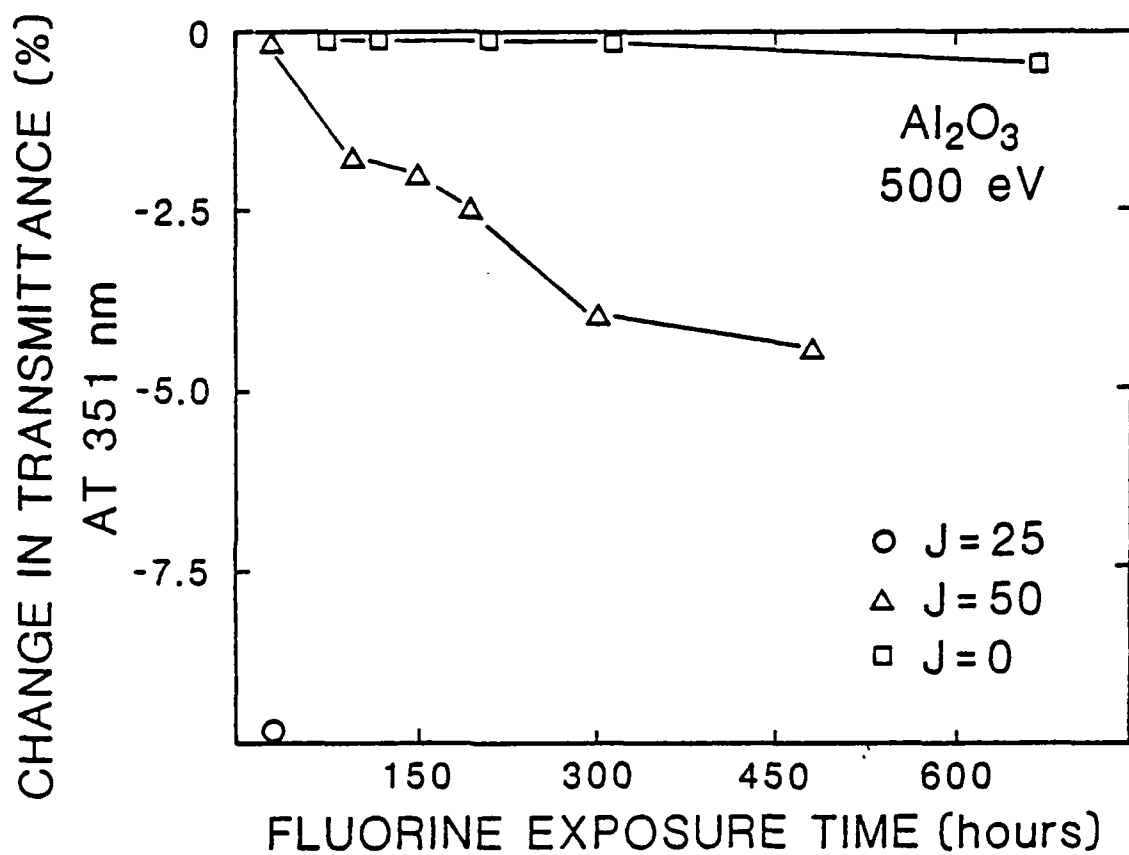
Figure III-21. Decrease in transmittance at 351 nm for Al$_2$O$_3$ coatings vs fluorine gas exposure time.

with no ion bombardment. Due to the limited number of coatings tested, no clear hypothesis about the mechanism(s) for fluorine gas attack can be formulated. These results along with the results for the other coatings (Ta_2O_5, SiO_2 and Al_2O_3/SiO_2 AR) are further discussed in Chapter VI.

III.3 Silicon Dioxide

Silicon dioxide (SiO_2) has been a standard material in metal-oxide-semiconductor devices for over two decades, as well as one of the standard low-index materials in multi-layer optical coatings. Thin films of SiO_2 have been produced by a variety of techniques: thermal oxidation,[80] electron-beam evaporation,[81] reactive rf diode sputtering,[12] ion beam sputtering,[14] ion implantation of SiO,[19] nozzle beam deposition,[18] laser evaporation,[73] laser chemical vapor deposition[74] and plasma enhanced chemical vapor deposition.[82] The values of refractive index (n) for the films deposited by these techniques varied from 1.43 to 1.46 (at λ=633 nm). The value of n for bulk SiO_2 is 1.46.

In this study, the SiO_2 coatings were electron-beam evaporated at a rate of 0.35 nm sec^{-1} with oxygen backfill pressure of 1.0×10^{-4} Torr. The coatings were deposited onto heated substrates (~275°C), and were bombarded with oxygen ions during deposition. The values of refractive index presented in this section were measured using an ellipsometer at λ=633 nm.

The values of n for SiO_2 coatings bombarded during deposition with 300 and 500 eV O_2^+ are listed in Table III-3. The empirically determined precision of the ellipsometry measurements is approximately 2% (n=1.44 ± 0.01). The values of n in Table III-3 do not vary by more than the precision of the measurement technique. Therefore, there is no

Table III-3

IAD conditions and refractive index values for SiO_2

E (eV)	J ($\mu A\ cm^{-2}$)	n (λ=633nm)
0	0	1.44
300	30	1.45
300	60	1.45
300	90	1.45
300	195	1.43
500	30	1.45
500	60	1.44
500	90	1.45
500	195	1.45

significant effect on the refractive index of SiO_2 due to ion bombardment during deposition.

The optical transmittance spectra of SiO_2 coatings deposited onto high-index substrates were measured. The differences in transmittance extrema (ΔT) for these spectra were calculated. All of the ΔT values were within the range of 0.067 to 0.069. There was no significant difference in the ΔT values for the IAD SiO_2 coatings within the measurement precision ($\pm$ 0.1%) of the spectrophotometer. The results from analysis of the transmittance spectra confirmed the refractive index values measured using the ellipsometer.

The optical transmittance spectra of 300 nm thick SiO_2 coatings deposited onto UV-grade fused silica substrates were measured. The spectra were analyzed for optical absorption at $\lambda=200$ nm as a qualitative measure of film stoichiometry. This analysis was performed to study the compositional stability of SiO_2 coatings deposited with O_2^+ bombardment. All but two of the coatings exhibited no optical absorption within the measurement precision of the spectrophotometer. The coatings bombarded during deposition with 300 and 500 eV O_2^+ at a current density of 195 μA cm^{-2} exhibited 1.0 and 1.3% absorption, respectively. These values correspond to an absorption coefficient of approximately 300 cm^{-1}. The absence of any measurable absorption in the other IAD SiO_2 coatings indicated that for moderate ion bombardment levels preferential sputtering was not a dominant mechanism as was the case for Ta_2O_5 (Figure III-3).

The absorption values were calculated from the difference in transmittance between the coated substrate and the uncoated substrate. The measured absorption values included the effects due to optical

scatter. However, the increase in optical scatter for these coatings was negligible compared to the measured absorption values. (Optical scatter characteristics of SiO_2 are discussed in a later paragraph.)

A recent XPS study[57] of the effects of ion bombardment on the composition of SiO_2 films indicated that preferential sputtering of oxygen occurred. The study involved Ar ion bombardment of a sample at a current density of 250 μA cm^{-2}. The results indicated that the oxygen deficiency was localized in the near surface region to a depth that corresponded with the ion penetration depth. Preferential sputtering is further discussed in Chapter VI.

The optical scatter characteristics of the coatings were examined using an angle-resolved scatterometer as described in Chapter II. The coatings were deposited onto polished silicon wafers and were multiple half-wave optical thickness at 633 nm so that scatter was primarily due to volume effects in the coatings. Figure III-22 illustrates the scatter characteristics of two SiO_2 coatings; one deposited without ion bombardment (J=0), and the other bombarded during deposition with 300 eV O_2^+ at a current density of 30 μA cm^{-2}. The scatter characteristic for an uncoated silicon wafer is illustrated for comparison.

As illustrated in Figure III-22, the optical scatter from the IAD coating (J=30) was less than that from the coating deposited without bombardment. Figure III-23 illustrates the scatter characteristics for a SiO_2 coating bombarded during deposition with 500 eV ions at a current density of 30 μA cm^{-2}. The IAD coating was compared with a coating deposited without ion bombardment (J=0), and a reduction in optical scatter was observed. Comparable reduction in scatter was observed for other IAD SiO_2 coatings relative to unbombarded coatings except for
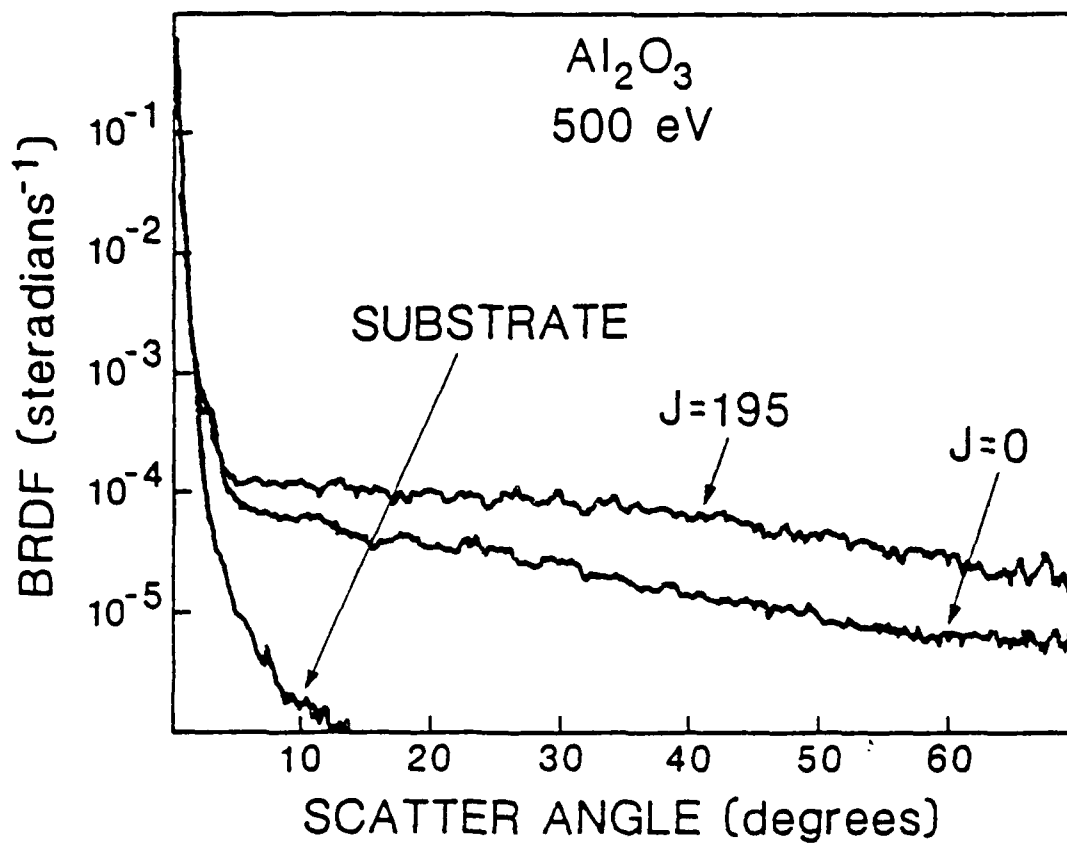
Figure III-22. BRDF vs scatter angle for two SiO_2 coatings. One deposited with no ion bombardment (J=0); the other bombarded during deposition with 300 eV O_2^+ at J=30 μA cm^{-2}.
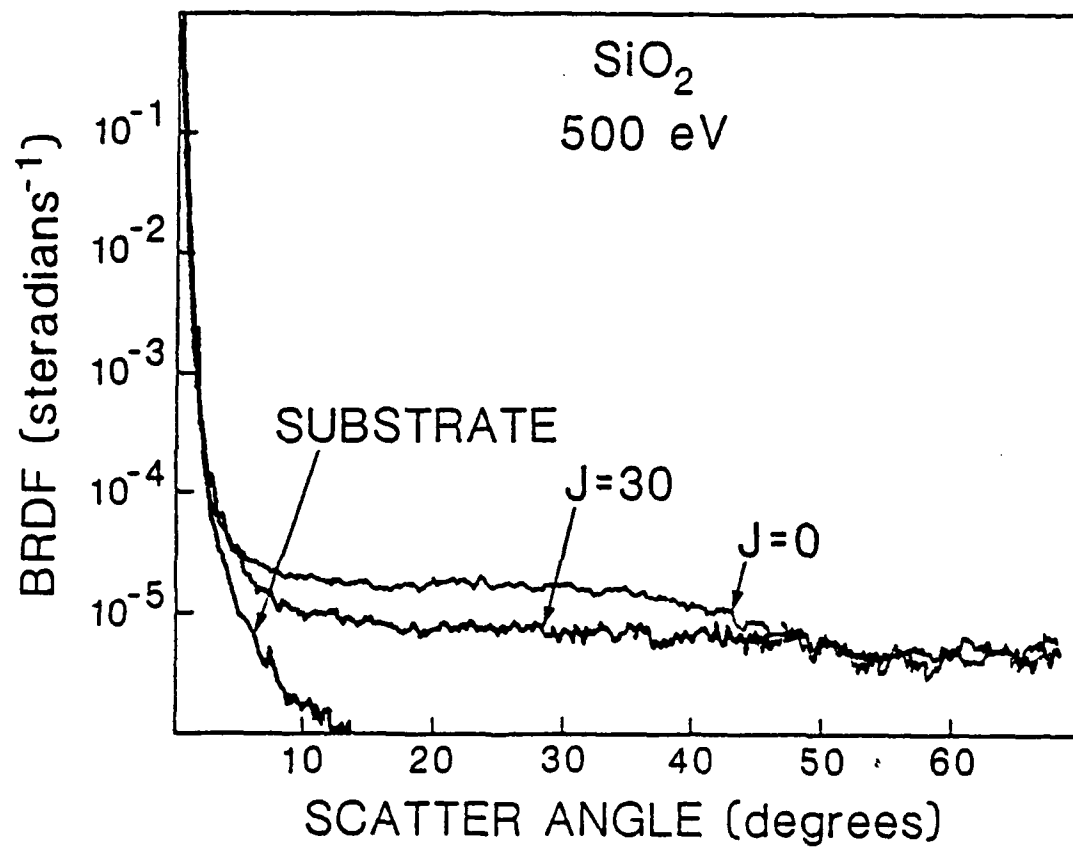
Figure III-23. BRDF vs scatter angle for two SiO$_2$ coatings. One deposited with no ion bombardment (J=0); the other bombarded during deposition with 500 eV O$_2^+$ at J=30 μA cm^{-2}.

coatings bombarded with very high levels of current density. For coatings bombarded during deposition with 300 and 500 eV O_2^+ at a current density of 195 μA cm^{-2}, the optical scatter increased by a factor of two times that for a coating deposited without bombardment (see Figure III-24). These results indicate that moderate levels of ion bombardment during deposition can reduce the amount of optical scatter for SiO_2 coatings. Similar results are reported for optical scatter from IAD SiO_2 coatings.[33]

A few SiO_2 coatings were exposed to humidity testing as described in Chapter II. The environmental stability of optical coatings is in a large part limited by their tendency to adsorb water vapor. This results in wavelength shifts to higher values as the coatings age. The coatings exposed to humidity testing were deposited onto heated high index sub-strates and bombarded with 500 eV O_2^+ during deposition. The trans-mittance spectra were measured immediately after the coatings were removed from the vacuum chamber and exposed to the ambient atmosphere. The transmittance spectra were re-measured after the coatings were exposed to 97% relative humidity at 35°C for six hours.

The SiO_2 coating deposited without bombardment exhibited a spectral shift to longer wavelengths of approximately 0.3%. The shift was most likely due to water adsorption into the film microvoids. The coatings bombarded during deposition with 500 eV O_2^+ exhibited no spectral shifts within the measurement precision ($\pm$ 0.5 nm) of the spectrophotometer. The humidity test results for the IAD SiO_2 coatings are similar to the results obtained for IAD Ta_2O_5 coatings (Table III-1) and results reported for Ar ion assisted SiO_2.[21]

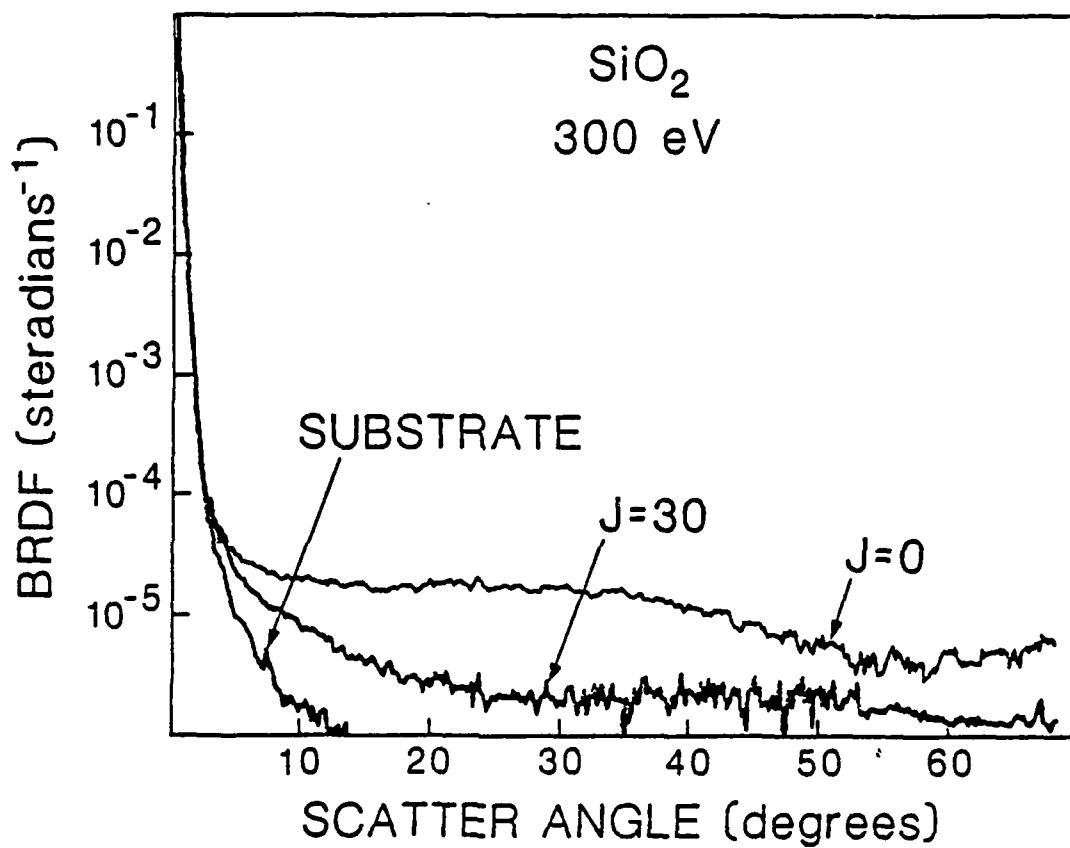Three SiO_2 coatings were exposed to fluorine gas tests at LANL. The
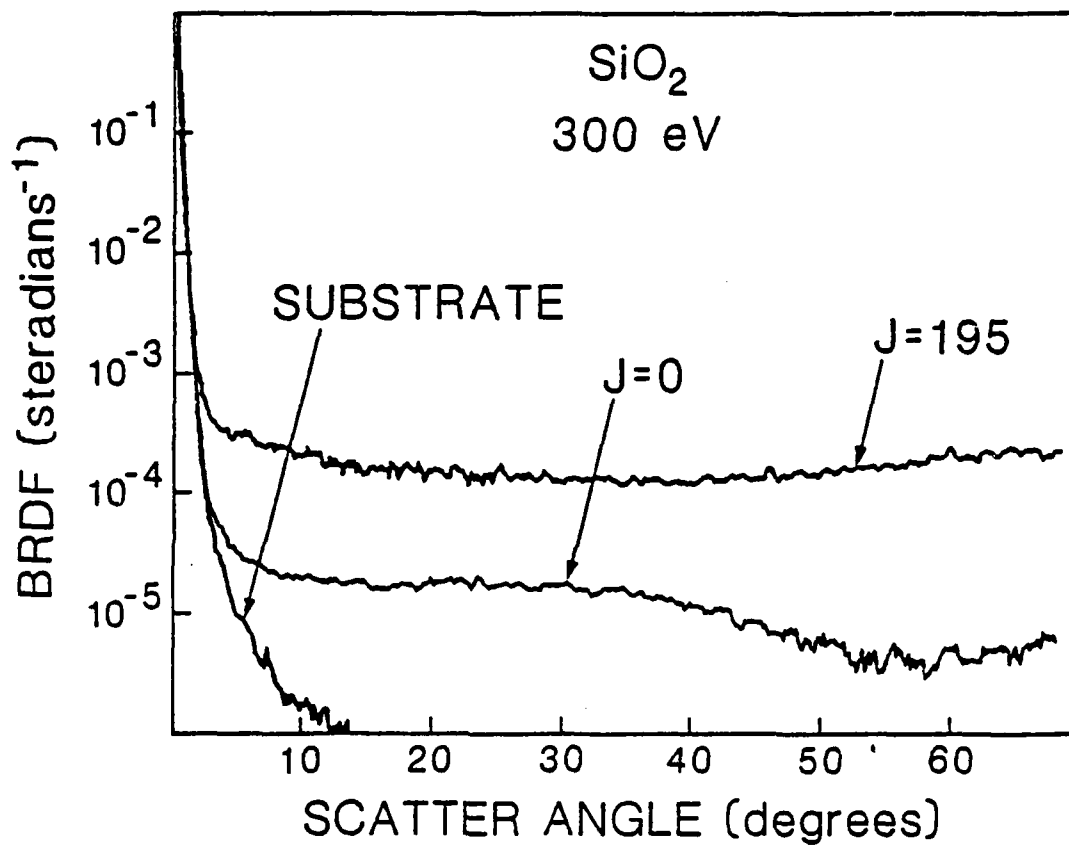
Figure III-24. BRDF vs scatter angle for two SiO$_2$ coatings. One deposited with no ion bombardment (J=0); the other bombarded during deposition with 300 eV O$_2^+$ at J=195 µA cm^{-2}.

coatings were exposed to a 0.5% dry F_2 in He gas mixture and their optical transmittance at 351 nm was measured at various time intervals. The three coatings were deposited onto heated fused silica substrates. Figure III-25 illustrates the results of the F_2 testing. The SiO_2 coating deposited with no ion bombardment (J=0) has suffered 0.5% loss in optical transmittance after 698 hours of exposure. This coating is still undergoing F_2 exposure. The SiO_2 coating bombarded during deposition with 500 eV O_2^+ at a current density of 50 μA cm^{-2} suffered approximately 4.5% loss in optical transmittance after 470 hours of exposure. The coating bombarded with 500 eV O_2^+ at a current density of 25 μA cm^{-2} suffered approximately 10% loss in optical transmittance after only 28 hours of exposure. It is unclear why the results for the IAD coatings are much worse than the coating deposited with no ion bombardment. The results for SiO_2 are very similar to the results for Al_2O_3 (Figure III-21). For both coating materials the J=0 sample was still undergoing F_2 testing after over 600 hours exposure. Due to the limited number of coatings tested, no clear hypothesis about the mechanism(s) for fluorine gas attack can be formulated. These results along with the results for the other coatings (Ta_2O_5, Al_2O_3 and Al_2O_3/SiO_2 AR) are further discussed in Chapter VI.

III.4 Hafnium Dioxide

Hafnium dioxide (HfO_2) thin films have been produced by electron-beam evaporation,[83] reactive sputtering[84] and oxidation of evaporated hafnium films.[85] The values of refractive index reported for HfO_2 films has varied from 1.95 to 2.08 (at λ=350 nm).[83,78] The value of n for bulk HfO_2 is 2.25.[55]
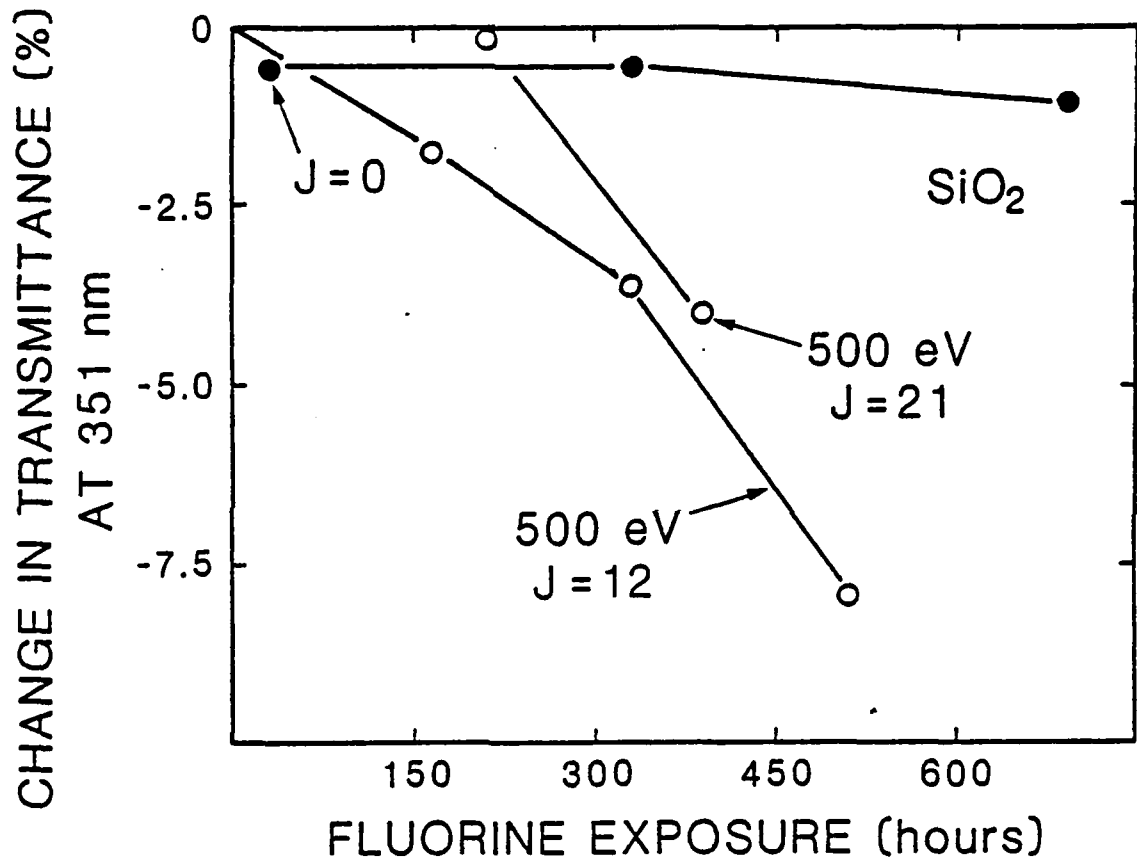
Figure III-25. Decrease in transmittance at 351 nm for SiO$_2$ coatings vs fluorine exposure time.

In this study, the HfO_2 coatings were electron-beam evaporated at a rate of 0.3 nm sec^{-1} with oxygen backfill pressure of 1.0 x 10^{-4} Torr. The coatings were deposited on heated substrates (~275°C), and were bombarded with oxygen ions during deposition. The values of refractive index and optical inhomogeneity were determined from transmittance and reflectance spectra as described in Chapter II.

A problem encountered in evaporating HfO_2 was material "spitting". Large particles of material were ejected from the HfO_2 evaporant even at electron gun conditions well below normal deposition conditions. Similar problems have been observed by others.[86] This material "spitting" resulted in coatings in which a large number of solid particles were incorporated. Figure III-26 is a dark-field Nomarski micrograph (20X) of a HfO_2 coating. The figure illustrates a large number of scatter sites in the coating. The sites are assumed to be particulates incorporated in the coating due to the material "spitting". Figure III-27 is a dark-field Nomarski micrograph of the same coating obtained at 100X. This figure illustrates that the scatter sites were indeed incorporated particulates. The size of the largest particulates was approximately 25 μm.

One of the problems associated with the material "spitting" was that it resulted in coatings with high optical scatter. The optical scatter characteristics of the coatings were examined using an angle-resolved scatterometer as described in Chapter II. Figure III-28 illustrates the scatter characteristic of a HfO_2 coating. The coating was the same one used to obtain the micrographs in Figures III-26 and -27. The optical scatter from this HfO_2 coating was approximately 100 times larger than that from the Ta_2O_5, Al_2O_3 and SiO_2 coatings examined in this study. All
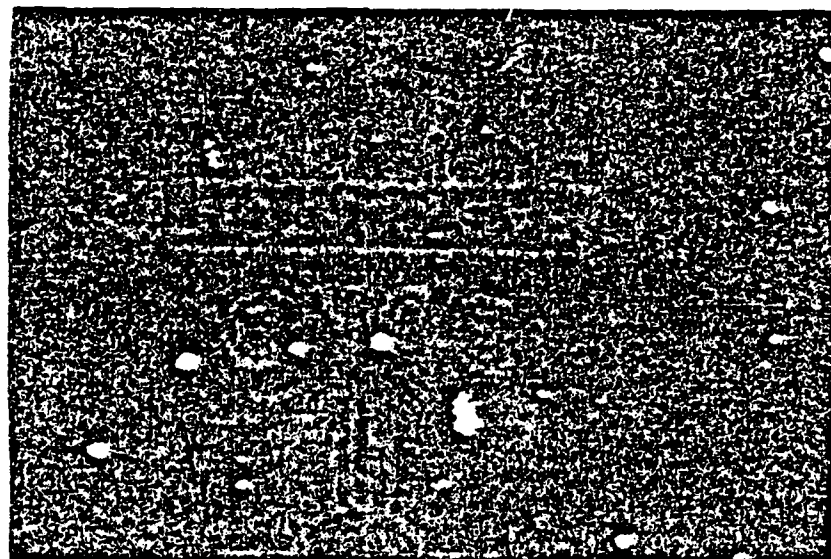
10 μm

Figure III-26. Dark field micrograph of a HfO$_2$ coating (20X).
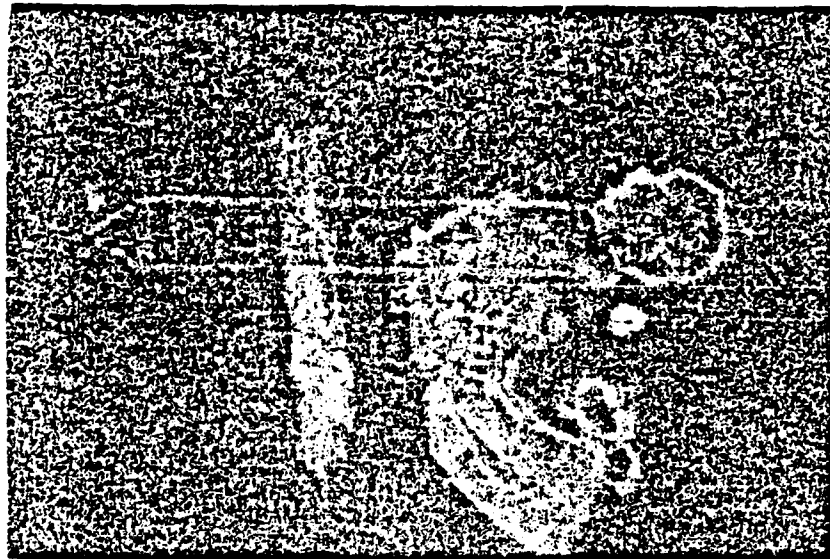
10 μm

Figure III-27. Dark field micrograph of a hfO$_2$ coating (100X).
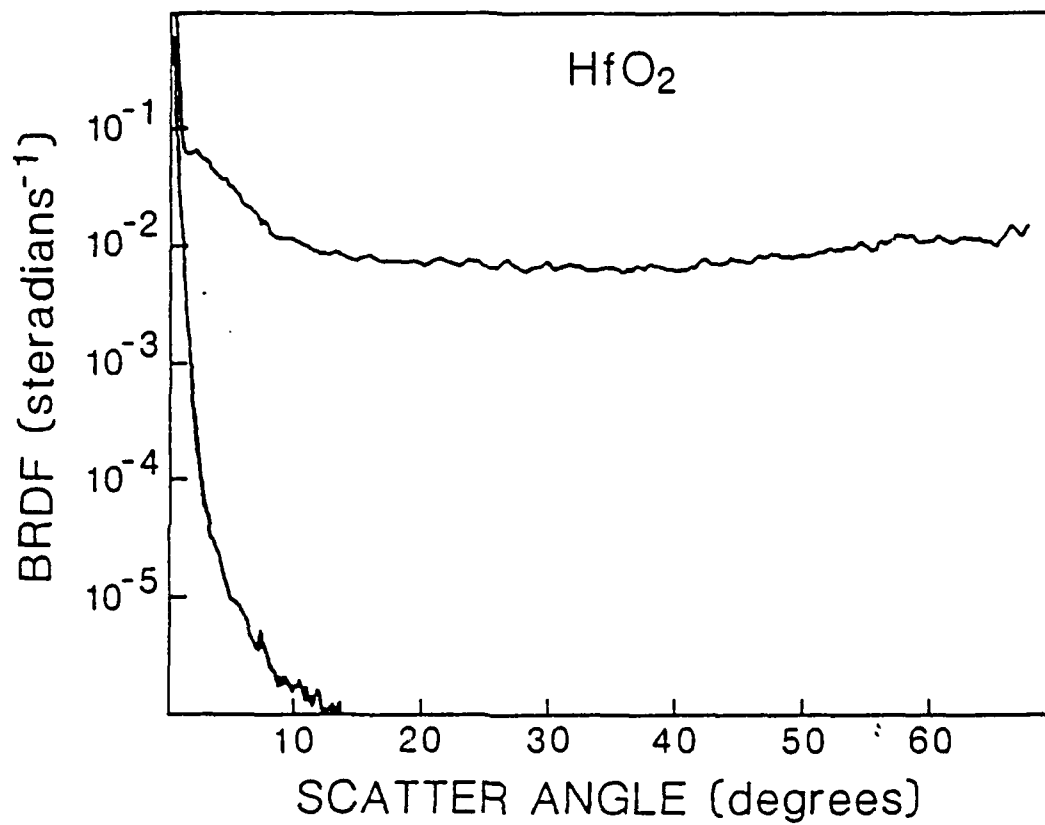
Figure III-28. BRDF vs scatter angle for HfO_2 coating.

of the HfO_2 coatings examined had similar scatter characteristics as that illustrated in Figure III-28.

Another problem encountered with the HfO_2 coatings was optical inhomogeneity. Evidence that the single-layer coatings were inhomogeneous was obtained by examining the reflectance spectra. The minimum reflectance values were lower than the reflectance value for the uncoated substrate. This indicated a negative inhomogeneity where the refractive index of the coating was highest adjacent to the substrate. A similar problem with optical inhomogeneity in HfO_2 coatings was reported by Baumeister and Arnon.[83] They reported negative inhomogeneity in HfO_2 coatings deposited over a range of conditions. Coatings deposited on heated and unheated substrates, at deposition rates of 0.1, 0.2 and 0.3 nm sec^{-1} and at various vacuum pressures all exhibited optical inhomogeneity.

The inhomogeneity of the refractive index in optical coatings has been represented by two different models. One model assumes the inhomogeneous coating can be represented as several thin homogeneous layers each with a slightly different value of n. An empirical relation has been developed by applying this model to inhomogeneous coatings.[87] The relation is

$$\Delta n/n \approx \Delta R/4.4R, \qquad (III-2)$$

where n is the average value of refractive index, Δn is the change in n over the coating thickness, R is the single surface reflectance of the uncoated substrate, and ΔR is the difference between the minimum coating reflectance and the uncoated substrate. The other model assumes that the

inhomogeneity is directly related to the size of the columnar micro-structure in a coating.[88] The model represents coating microstructure as an array of close-packed cylindrical columns. For a coating with negative inhomogeneity (i.e. n decreasing with thickness), the model is varied to allow columns with decreasing diameters as the coating thickness increases. The columns form truncated cones. In this variation, the film packing density decreases with thickness.

The relationship developed by Arndt et.al. will be used to analyze the HfO_2 coatings in this study.[87] Figure III-29 is the reflectance spectrum for a HfO_2 coating bombarded with 300 eV O_2^+ at a current density of 12 μA cm^{-2}. This result is typical of the HfO_2 coatings deposited in this study. The value of refractive index was 1.98. The value of ΔR was -2.1%. The calculated value of Δn was -0.24. Assuming a linear variation in n as a function of film thickness, the following two relations can be developed

$$n_{sub/f} = n + \Delta n/2 \qquad (III-3)$$

and
$$n_{air/f} = n - \Delta n/2. \qquad (III-4)$$

The value of refractive index at the substrate/film interface is $n_{sub/f}$; the value of refractive index at the air/film interface is $n_{air/f}$. The value of $n_{sub/f}$ for the coating whose reflectance spectrum is illustrated in Figure III-29 was 2.10. The value of $n_{air/f}$ was 1.86. Table III-4 lists the average values of Δn for the HfO_2 coatings examined in this study.
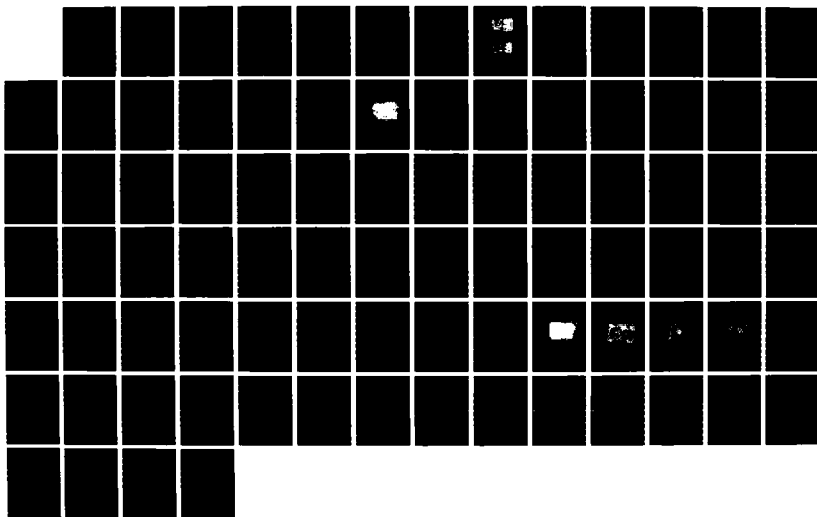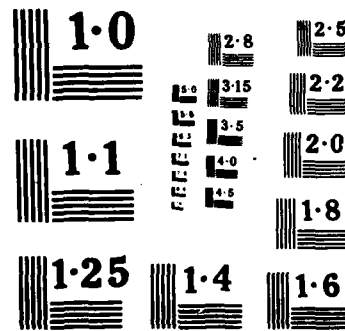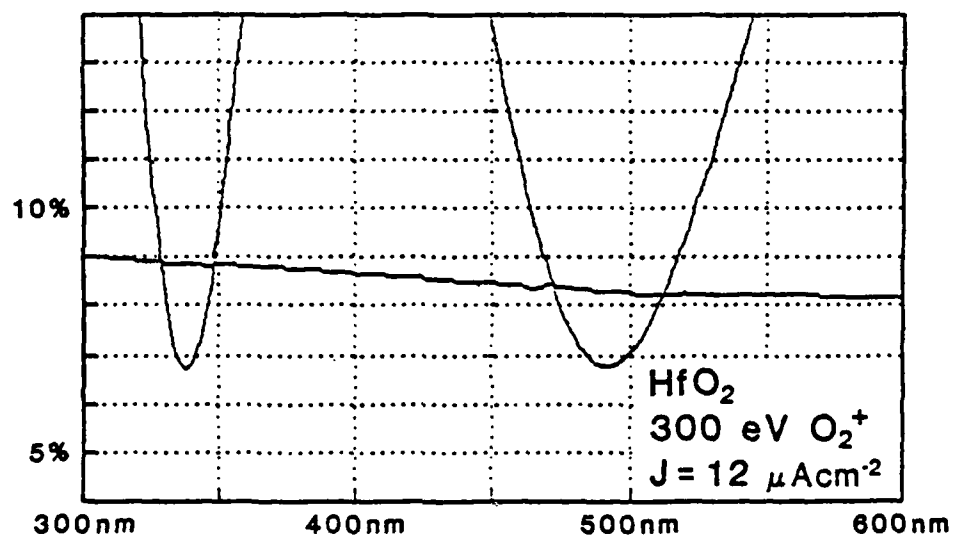
Figure III-29. Reflectance spectrum of a HfO$_2$ coating bombarded during deposition with 300 eV O$_2^+$ at J=12 μA cm^{-2}.

Table III-4

IAD conditions and Δn values for HfO_2

E(eV)	J($\mu A\ cm^{-2}$)	n	ΔR	Δn
0	0	1.98	-0.010	-0.11
300	12	1.98	-0.020	-0.23
300	30	2.10	-0.030	-0.35
300	50	1.99	-0.015	-0.17
500	12	2.00	-0.015	-0.17
500	20	1.98	-0.020	-0.23
500	60	2.04	-0.015	-0.17

CHAPTER IV

RESULTS FOR HEAVY METAL FLUORIDE GLASS COATINGS

Heavy metal fluoride (HMF) glasses have attracted considerable interest as multispectral transmissive optical components, laser host materials and optical fibers. HMF glasses were discovered by Lucas, Paulain and coworkers in 1974. The early materials were fluorozirconates, where ZrF_4 was the primary constituent (> 50 mol %), BaF_4 was the principal modifier (~ 30 mol %) and other metal fluorides (ThF_4 and LaF_3) were the tertiary constituents. Other HMF glasses have been made and studied (for example, fluorohafnate glasses where HfF_4 was the primary constituent). The concerns with HMF glasses center around their stability and their glass formation ability. A wide working range, defined as the difference between the crystallization temperature (T_x) and the glass transition temperature (T_g), is required for fiber fabrication and to cast large preforms of good optical quality. T_g is defined as the temperature near which the liquid-to-glass transition occurs in a material; T_x is defined as the temperature at which the liquid-to-crystal transition occurs. A typical value for the difference, $\Delta T = T_x - T_g$, for fused silica is approximately 400°C.[89] For the better HMF glasses, however, ΔT is approximately 80-100°C.[90] This is a relatively narrow working range and specialized fabrication techniques are required to achieve highly uniform and crystal-free fibers.

On the other hand, an attractive property of these materials is their low intrinsic scatter losses. However, their tendency to form defects (bubbles, micro-crystallites and non-uniformities) has limited

their actual performance to date. Work by Poignant[91] predicted the scatter loss to be Rayleigh in character (λ^{-4} dependence) and equal to 2.7×10^{-3} dB/km at 4 μm. This value is approximately one-half the measured values for silicates. Measurements at 0.633 μm on ZBLA fibers resulted in values of 4.3 dB/km, as low as Suprasil 1 fibers, but still twice the theoretical values.[92] Recent work on carefully prepared bulk HMF glasses reported results for 13 of 15 samples within the predicted values for scatter loss, and the values were one-half those obtained for fused silica.[93] Thus, a key parameter in maintaining the intrinsic properties of HMF glass materials is temperature control in all processing techniques (fabrication, coating, etc.)

HMF glasses possess desirable optical properties, including a broad transmittance range from the mid-IR (~7 μm) to near-UV (~0.3 μm), low absorption and scatter losses, low dispersion and index of refraction, and low thermal distortion.[94] However, despite their promising optical characteristics, many compositions are relatively soft and hygroscopic. For example, it has been shown that the solubility of typical fluoro-zirconates is many orders of magnitude greater than that of high silicates.[95] Also, measurements of fiber strength reveal that while initial strengths are high, HMF optical fibers degrade rapidly when exposed to humidity, and that protective Teflon coatings do not serve as effective barriers against moisture attack. This susceptibility to attack by moisture indicates that hermetic coatings are required to protect HMF glasses. Moreover, because HMF glasses are chemically sensitive, an additional requirement is that coatings must be applied in a non-damaging way. Compounding the problems above, fluoride glass materials have low softening temperatures, typically ~200°C. This

precludes application of standard thin film deposition techniques which require a substrate temperature of 250-300°C. The elevated substrate temperature is required to produce thin films which are durable, non-porous and have good substrate adhesion; otherwise, the film does not provide a good hermetic coating.

The purpose of this study was to investigate the use of IAD to deposit protective and anti-reflection (AR) coatings on HMF glass substrates in order to obtain good quality coatings at reduced temperatures. Other techniques for depositing thin film coatings onto substrates at reduced temperatures have been reported.[70,96,97] However, these techniques, based on bombardment of the growing film with energetic particles, have inherent disadvantages in that it is not possible to independently control nor accurately measure the important experimental parameters involved. Using IAD, the effects of ion energy and current density on coating properties can be independently examined and optimized. The results reported are preliminary, as only a limited number of samples and conditions were investigated. The coating materials selected for this investigation were MgF_2, SiO_2 and Al_2O_3. Single-layer coatings of MgF_2 and SiO_2 were deposited onto substrates of HfF_4-BaF_2-LaF_3-AlF_3 (HBLA) glass, and an Al_2O_3/SiO_2 AR coating was deposited onto a substrate of ZrF_4-BaF_2-LaF_3-AlF_3 (ZBLA) glass. Tests were performed to determine film and substrate environmental durability, abrasion-resistance and adhesion. The optical properties of the coatings were also characterized.

The MgF_2 film material was evaporated at 0.3 nm sec^{-1} using a resistively heated boat, and the growing film was bombarded with 300 eV Ar ions at a current density of 5 μA cm^{-2} during deposition. The

temperature was approximately 100°C, due to heating from the boat. The SiO_2 and Al_2O_3 film materials were electron-beam evaporated at rates of 0.3 nm sec^{-1} with oxygen backfill pressure of 1.0×10^{-4} Torr. The growing films were bombarded with 300 eV O_2 ions at a current density of 30 μA cm^{-2} during deposition. The substrate temperature was approximately 150°C.

IV.1 Environmental Stability

An HBLA glass sample was coated with 0.5 μm IAD MgF_2 film, and another sample was left uncoated. A drop of water was placed on each sample for approximately 16 hours. The samples were then examined using a Nomarski microscope. The two micrographs are shown in Figure IV-1. The results for the uncoated sample illustrate the known susceptibility to aqueous corrosion of an unprotected fluoride glass surface. The result for the coated sample shows that it did not suffer any noticeable degradation, and indicates that an IAD MgF_2 coating might serve as an effective barrier against moisture penetration. Figure IV-2 is a micrograph of an HBLA glass sample coated with 0.5 μm IAD SiO_2 and subjected to a water drop test. There is no observable difference in the film exposed to the water drop relative to the portion not exposed. A ZBLA glass sample coated with a two-layer Al_2O_3/SiO_2 AR coating was also examined. The sample was exposed to a water drop test as described above. Again, there is no noticeable degradation in the film exposed to the water drop; it appears exactly as the portion not exposed.

Humidity cycle tests were also conducted to examine film stability properties. Films were exposed to 97% humidity at 35°C for six hours after removal from the coating chamber. Spectral shifts in film trans-

a
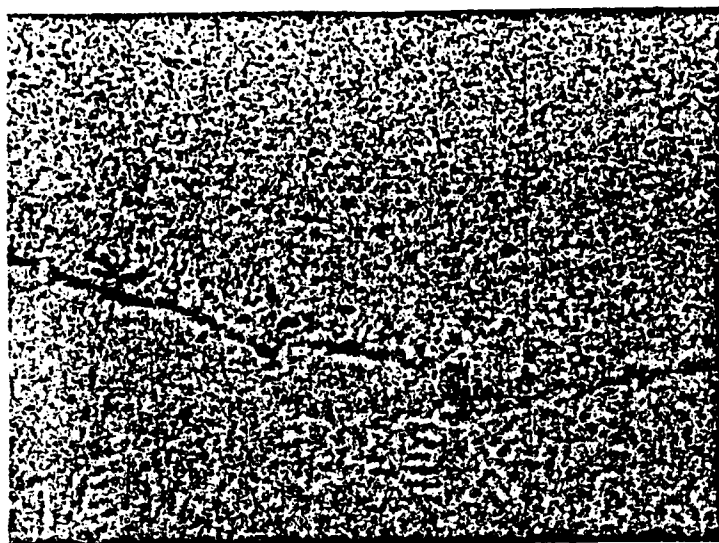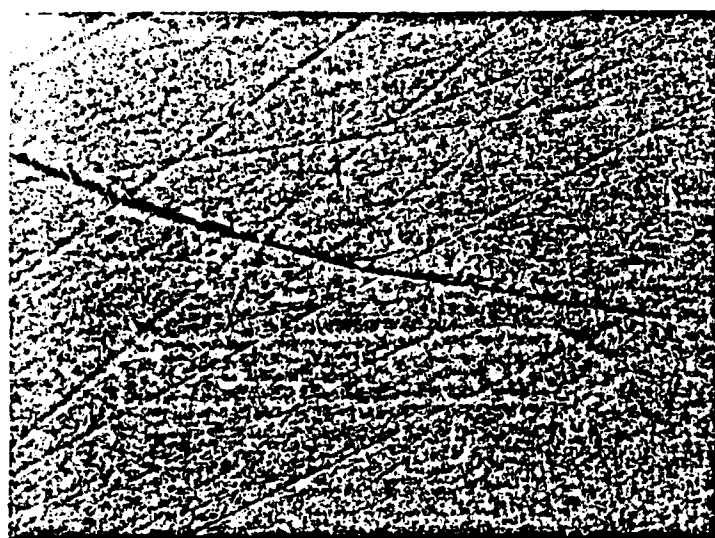
10 μm

b

Figure IV-1. Micrograph of a) an uncoated HBLA glass sample, and b) HBLA sample coated with 0.5 μm IAD MgF_2 coating after water drop test.
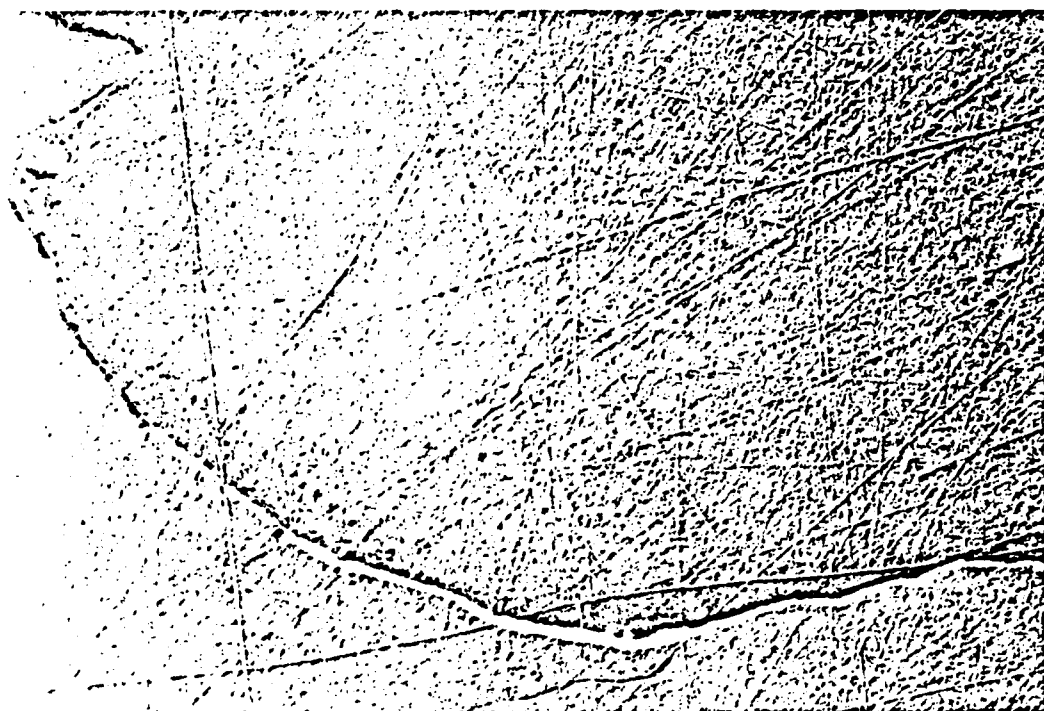
10 μm

Figure IV-2. Micrograph of a HBLA sample coated with 0.5 μm IAD SiO$_2$ after water drop test.

mittance curves were observed for films deposited without IAD, indicating that the films adsorbed water. However, for all IAD films examined, no spectral shifts were observed in the spectrophotometer traces (see Figure III-8). These results, as well as previous observations of reduced optical scatter and increased refractive index,[33,37,38] are consistent with IAD films having increased packing density and being less susceptible to water adsorption. Thus, overcoating a fluoride glass with an IAD coating may offer adequate protection from moisture attack and allow the use of HMF glasses in adverse environments.

IV.2 Abrasion Resistance

The effect of a coating on the abrasion resistance of HMF glass substrates was investigated. Samples were subjected to an eraser-rub test and examined using a Nomarski microscope. A sample was divided into two sections; one section was coated with 0.5 μm IAD MgF_2, and the other section was left uncoated. The sample was then subjected to a 10-stroke eraser rub test. Figure IV-3 is a micrograph of the uncoated HBLA glass section and the IAD coated section. The figure shows that the unprotected HMF glass was soft and subject to abrasion, while the IAD coated section was hard and much less subject to abrasion. The abrasion resistance for two MgF_2 coatings on glass substrates was investigated. It is well established that MgF_2 films deposited onto unheated substrates are soft; substrate temperatures of ~250°C are required to produce durable films. One sample was coated with 0.5 μm IAD MgF_2, and the other was coated with 0.5 μm MgF_2 deposited without Ar ion bombardment. The samples were then subjected to a 10-stroke eraser rub test. Results are shown in figure IV-4. The unbombarded (J=0) sample was
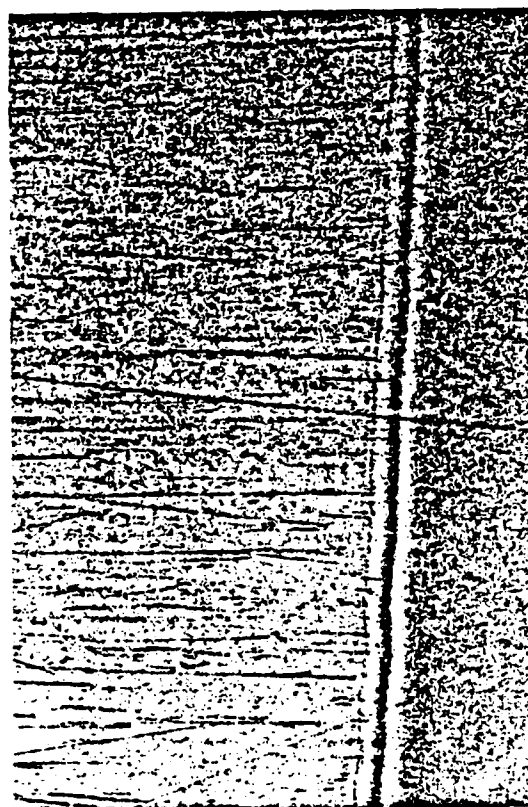
10 μm

Figure IV-3. Micrograph of a HBLA sample after eraser rub test. The left side of the figure is the uncoated section; the right side is the section coated with 0.5 μm IAD MgF$_2$.

a

b
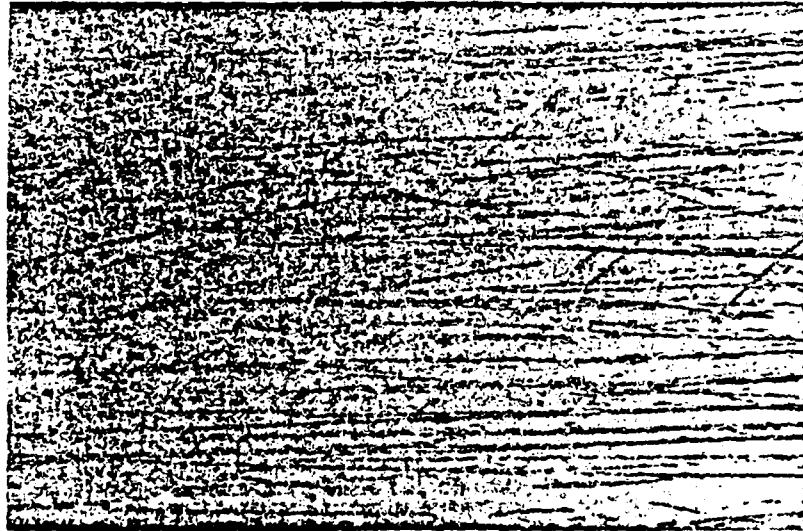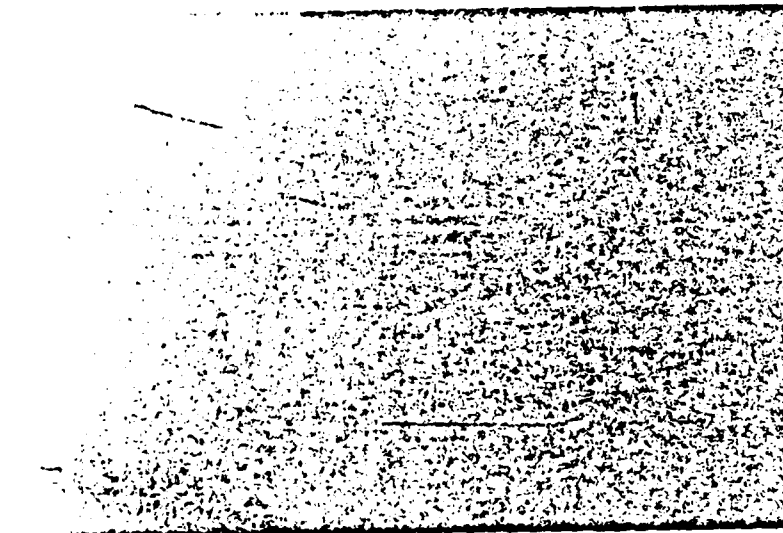
10 µm

Figure IV-4. Micrograph of two MgF$_2$ coatings after eraser rub test.
a) Sample coated with 0.5 µm MgF$_2$ deposited with no ion bombardment,
and b) sample coated with 0.5 µm IAD MgF$_2$.

scratched, whereas the bombarded sample was much less scratched. This illustrates that the IAD coated sample was more durable than the sample coated without bombardment. Another HMF sample was divided into two sections. One section was coated with 0.5 μm IAD SiO_2, and the other section was left uncoated. Results similar to those obtained for the IAD MgF_2 coated samples were obtained. The coated section was much less scratched than the uncoated section. Although the abrasion resistance test used was qualitative in nature, it appears that harder films may be obtained using IAD. These results indicate that overcoating a fluoride glass with an IAD coating can enhance the durability of HMF glasses.

IV.3 Film Adhesion

All samples were subjected to a tape-pull test to examine the effect of IAD on film adhesion. Coatings deposited without IAD had poor adhesion to the glass substrates. None of the samples coated with ion bombardment during deposition experienced delamination.

IV.4 Optical Properties

Transmittance and reflectance spectra for all samples were obtained using a dual-beam spectrophotometer. One important parameter that can be qualitatively characterized from spectrophotometric measurements is film stoichiometry. Poor film stoichiometry leads to a higher UV cutoff wavelength in transmittance. The transmittance spectra of the coated and uncoated HMF glass samples were examined, and in no case was the UV cutoff wavelength higher for an IAD coated sample relative to the uncoated substrate. This indicates that ion bombardment at these conditions is not detrimental to film stoichiometry for low temperature

coating. Another film property that can be obtained from spectrophoto-metric measurements is index inhomogeneity. The presence of an inhomo-geneity can be deduced from the transmittance and reflectance data at wavelengths for which the film is multiple half-wave in optical thick-ness. Index inhomogeneity can often occur in low temperature coatings. *No detectable index inhomogeneity was present in any low temperature IAD* coating deposited on HMF substrates in this study. The transmittance spectra for an uncoated ZBLA glass substrate and a two-layer Al_2O_3/SiO_2 AR coating are shown in Figure IV-5. Note that the spectrum for the AR coating touches that of the uncoated glass at approximately 500 nm, and that the optical characteristics are good above 400 nm; below 400 nm the coating becomes absorbing.

In summary, IAD techniques have been successfully applied to deposit MgF_2, SiO_2 and Al_2O_3/SiO_2 thin film structures on HMF glass surfaces at *low substrate temperatures (100-150°C). The coatings deposited using* IAD were hard, dense and improved the durability of the fluoride glass. Environmental stability and corrosion resistance of the optical surfaces were significantly improved; abrasion resistance was improved; excell-ent film adhesion was obtained; film optical properties were good and shown to be compatible with the HMF glass material. The demonstrated properties enhance the prospects for the use of HMF glass materials in a variety of applications. Optimization of the coating process should enable further improvements in fluoride glass durability for use in harsh environments.
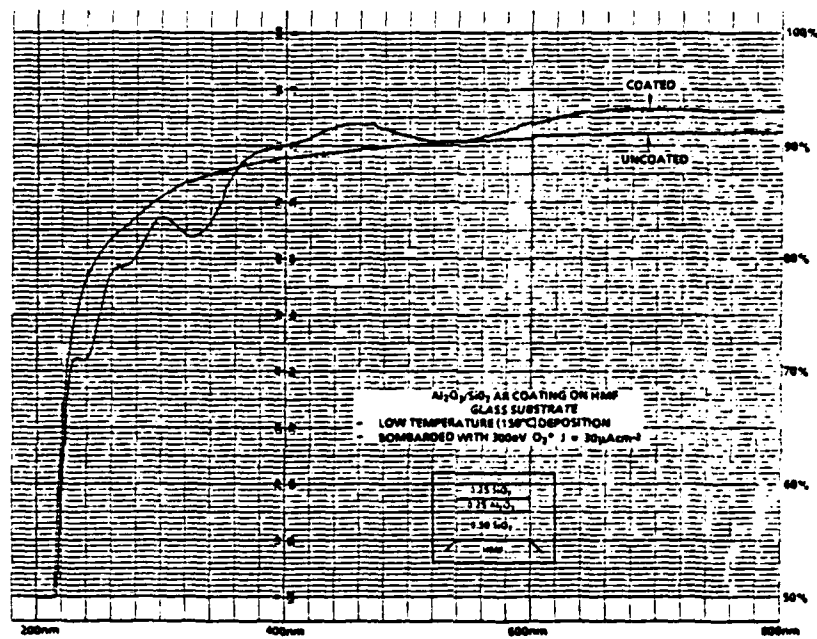
Figure IV-5. Transmittance spectra for a two-layer Al_2O_3/SiO_2 AR coating deposited on ZBLA sample.

CHAPTER V

MULTI-LAYER COATING RESULTS

Many studies have been conducted to investigate the sources of
damage in optical coatings, and, using empirical techniques, to improve
their damage thresholds.[77,98-100] This parametric study was an initial
attempt to compare electron-beam deposited coatings to ion assisted
electron-beam deposited coatings. The parameters which were varied were
oxygen-ion energy and current density. The effects of different filament
materials in the ion source on laser-induced damage threshold (LIDT)
values were studied. A number of Al_2O_3/SiO_2 and Ta_2O_5/SiO_2 anti-
reflection (AR) coatings were laser damage tested at Los Alamos National
Laboratory (LANL). The multi-pulse laser damage tests were conducted at
351 nm with a pulse repetition frequency of 35 pps. The results and
conclusions from this laser damage study of IAD coatings must be viewed
with caution due to the limited number of samples examined.

V.1 Laser Damage Facility

The LANL laser damage test facility is illustrated in Figure V-1.[101]
The laser beam was relayed from the laser room (not shown in the figure)
and was reflected twice at small angles before being focused in the test
plane. A small fraction of the laser intensity was transmitted through
the turning mirrors to power a photodiode array and a vacuum photodiode
for spatial and temporal profiling, respectively. The spatial beam
profile was measured with a silicon-photodiode array having a 25 μm
element spacing. Measurements were made ir both the vertical and
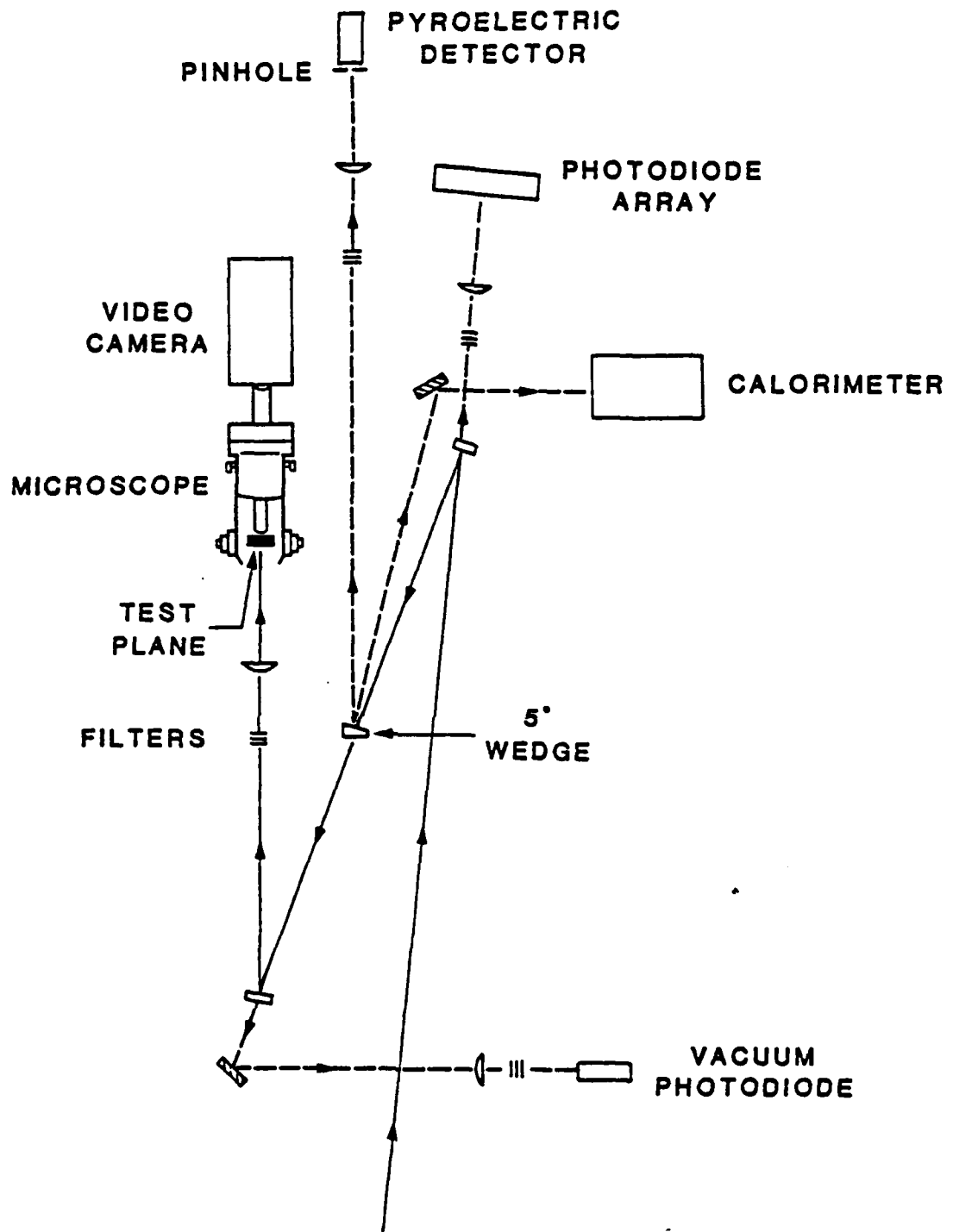
Figure V-1. Schematic of laser damage test facility.

horizontal axes of the test plane. Figures V-2a and -2b illustrate the horizontal and vertical spatial profiles.[102] The e^{-2} beam diameters were measured in the test plane to be 0.99 and 0.21 mm, respectively. The temporal beam profile, illustrated in Figure V-2c, was measured with a fast vacuum photodiode and a storage oscilloscope. The full-width half-maximum (FWHM) pulse width was 9 nsec. A 5^0 uncoated Suprasil wedge directed a fraction of the laser intensity to a calorimeter and a pinhole/pyroelectric detector combination to monitor average power and peak fluences, respectively. The documented beam characteristics were measured in the test plane, and, in addition, the characterization equipment was used to monitor beam quality and peak laser fluence during testing. Damage was observed visually in real time with a 60X stereo zoom microscope. A high resolution video system can be attached to the microscope to record images of damage onset and growth. At high laser fluence values (>> damage threshold values) a "burn pattern" replicating the beam shape can be produced in the coating. A micrograph of a "burn pattern" for an Al_2O_3/SiO_2 AR coating observed with a Nomarski microscope is illustrated in Figure V-3.

All of the damage testing was n-on-m, where m sites were irradiated at each laser fluence for a maximum of n pulses. Ten discrete sites were irradiated at each test fluence, and each site was exposed to the laser for 4 sec (140 pulses). Damage was defined as any visible change in the coating observed under 60X microscope examination (microscopic damage). Figure V-4 depicts a test area for an Al_2O_3/SiO_2 AR coating irradiated at a laser fluence of 7 J cm^{-2}. The coating was bombarded during deposition with 300 eV O_2^+ at a current density of 10 μA cm^{-2}. As illustrated in the micrograph a dense collection of damage pits formed (~2-4 μm in size)
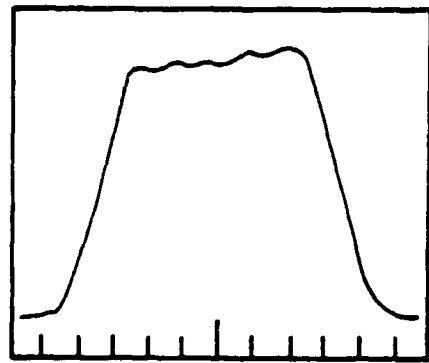
HORIZONTAL PROFILE
e^{-2} diameter = 0.99mm

(a)
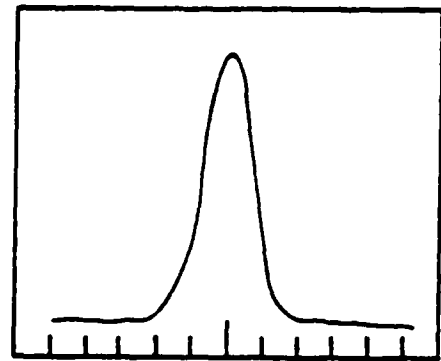
VERTICAL PROFILE
e^{-2} diameter = 0.21mm

(b)
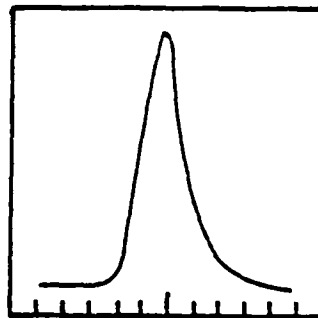
TEMPORAL PROFILE
FWHM = 9 nsec

(c)

Figure V-2. Horizontal and vertical spatial profiles, and the temporal profile of the laser beam.
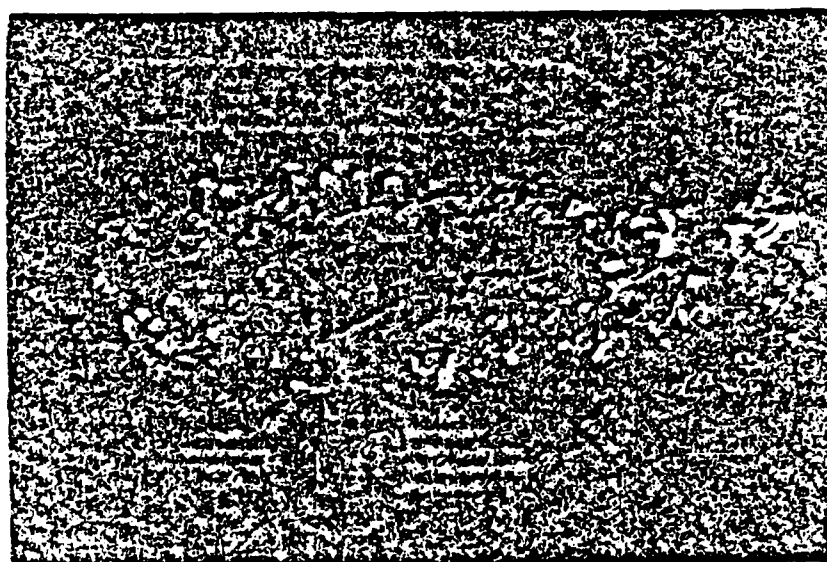
10 µm

Figure V-3. Micrograph of a "burn pattern" in an Al_2O_3/SiO_2 AR coating.
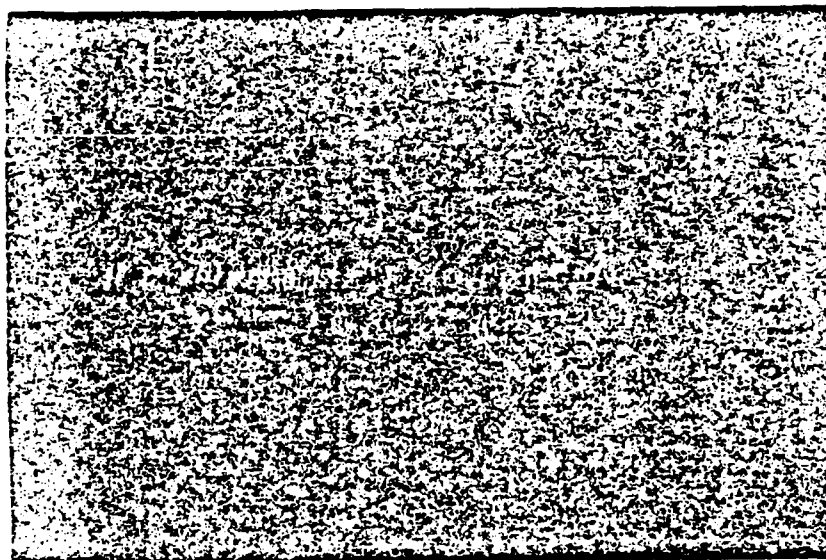
10 µm

Figure V-4. Micrograph of an Al_2O_3/SiO_2 AR coating irradiated at a laser fluence of 7 J cm^{-2}.

but no growth occurred with continued irradiation. The scientists at
LANL reported that for most of the coatings in this study damage occurred
in the first few laser pulses and didn't grow with continued irradiation.
The coatings were tested at several fluence levels between the value at
which 0 of 10 sites damaged and the value at which 10 of 10 sites
damaged. The fraction of damage sites was plotted as a function of laser
fluence, in units of Joules cm^{-2}. Figure V-5 illustrates a sample damage
probability curve for an Al_2O_3/SiO_2 AR coating. The open circles
represent the fraction of ten test sites which damaged at a particular
test fluence. A linear regression fit was performed on the data result-
ing in a sloped, fitted line from a fluence at which all ten sites
damaged to a lower fluence at which no damage occurred. The LIDT value
was defined as the zero-percent crossing of the fitted line (zero-
probability intercept). Note that the conventional definition of LIDT
value is the average value of the minimum fluence that always causes
damage and the maximum fluence at which no damage occurs.

The damage probability curves contain more information than just the
LIDT value. Foltyn has developed a simple model which correlates the
slope of damage probability curves with defect density and laser beam
spot size.[103] The model predicts steep slopes if the laser beam is large
compared to the mean defect spacing in a coating. This implies that if
the beam is smaller than the defect spacing, then a large amount of data
spread would be present in the damage probability curves. He suggested
that the zero-probability intercept value was independent of spot size.
Thus, damage probability curves with steep slopes indicate coatings with
a dense population of defects. The LIDT values of various thin film
coatings were measured as a function of laser beam spot size by Stewart
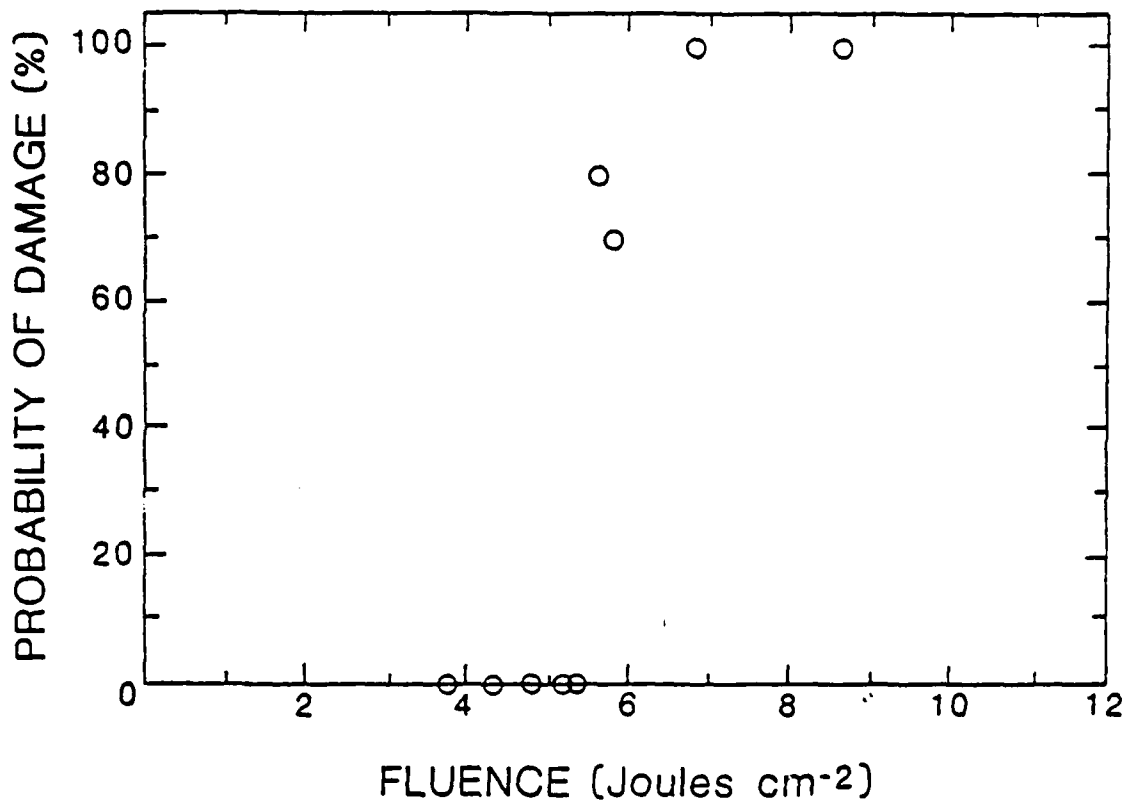
Figure V-5. Damage probability plot for an Al_2O_3/SiO_2 AR coating.

and Guenther.[104] The laser beam diameter (e^{-1}) used in the study varied from 9 to 300 μm. The measured LIDT values increased as the beam diameter decreased indicating that a smaller number of defects were irradiated with each laser pulse. Also, the data spread increased as the spot size decreased. This suggested that the damage process was defect or impurity dominated because the probability of missing a defect increased with decreasing spot size.

The AR coatings in this study were deposited onto Corning 7940 fused silica substrates with bare surface LIDT values ~8 J cm^{-2}.[102] The coating design was SLLHL where S was the substrate, L was quarter-wave thick SiO_2 and H was quarter-wave thick Al_2O_3 or Ta_2O_5. The substrates were cleaned as described in Section II-3. The substrates were subjected to a 2 hour vacuum bake-out ($325°C$) and Ar^+ cleaning before coating. The base pressure in the vacuum system before coating was ~3 x 10^{-8} Torr.

V.2 Al_2O_3/SiO_2 Laser Damage Results

The zero-probability LIDT values for Al_2O_3/SiO_2 coatings bombarded with 300 and 500 eV oxygen ions are plotted versus O_2^+ current density in Figure V-6. Tantalum (Ta) filaments were used in the ion source for all the results in Figure V-6. The values plotted are the average LIDT values for coatings deposited under the same conditions. The error bars represent the range of LIDT values obtained for all the coatings deposited under the same conditions. With one exception, it appears that the IAD coatings did not have higher LIDT values than the coatings deposited with no ion bombardment (J=0). The coatings bombarded with 300 eV O_2^+ at a current density of 10 μA cm^{-2} had an average LIDT value of 6.1 J cm^{-2} with a ±7% variation for the two coatings tested. This represents a 65%
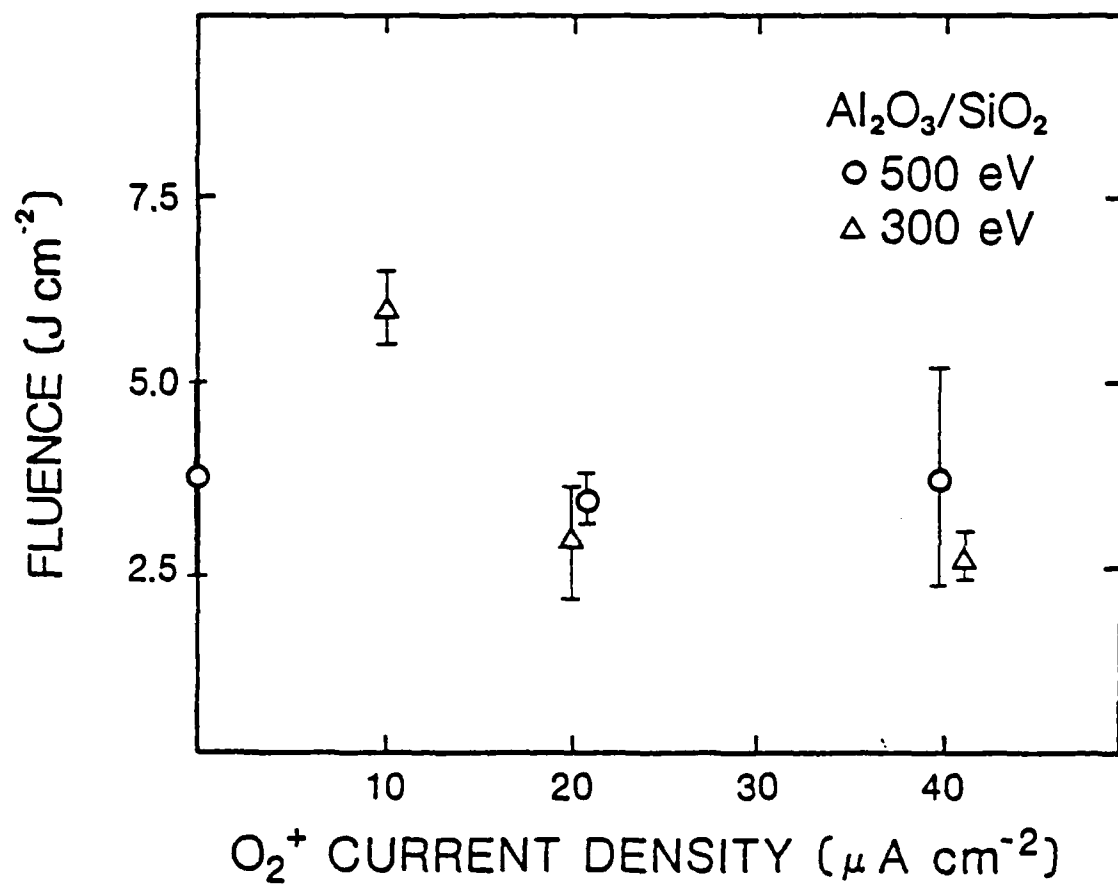
Figure V-6. Laser-induced damage threshold values for Al₂O₃/SiO₂ AR coatings vs O₂⁺ current density.

increase in LIDT value over the J=0 coatings. However, these were the only IAD coatings that exhibited an increase in LIDT value. Further testing of coatings deposited at this condition is required before any definite conclusions can be made.

Figure V-7 illustrates the effects of different cathode filament materials in the ion source on LIDT values. A contamination analysis of IAD TiO_2 coatings indicated that tungsten (W) filament material was incorporated into the coatings.[41] The quantity of W present in the TiO_2 coatings increased as the ion current density increased. The amount of W ranged from 130 to 510 ppm. As part of this study a number of IAD Al_2O_3/SiO_2 AR coatings were deposited using W filaments in the ion source ("W coatings"). Another set of coatings were deposited using identical IAD conditions except Ta filaments were used in the ion source ("Ta coatings"). The purpose of this comparison was to attempt to control one defect in IAD coatings and to measure LIDT values for coatings in which different filament materials were used.

As observed in the figure the "Ta coatings" had LIDT values consistently higher than the "W coatings". The largest difference is for the higher energy (500 eV), higher current density (40 μA cm^{-2}) case. The average value of the increase in LIDT for the "Ta coatings" was 40%. This exceeded the run-to-run variations in LIDT values which was ±25%. The analysis for run-to-run variations is presented in the following paragraph. The results appear to indicate an improvement in LIDT value for "Ta coatings" over "W coatings".

The laser damage results were analyzed for both sample-to-sample variations and run-to-run variations in LIDT values. Sample-to-sample variations were calculated for three sets of two coatings each deposited
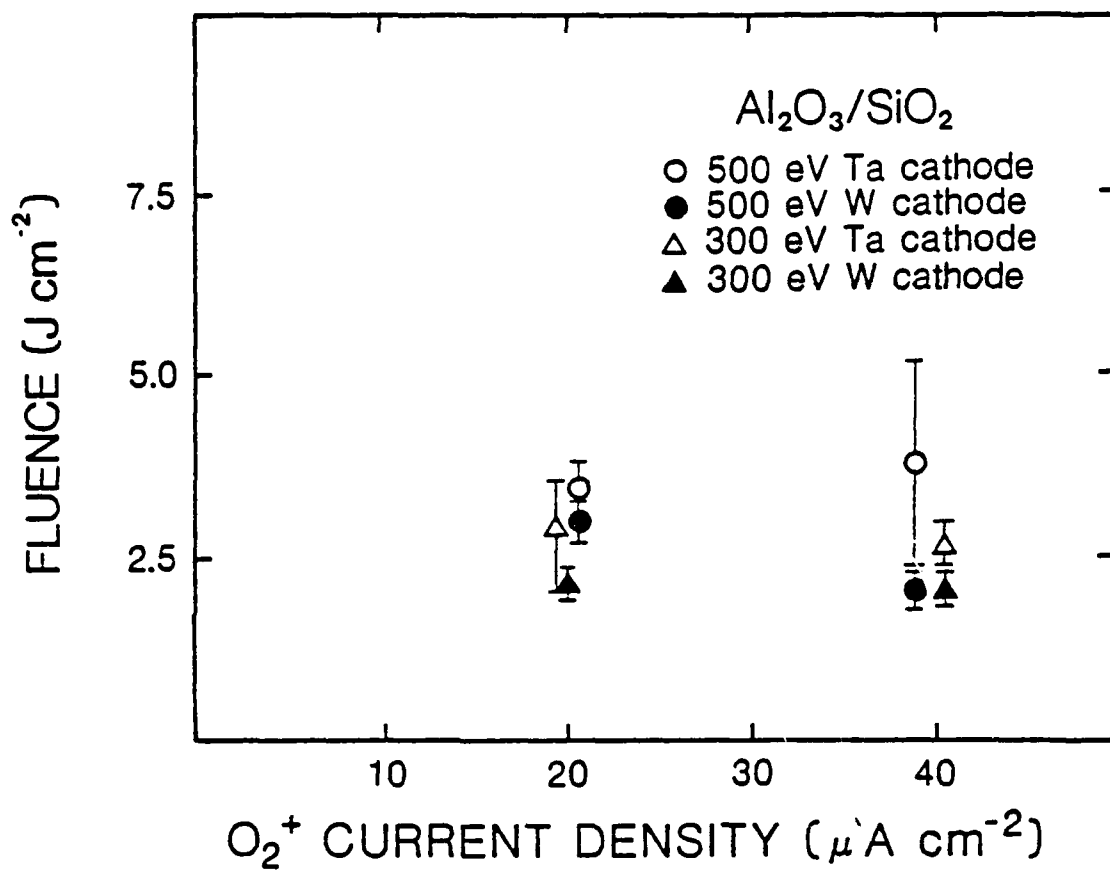
Figure V-7. Laser-induced threshold values for Al_2O_3/SiO_2 AR coatings deposited using tungsten or tantalum filaments in the ion source vs O_2^+ current density.

at the same time. Run-to-run variations were calculated for three sets of two coatings each deposited using identical IAD conditions but at different times. The coatings used to calculate sample-to-sample variations were bombarded during depositicn with 300 eV O_2^+ at current densities of 10, 20 and 40 μA cm^{-2}, respectively. The average value of the sample-to-sample variations was $\pm 14\%$. The coatings used to calculate run-to-run variations were a set of J=0 coatings and coatings bombarded during deposition with 300 and 500 eV O_2^+ at current densities of 20 and 40 μA cm^{-2}, respectively. The average value of the run-to-run variations was $\pm 25\%$. Foltyn et.al.[105] reported sample-to-sample variations of $\pm 10-20\%$ and run-to-run variations of $\pm 20-50\%$ for other coatings tested at LANL. They also reported that for damage thresholds measured several times for the same coating, the results agreed to within $\pm 5\%$.

V.3 Ta$_2$O$_5$/SiO$_2$ Laser Damage Results

The zero-probability intercept fluence values for Ta$_2$O$_5$/SiO$_2$ AR coatings bombarded with 300 and 500 eV O_2^+ are plotted versus O_2^+ current density in Figure V-8. Only a limited number of coatings (9) were tested which precluded examining laser damage for wide variations in the parameter set. This also limited the number of coatings that could be tested which were deposited with similar IAD conditions but in different runs. For the conditions examined, it appears that the IAD coatings did not have higher LIDT values than the coatings deposited with no ion bombardment (J=0). The LIDT values for coatings bombarded during deposition with 500 and 300 eV O_2^+ at current densities of 40 and 60 μA cm^{-2}, respectively, were ~32% lower than the J=0 coatings. This decrease in LIDT values is consistent with the increase in optical
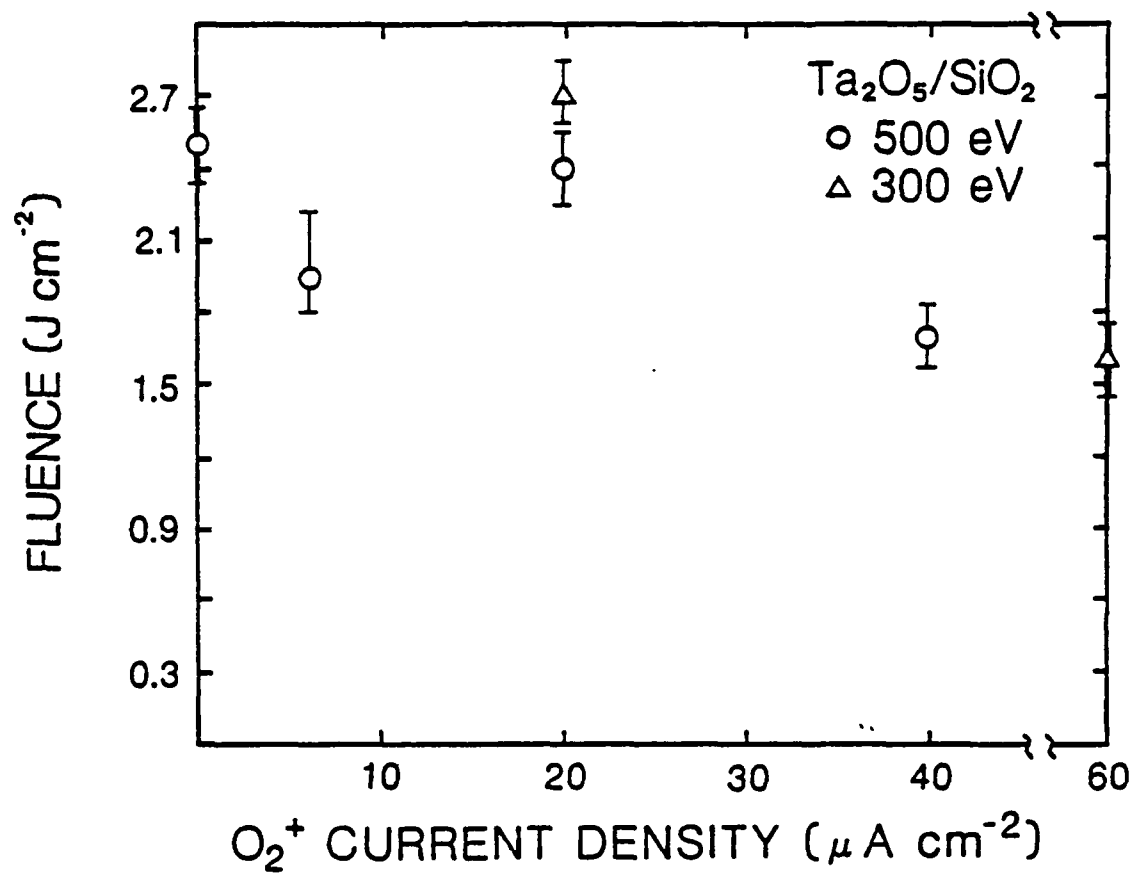
Figure V-8. Laser-induced damage threshold values for Ta_2O_5/SiO_2 AR coatings vs O_2^+ current density.

absorption for single-layer Ta_2O_5 coatings deposited using identical IAD conditions (Figure III-3).

Run-to-run variations were calculated for three sets of two coatings each deposited using identical IAD conditions but at different times. The coatings used to calculate run-to-run variations were bombarded during deposition with 300, 500 and 500 eV O_2^+ at current densities of 20, 6 and 40 μA cm^{-2}, respectively. The average value of the run-to-run variations was $\pm 7\%$.

It appears for the Ta_2O_5/SiO_2 AR coatings examined in this study that ion assisted deposition does not improve their laser damage resistance at 351 nm. However, the results for single-layer Ta_2O_5 coatings obtained in this study indicated that IAD produced coatings with increased values of refractive index and improved environmental stability. Further exploration of the mechanisms for laser damage in IAD Ta_2O_5 coatings is warranted.

V.4 Al_2O_3/SiO_2 Fluorine Test Results

Three Al_2O_3/SiO_2 coatings were exposed to fluorine gas tests at LANL. The coatings were exposed to a 0.5% dry F_2 in He gas mixture. The optical transmittance of the coatings at 351 nm was measured at various time intervals. Figure V-9 illustrates the results of the F_2 testing. The coating deposited with no ion bombardment (J=0) exhibited ~20% loss in transmittance after only 47 hours exposure to F_2. The coatings bombarded during deposition with 500 eV O_2^+ at current densities of 40 and 80 μA cm^{-2} exhibited 6% and 3% loss in transmittance, respectively. The tests were terminated after only 47 hours because the decrease in optical transmittance occurred very rapidly. The fluorine resistance of
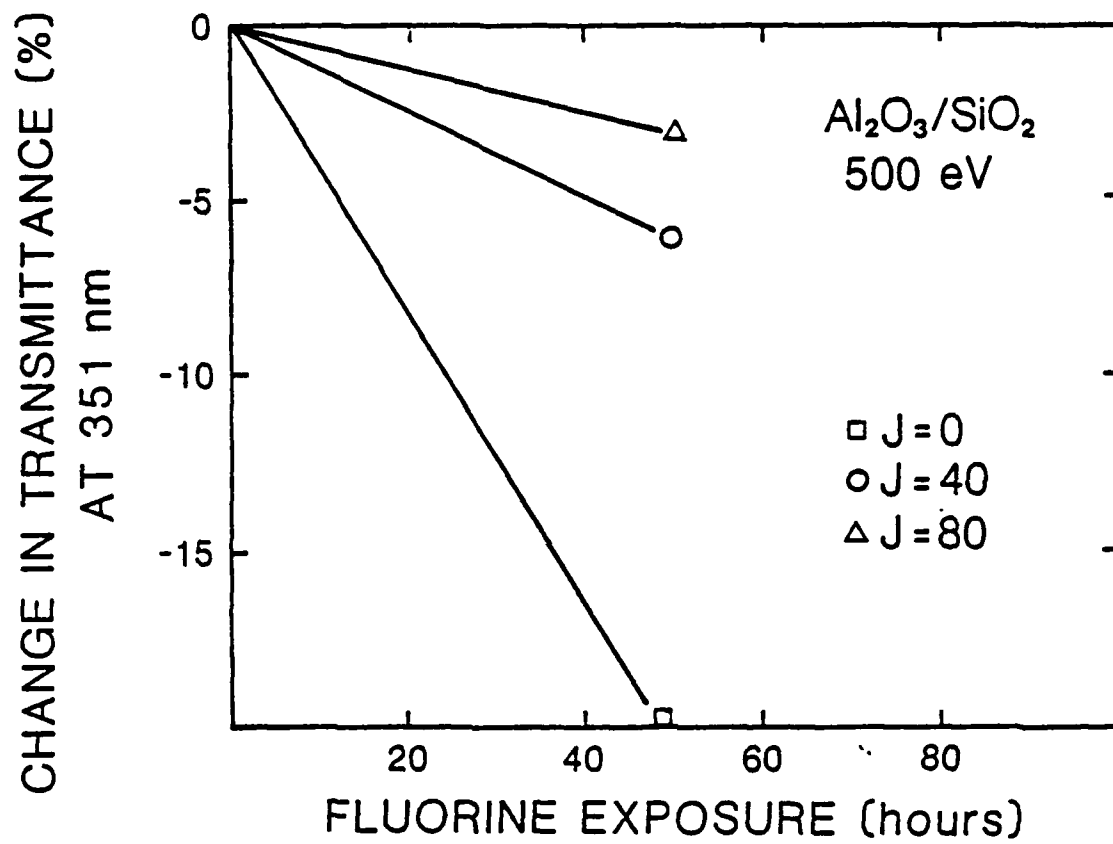
Figure V-9. Decrease in transmittance at 351 nm for Al_2O_3/SiO_2 AR coatings vs fluorine gas exposure time.

these coatings was extremely poor relative to required performance criteria. Further discussion relative to the combined results of other IAD coatings (Ta_2O_5, Al_2O_3 and SiO_2) is given in Chapter VI.

CHAPTER VI

DISCUSSION

VI.1 Ion Interactions

As discussed in Chapter I, the properties of thin film coatings are
very dependent on microstructure. The differences in the properties of
materials in thin film form from those of the bulk material result from
the columnar microstructure of thin films. Ion bombardment has been
shown to play an important role in controlling the properties of coatings
deposited by reactive rf diode sputtering,[12,72] reactive dc diode
sputtering,[53] ion beam sputtering,[15,106] plasma-assisted chemical vapor
deposition[16,82] and ion assisted deposition(IAD).[22,29,33,37] The
discussion in this chapter is limited to the effects observed in IAD
coatings for which the ion energy and current density were independently
controllable and accurately measurable. Increases in the value of
refractive index, stability to humidity exposure and decreases in optical
scatter relative to unbombarded coatings were observed for the IAD
coatings in this study. These results are discussed in terms of ion-
surface interactions.

When a low energy ion (<1 keV) is incident on a film, it penetrates
the surface with a range up to a few nanometers, depending on the film
density and atomic weight and the ion and film atomic masses. Harper
et.al.[107] suggested an equation to calculate the depth of penetration (d)
for low energy ions (0.2 to 1 keV). They formulated the equation by
extrapolation of data from Aspnes and Studna.[108] The equation is

$$d(\text{Å})=1.1W_t E^{2/3}/2\rho_t(Z_i^{1/4}+Z_t^{1/4})^2, \qquad (VI-1)$$

where W_t and ρ_t are the atomic weight and density of the target material, Z_i and Z_t are the atomic number of the incident ion and target material, and E is the ion energy. For a compound target the mean atomic number of the elements is used. Table VI-1 lists the values of d for a number of materials and various ion energies. As the ion penetrates through the material it loses energy by transfer to atoms via knock-on collisions and electronic excitations.[109] A collisional casacade occurs in which the knock-on atoms collide with other film atoms. When the incident ion and the knock-on atoms come to rest, a substantial part of their energy is transferred to lattice vibrations of neighboring atoms in the film.

A number of researchers have reported details of low energy ion-surface interactions that result from ion bombardment of a growing film. Marinov reported enhanced adatom migration due to binary collisions between incident ions and silver (Ag) adatoms. The collisions produced momentum changes in the Ag adatoms parallel to the substrate surface.[20] Eltoukhy and Greene reported enhanced bulk and surface diffusion coefficients as a function of ion bombardment conditions.[23] Carter and Armour discussed the displacement of surface atoms and the creation of lattice defects as well as desorption of physisorbed atoms due to low-energy ion bombardment.[110] In a critical review of the effects of low-energy particle bombardment of growing films,[25] Greene and Barnett identified enhanced adatom surface mobility, sputtering and preferential sputtering as the major ion-surface interactions during film growth. They used these effects to interpret experimental results obtained for a number of semiconductor materials (GaAs, InSb and GaSb). They reported enhanced reaction rates due to the activation energies supplied by the incident

Table VI-1

Depth of Penetration (d) for Oxygen Ions ($Z_i=8$)

	Ta_2O_5	Al_2O_3	HfO_2	SiO_2	ZrO_2
W_t	442	102	210	60	123
P_t	8.2	3.9	9.7	2.6	5.6
Z_t	40.5	10.5	40	11	24
d(Å) for E_0=200 eV	57	40	23	35	54
E_0=250 eV	65	47	27	41	63
E_0=300 eV	74	53	30	46	71
E_0=500 eV	105	75	43	65	100

ions. Takagi reviewed the energy ranges over which ion-surface effects would occur.[111] McNeil et.al. reported reduction in optical scatter for magnetron and ion beam sputtered coatings.[44] They related increased adatom mobility to reductions in surface microroughness.

The identification of enhanced adatom surface mobility as a primary result of low-energy ion bombardment is useful for thin film growth modeling. Macleod has improved standard two-dimensional thin film growth models by including a relaxation parameter.[6] This parameter is essentially the adatom diffusion distance normalized to the atomic diameter. By increasing the value of the relaxation parameter, simulated packing density increases. The model illustrates the basic relation between adatom surface mobility and the evolution of film microstructure. Messier et.al. reported apparent bombardment-induced increases in surface diffusion lengths of 1 to 10 nm.[7] In another report, they identified the redistribution of adatoms through downward sputtering as a primary effect of particle bombardment of a growing film.[112] This effect drastically altered the adatom distribution function in their model. However, for low-energy ion collisions with a growing film, models to simulate experimental results are still lacking.

VI.2 Thermal Spike Model

One model which has been studied to simulate ion bombardment effects is the thermal-spike model. This model attempts to relate film microstructure changes in IAD coatings to thermally-activated adatom diffusion induced by expanding thermal spikes. The mechanism for the thermal spike is as follows.[113] An incident ion penetrates the film surface, creates a collisional cascade and transfers a substantial part of its energy to

vibrational excitations in the film. This results in a sudden delivery of heat to a restricted volume of material--thus the term thermal spike. The material in the spike behaves initially like a hot gas extending over a volume which contains up to 100 atoms for low-energy (100 eV) ion bombardment. As the spike spreads, the temperature decreases, and it influences a larger number of atoms. Its effect may be approximated as atoms hopping between lattice sites, i.e. thermally-activated atomic diffusion.

Hirsch and Varga have applied the theory of bombardment-induced thermal spikes to their results for Ar^+ bombardment of germanium (Ge) films.[66] They deposited 2 μm thick Ge films while simultaneously bombarding them with Ar^+ at various current densities and energies between 65 to 3000 eV. The properties they measured were film stress and argon content in the films. They defined the critical ion current density value (J_c) as the minimum value of J_c for which no film cracking occurred. Fracture lines were present in ~1 μm thick Ge films deposited without bombardment. They obtained the critical value for each of six ion energies over the range 65-3000 eV. They related the lack of film cracking to a stress "annealing" mechanism. They suggested that the "annealing" mechanism was a consequence of an atomic activated rearrangement process induced by thermal spikes. Using the development of Seitz and Koehler[113] they analyzed their results as follows.

The number of atoms (N) participating in an activated rearrangement process is given as

$$N = 0.016 p (E/E_0)^{5/3}, \qquad\qquad (VI-2)$$

where E is the energy deposited in the spike by the incident ion, and E_0 is the activation energy of the process. The coefficient p depends on material thermal diffusivity and the number of neighbors with which an atom can interact. The value of p ranges from 1-10 for most materials.[113] At an ion flux of Γ_c(ions cm^{-2} sec^{-1}), the number of film atoms involved in an activated rearrangement process is $N\Gamma_c$. They reported an empirically determined relation between the critical ion flux value (Γ_c) and ion energy (E) as[66]

$$\Gamma_c \approx 3.9 \times 10^{16} E^{-3/2}. \qquad \text{(VI-3)}$$

Substituting equation (VI-2) into (VI-3) yields

$$N\Gamma_c \approx 6.2 \times 10^{14} p E_0^{-5/3}(E^{5/3}/E^{3/2}). \qquad \text{(VI-4)}$$

The effect of replacing the empirically determined exponent (3/2) by the exponent determined from the thermal-spike model (5/3) is not significant (maximum difference over the energy range studied is approximately a factor of three at 3 keV). Thus equation (VI-4) can be rewritten as

$$N\Gamma_c \approx 6.2 \times 10^{14} p E_0^{-5/3} \approx \text{constant}. \qquad \text{(VI-5)}$$

This equation states that the critical current density varies with the ion energy such that the rate at which atoms can participate in rearrangements remains constant. For the deposition conditions employed by Hirsch and Varga, the flux of Ge atoms was ~9.7×10^{14} atoms cm^{-2} sec^{-1} (deposition rate of 0.22 nm sec^{-1}). They assumed this was the constant

term in equation (VI-5) and substitution yields

$$pE_0^{-5/3} \approx 1.6. \qquad \qquad (VI-6)$$

Assuming a value for p of 5, the value of E_0 is approximately 1.98 eV. This is close to both the self-diffusion activation energy for Ge and the activation energy for the diffusion of vacant lattice sites.[66] Thus they concluded that the "annealing" effect occurred at a current density value that ensured all the Ge adatoms were subjected to an activated rearrangement process in a thermal spike.

This analysis by Hirsch and Varga related ion bombardment conditions to stress relief in Ge coatings. No attempt was made to relate film densification to ion bombardment conditions. In fact until recently[114] no results from including thermal spike effects in thin film growth models have been reported.

A two-dimensional computer simulation of IAD film microstructure was reported recently by Muller.[114] The incident ions were assumed to create thermal spikes which activated atomic hopping at a high rate between lattice sites. The results showed that film columnar growth was modified due to enhanced adatom mobility. Closed microvoids were formed due to atomic "bridging" that occurred across long cavities between columns. However, the calculations indicated that densification due to ion bombardment was not obtained using the thermal spike model.

VI.3 Muller Model

Another model to simulate the dynamics of ion assisted film growth has been developed by Muller.[115] This model performs calculations by

employing a modified version of a Monte Carlo TRIM.SP (transport of ions in matter) program.[115] The simulation model explains quantitatively the experimental observed increase in film density for IAD coatings.[29,37] Its development is very recent, and collaboration has been initiated to model IAD effects on Ta_2O_5 and Al_2O_3 obtained in this study. At this time no results from this effort are available. The model has been applied to IAD ZrO_2 and CeO_2 coatings,[117,118] and the computational results have been compared to the experimental results.[29,30]

In the model it is necessary to consider the ion bombardment as occurring between the times of arrival of vapor atoms. The ion assisted film growth can be visualized as the deposition of an amount of vapor material ($\Gamma_v \Delta t$) which is subsequently modified by ion bombardment for a time Δt (Γ_v is the vapor flux (atoms cm^{-2} sec^{-1})). The deposition of additional vapor material follows, and an alternating sequence of ion bombardment and deposition continues.

The simulation model is described as follows.[118] The incident ions create a collisional cascade in a film producing knock-on atoms (Figure VI-1). The incident ions and knock-on atoms are followed throughout their travel until their energy falls below a predetermined energy. The ions cause surface depletion due to sputtering and inwardly recoiling film atoms. These create vacanies which are at or near the surface, while inwardly recoiled atoms become trapped below the surface in microvoids. The microvoids originate due to low-mobility vapor atoms (typical columnar film growth) and vacancies created from previous ion bombardment. The surface vacancies are partially refilled in the next sequence of arriving vapor material. The vapor material distribution of the deposited layer is chosen such that the resulting film density equals
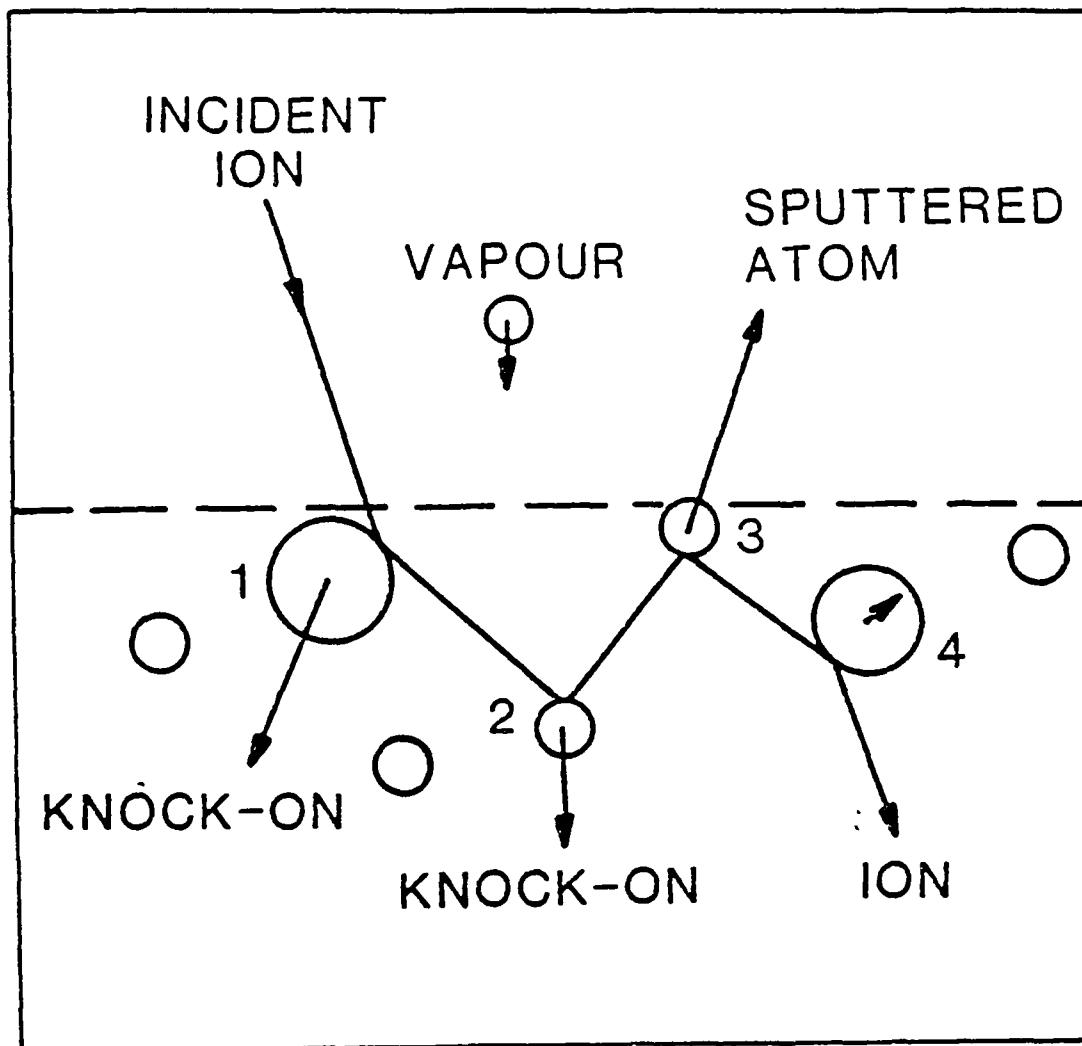
Figure VI-1. Simplified schematic of ion-film interactions.
(from reference 116)

that value which would be attained without ion bombardment. The arriving

vapor material refills the surface vacancies to a depth of ~2 monolayers

(refilling depth). This is reasonable considering low thermal adatom

surface mobility.

The calculations performed in the model require terms for the vapor

flux, ion flux, backscattered (or reflected) ion flux, sputtered atom

flux, number of vacancies created per incident ion and number of inwardly

recoiled atoms per incident ion. The calculations also require ion

incorporation probability distribution and matter transport distribution

functions. The output from the calculations is film density as a

function of film depth ($p(x)$) or the average film density. The former is

a very time intensive calculation. Ion incorporation and implantation of

recoiled surface atoms lead to a film densification slightly below the

surface of the growing film (Figure VI-2).

The model has been applied to calculate the time dependent density

distribution of ZrO_2 bombarded during deposition with 1200 eV O_2^+.[117]

The density distribution showed a slight surface depletion (~2 nm deep)

and an ~13% increase in density below the depletion region (see Figure

VI-2). Müller also calculated the average density as a function of ion

flux. The results matched the experimentally observed values[29] as the

ion current density increased to the critical value. The calculations

did not incorporate any mechanism to account for density saturation.

The model has been applied to calculate the average film density of

CeO_2 bombarded during deposition with O_2^+.[118] The density was calculated

as a function of both ion flux and energy. The computed values of

density increased as ion flux values increased matching the experimental

results[117] extremely well. The calculations of density as a function of
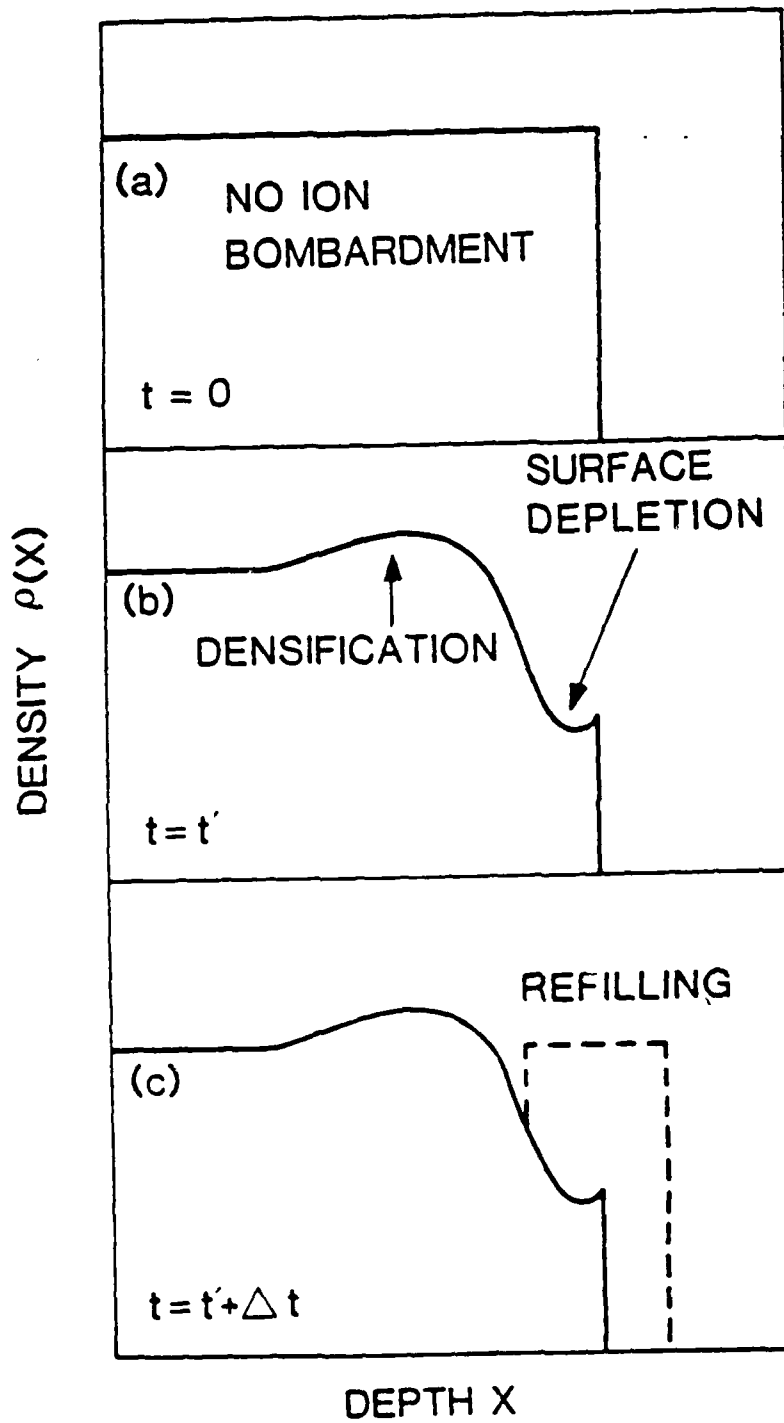
Figure VI-2. Calculated film density vs depth from Müeller's model
(from reference 116)

ion energy showed that the density reached a maximum value for an intermediate value of O_2^+ energy (~350 eV). At this energy the amount of material transported from the surface region deeper into the film reached an optimum value. The computed results match the experimental results extremely well except for the highest ion energy (1200 eV O_2^+) case. These results are similar to the experimental results obtained for Ta_2O_5 in this study. Recall that a larger value of refractive index was obtained for bombardment with 300 eV O_2^+ than with 500 eV O_2^+. The Ta_2O_5 results also indicate that only minor densification occurred for coatings bombarded with 200 eV O_2^+. The results from modeling CeO_2 showed that lower energy ions can drive very few atoms from the surface region deeper into the film causing only minor densification. Although CeO_2 and Ta_2O_5 have different material properties (bulk densities, unbombarded film densities, binding energies) the trends obtained experimentally and numerically for IAD CeO_2 coatings are comparable to those observed experimentally for IAD Ta_2O_5 coatings.

VI.4 Preferential Sputtering

The calculation of extinction coefficients for the Ta_2O_5 coatings indicated that bombardment at increasing values of O_2^+ current density resulted in larger values of k (Figure III-3). These results also indicated that bombardment with higher energy ions at a fixed current density resulted in larger values of k. The larger values of optical absorption in the coatings was attributed to preferential sputtering of oxygen in the Ta_2O_5 molecule. The term preferential sputtering is used to describe the phenomenon in which different atoms of a solid are not sputtered proportionally to their atomic concentration at the surface.[119]

The results for Al_2O_3 and SiO_2 did not exhibit the same increase in optical absorption due to ion bombardment as Ta_2O_5. The underlying mechanism(s) for the preferential loss of oxygen from a material is not well understood. However, the differences in behavior for IAD Ta_2O_5, Al_2O_3 and SiO_2 may offer some evidence to help explain preferential sputtering.

Structural and compositional changes have been frequently observed in oxide materials under ion bombardment.[120-127] An early study by Kim et.al.[120] utilized electron spectroscopy for chemical analysis (ESCA) to monitor alterations to metal-oxide surfaces following Ar^+ bombardment. They developed a model based on thermodynamics (values of standard free energy of formation) to explain preferential sputtering of oxygen. The model predicted and their measurements confirmed that Al_2O_3, SiO_2 and Ta_2O_5 were stable to ion bombardment. Subsequent studies utilizing RBS,[121] Auger electron spectroscopy (AES)[122,124] and ESCA[123,126] resulted in evidence which contradicted the model and results of Kim et.al. In a very thorough study, Holm and Storp[123] studied the effects of 1 and 5 keV Ar^+ bombardment on eight oxide materials (Mo, W, Nb, Ta, Ti, Zr, Si and Bi-oxides). They reported reduction in all the oxides studied, and concluded that the thermodynamic model can not be considered universally valid. Their results showed that the product of the ion energy times the ion current density which caused reduction of a specific amount was not a constant. They reported that to maintain the same reduction rate with 1 keV Ar^+ as with 5 keV Ar^+ required a current density ~7.5 times as large. This result was attributed mainly to the energy dependence of the penetration depth of the ions. Another study by Murti et.al. found that the amount of reduction increased as the value of ion current density

increased for 35 keV O_2^+ bombardment of Ta_2O_5.[60] Holloway and Nelson[126] investigated preferential sputtering of 100 nm thick Ta_2O_5 films bombarded with 0.5 and 5 keV Ar^+ at current densities up to 200 μA cm^{-2}. These results correlate with the IAD results illustrated in Figure III-3. In recent work, Thomas and Hofmann measured the compositional stability of SiO_2 to bombardment by He^+, Ne^+, Ar^+ and Xe^+ (0.5-2.0 keV).[127] They reported that for current densities greater than 250 μA cm^{-2} SiO_2 was reduced 5-10%. The amount of reduction was primarily dependent on the ion species and only mildly on ion energy. They also reported that the depth of the reduced region correlated with the calculated mean ion penetration depth.

Based on the results obtained in this study for IAD Ta_2O_5, Al_2O_3 and SiO_2, together with the results reported in these other studies, a number of simple mechanisms to explain preferential sputtering will be examined. The first criteria for compositional changes in oxide coatings are those based on thermodynamic considerations. One of these is a bond-type criteria which evaluates the response to ion bombardment on the basis of the ionicity equation of Pauling.[119] The equation has the form

$$i = 1 - \exp[-0.25(X_A - X_B)^2], \tag{VI-7}$$

where i is the ionicity of a compound (AB), with X_A and X_B equal to the electronegativities of atoms A and B, respectively.[128] Ionicity measures the degree of the ionic nature of a chemical bond, i.e., as $i \rightarrow 1$ the bonding strength of a compound increases. Calculations of i for Ta_2O_5, Al_2O_3 and SiO_2 yield values of 0.63, 0.59 and 0.47, respectively (see Table VI-2). According to this criteria Ta_2O_5 should be more stable than

Al_2O_3 and SiO_2 to bombardment-induced compositional changes. A second thermodynamic criterion is an energy criterion based on the standard free energy of formation (ΔG^0).[120] With this criterion, the tendency to reduce an oxide material is related to the energy difference between the initial and final states. The values of ΔG^0 for Ta_2O_5, Al_2O_3 and SiO_2 are 20.4, 16.4 and 8.3 eV/atom, respectively.[55] According to this criterion Ta_2O_5 should be more stable to bombardment-induced composition-al changes. A third thermodynamic criterion is a surface binding energy (E_b) criterion where E_b is approximated by the total and partial heats of atomization (ΔH_a, ΔH_p).[119] For example,[59] the sputtering of TiO_2 into elemental constituents involves the total heat of atomization as

$$TiO_2 \rightarrow Ti + 2O, \qquad \Delta H_a = 6.4 \text{ eV/atom.}$$
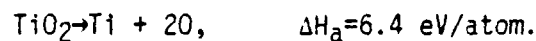
The sputtering of TiO_2 such that the stoichiometry evolves to a sub-oxide form involves the partial heat of atomization as

$$2TiO_2 \rightarrow Ti_2O_3 + O, \qquad \Delta H_p = 5.1 \text{ eV/atom.}$$

With this criterion, materials can be identified in which oxygen is more loosely bound than in other oxide materials. The criterion is based on the fact that the values of ΔH_a for some oxides tend to minimize for a particular degree of oxygen loss. Thus processes with the smallest value of ΔH_a are expected to have the highest preferential sputtering yield. A relative ranking of materials predicted to lose oxygen based on their values of ΔH_a[55] is as follows: Ta_2O_5, TiO_2, Al_2O_3, SiO_2 and ZrO_2. This criterion predicts that Ta_2O_5 and TiO_2 will reduce while Al_2O_3, SiO_2 and

Table VI-2

Electronegativity, Ionicity and Standard Free Energy of Formation

	X	i	$-\Delta G^o$(eV/atom)
Ta	1.5		
Al	1.6		
Si	1.9		
0	3.5		
Ta_2O_5		0.63	20.4
Al_2O_3		0.59	16.4
SiO_2		0.47	8.3

ZrO_2 will not. The results obtained in this study for Ta_2O_5 agree with this criterion. However, results reported for ion assisted ZrO_2 coatings[29] and TiO_2 coatings[41] disagree with this criterion. Thus, it is unclear how well this criterion can predict bombardment induced compositional changes.

The criteria based on thermodynamic considerations predicted conflicting behaviors for the various oxide materials. From the evaluation of these criteria it remains unclear which, if any, of the thermodynamic properties (ionicity, energy of formation, heat of atomization) governs the compositional stability of oxide materials subjected to ion bombardment. Another mechanism on which to base a criterion for compositional changes is collisional processes. The elastic-collision energy transfer criterion is based on binary-collision model calculations.[129] The incident ion is modeled as transferring its kinetic energy in a series of elastic collisions with lattice atoms. The collisions are assumed to be independent binary events between a moving particle and a lattice atom at rest. For elastic collisions, the energy is not equally distributed among the different mass atoms in a solid. To evaluate this criterion, the energy transfer factor (γ) for each binary collision must be calculated. The energy transfer factors are given by

$$\gamma = 4M_1M_2/(M_1+M_2)^2, \qquad\qquad (VI-8)$$

where M_1 and M_2 are the atomic masses of the colliding atoms. The calculated values of γ for oxygen ion bombardment of all the materials examined in this study are

$$\gamma_{0 \to Ta} = 0.298$$

$$\gamma_{0 \to Al} = 0.935$$

$$\gamma_{0 \to Si} = 0.926$$

$$\gamma_{0 \to 0} = 1.000.$$

The large difference in atomic mass between oxygen and tantulum results in a more efficient energy deposition to the oxygen atoms ($\gamma_{0 \to 0} > \gamma_{0 \to Ta}$). This results in a correspondingly higher sputtering yield for the oxygen atoms in the Ta_2O_5 molecule. The value of $\gamma_{0 \to Al}$ is very close to $\gamma_{0 \to 0}$; therefore the energy of the bombarding oxygen ion is distributed almost evenly between Al and O in Al_2O_3. Likewise, the value of $\gamma_{0 \to Si}$ is very close to $\gamma_{0 \to 0}$; therefore the energy of the bombarding oxygen ion is distributed almost evenly between Si and O in SiO_2 as well. Thus, this criterion predicts preferential oxygen sputtering will occur in Ta_2O_5 more than in Al_2O_3 and SiO_2 which agrees with the results obtained in this study.

Increases in the values of optical absorption for increasing ion bombardment conditions for oxygen ion assisted deposition of CeO_2 were reported by Netterfield et.al.[30] They attributed the increases in absorption to the preferential sputtering of oxygen in the CeO_2 molecule. The values of γ for oxygen bombardment of CeO_2 are

$$\gamma_{0 \to Ce} = 0.368$$

$$\gamma_{0 \to 0} = 1.000.$$

The large difference in atomic mass between oxygen and cerium results in a more efficient energy deposition to the oxygen atoms ($\gamma_{0 \to 0} > \gamma_{0 \to Ce}$).

The experimental results are consistent with the predictions of the energy transfer criterion.

One factor that must be considered in this criterion is that the bombardment in this study was with O_2^+ not O^+. However, a theoretical and experimental study conducted to evaluate the sputtering yields for atomic and molecular ions reported that the sputtering yield of a molecular ion ($Y[X_j^+]$) can be expressed in terms of the sputtering yields of the constituent atomic ions ($Y[X^+]$).[130] This can be written as $Y[X_j^+(jE)]=jY[X^+(E)]$, where E is energy. The results were constant regardless of the details of the process by which the molecular ion dissociates upon impact with the surface. Comparison of calculated and experimental sputtering yields of O_2^+ and O^+ were within 10% of each other. Thus, calculation of γ using the atomic mass of O appears valid.

Evidence from other studies support the predictions of the energy transfer criterion. The work of Thomas and Hofmann[127] discussed above, showed that the least amount of reduction in SiO_2 occurred for bombardment by Ne^+ and Ar^+ compared to that for He^+. The energy transfer factors for Ne^+ bombardment are

$$\gamma_{Ne \to O} = 0.988$$
$$\gamma_{Ne \to Si} = 0.972.$$

The energy transfer factors for Ar^+ bombardment are

$$\gamma_{Ar \to O} = 0.816$$
$$\gamma_{Ar \to Si} = 0.969.$$

For each ion species the values of $\gamma_{\to O}$ and $\gamma_{\to Si}$ are close to each other; therefore the energy of the bombarding ion is distributed evenly between Si and O. They reported that He^+ reduced the surface more severely than Ne^+ or Ar^+ bombardment. The values of γ for He^+ bombardment are

$$\gamma_{He \to O} = 0.640$$
$$\gamma_{He \to Si} = 0.438.$$

Because $\gamma_{He \to O} > \gamma_{He \to Si}$ the energy transfer to oxygen atoms is greater than to silicon atoms. This results in a correspondingly higher oxygen sputter yield for He^+ bombardment as reported by Thomas and Hofmann.

The effects of bombardment with 1 keV He^+ and Ar^+ on the composition of Ta_2O_5 were studied.[61] Although pronounced oxygen depletion was observed for bombardment with both species, the amount of reduction was much less for Ar^+ bombardment. The energy transfer factors for He^+ bombardment are

$$\gamma_{He \to O} = 0.640$$
$$\gamma_{He \to Ta} = 0.085.$$

The energy transfer factors for Ar^+ bombardment are

$$\gamma_{Ar \to O} = 0.816$$
$$\gamma_{Ar \to Ta} = 0.593.$$

The ratio of the energy transfer factors (γ_O / γ_{Ta}) is approximately 7.5 for He^+ bombardment and approximately 1.4 for Ar^+ bombardment. Thus, the

efficiency of the energy transfer to the oxygen atoms is much greater for He^+ bombardment than for Ar^+ bombardment. This results in a correspond-ingly higher oxygen sputter yield for He^+ bombardment as reported. These results in which the reduction was dependent on the mass of the ion species support the energy transfer criterion.

VI.5 Raman Results

Measurement of the Raman spectra for a number of Ta_2O_5 coatings indicated that various ion-induced crystalline phase changes occurred (Figure III-9 and Table III-2). Knowledge and control of the crystalline phase composition and structure in thin film optical coatings is import-ant. Crystalline phase and structure in large part determine coating properties such as refractive index, stress and resistance to high energy laser damage.[12,46] A number of studies have shown that deposition conditions allow repeatable control of coating crystalline phase and grain size.[12,16,54] Pawlewicz et.al. deposited TiO_2 coatings using reactive rf diode sputtering.[12] They reported values of n from 2.0 to 2.5 (at λ=1 μm) depending on average crystalline grain size in the coat-ings. The largest value of n occurred for the largest grain size(60 nm). The average grain size increased as the rf power density during deposi-tion increased. They also reported that laser damage threshold values (at λ=1.06 μm) decreased as average grain size increased. The highest laser damage threshold values were obtained for glassy TiO_2 coatings. Williams and Hess deposited TiO_2 thin films using plasma-assisted chem-ical vapor deposition.[16] They reported a direct dependence of grain size and phase composition on plasma characteristics during deposition.

Exarhos and Morse used time-resolved Raman spectroscopy (TRRS) to

study laser damage (at λ=532 nm) in TiO_2 coatings.[46] Using TRRS,
in which Raman spectra were obtained at various time delays following the
damage pulse, they reported an irreversible transition from the anatase
to the rutile phase during the damage process. They explained the
damage mechanism as one due to mechanical stress developed in the
coating. The rutile phase is denser than the anatase phase (4.27 vs.
3.90 g cm^{-3}). Thus, the phase transition led to localized bond strains
and eventual microcrack formation in the coatings. They also reported
larger values of laser damage threshold for rutile coatings than for
anatase coatings.

The instability of anatase TiO_2 coatings exposed to pulsed laser
irradiation resulted from observed phase transitions to the rutile phase
due to localized heating. In another study, Exharos studied the Raman
spectra of TiO_2 coatings under CW CO_2 laser irradiation.[131] The CO_2
laser was used as a localized heating source for the coatings. He
reported an irreversible transition from the anatase to rutile phase
which started at ~800°C and was complete at ~900°C. He reported that
microcracks developed in coatings undergoing phase transition.

Knowledge of the fundamental mechanism(s) that occur during energet-
ic particle bombardment of materials would allow controlled variations of
the crystalline phase composition and structure in coatings bombarded
during deposition with low-energy ions. Results of bombardment-induced
crystallization in materials have been reported, mostly for high energy
(>20 keV) bombardment.[59-61,132] However, these results may assist in
the selection of criteria to predict the structural effects that occur
due to simultaneous low-energy ion bombardment during deposition. Murti
et.al. examined the effects of 35 keV O_2^+ bombardment on Ta_2O_5.[60] They

reported that Ta_2O_5 was among the most easily amorphized substances examined. The material amorphized for current densities as low as $5~\mu A~cm^{-2}$. They also found that the material re-crystallized as a lower oxide with increased levels of ion bombardment. They summarized the overall structural and compositional effects as follows:

$$Ta_2O_5(crystalline) \rightarrow Ta_2O_5(amorphous) \rightarrow Ta_2O_{5-x}(amorphous) \rightarrow$$

$$\rightarrow Ta_2O_{5-x}(amorphous) + \delta\text{-}Ta\text{-}O(crystalline).$$
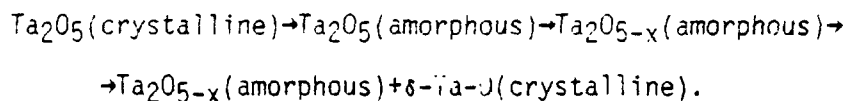
The notation δ-Ta-O represents a form of tantalum oxide of unestablished composition. The results for IAD Ta_2O_5 coatings in this study qualitatively agree with their observations for high energy O_2^+ bombardment.

Kelly has compiled a large data base of available information about bombardment-induced effects in oxides.[61,132] He stated that it is a fairly general result that ion bombardment of a material causes either amorphization or crystallization depending on material properties and bombardment dose. Naguib and Kelly proposed a mechanism to explain structural changes observed in a large number of materials.[59] The model is based on the accumulation of "amorphous zones". They postulated that an incident ion can be regarded as creating a small, hot, disordered region equivalent to a liquid surrounded by a crystal (i.e. a thermal spike). The amorphous-crystal interface ("crystallization front") migrates as the spike spreads. The region cools rapidly and crystallization sets in when the temperature falls below the material melting point(T_m). The condition that the region will not crystallize is whenever the distance moved by the "crystallization front" is less than the mean atomic spacing. This mechanism led to a temperature ratio

criterion to determine the response of a material to ion bombardment. The criterion is

$$T_c/T_m > 0.3 \text{ (amorphization)}$$
$$T_c/T_m < 0.3 \text{ (crystallization)}.$$

Here T_c, in degrees Kelvin, is the macroscopic crystallization temperature of a material. The criterion, $T_c/T_m > 0.3$, states that a material will amorphize or remain amorphous if the temperature ratio exceeds 0.3. The criterion has its physical basis in the thermal-spike model. However, whether or not that model is valid, a phenomenological criterion for predicting bombardment-induced amorphization or crystallization was established. The validity of the criterion was tested for 34 cases and found correct for 33 of them. Thus, the criterion can be considered valid based on empirical results without reliance on the validity of the thermal-spike model.

The results of applying ion bombardment during the deposition of Ta_2O_5 coatings in this study, and TiO_2 and ZrO_2 coatings[33,29] in other studies appear to agree with the predictions of the temperature ratio criterion. The ratio values for Ta_2O_5, TiO_2 and ZrO_2 are 0.47, 0.31 and 0.27, respectively.[55] The criterion predicts that Ta_2O_5 should amorphize and ZrO_2 should crystallize under ion bombardment. Martin et.al. reported that ZrO_2 coatings were amphorous when deposited on unheated substrates with no ion bombardment.[29] The cubic phase structure was found in coatings bombarded during deposition with 1200 eV O_2^+ at current densities greater than 5 $\mu A \, cm^{-2}$. Both cubic and monoclinic phase structures were found in ion-assisted coatings deposited on heated

substrates. It is not clear what the criterion predicts for TiO_2 because the value of its ratio lies close to the boundary value of 0.3. Ion-induced phase transitions were reported for TiO_2 coatings bombarded during deposition with 500 eV O_2 ions.[33] Thus, it appears that the temperature ratio criterion can be used to predict crystalline structural effects in coatings due to ion bombardment during deposition.

VI.6 RBS Results

Measurements of the relative ratio (O:Ta) for a number of IAD Ta_2O_5 coatings were accomplished using Rutherford backscattering spectroscopy (RBS) (see Figure III-11). These measurements revealed a potential problem in using RBS to determine the composition of metal oxide thin films. It was discovered that significant deviations (27%) from publish-ed stopping powers for oxygen had to be applied in the data analysis. Thus caution must be used when analyzing the RBS results due to the uncertainty introduced by the oxygen stopping power. To better under-stand the origin of the uncertainty in oxygen stopping power a simple review of the RBS technique is required.[63]

The RBS technique consists of placing a target in a beam of mono-energetic helium ions. Scattered particles from the target are detected and analyzed. The backscattering analysis allows the atomic masses of elements to be distinguished and their distribution with depth to be determined as a function of detected energy. Figure VI-3 is a back-scatter spectrum for Ta in a Ta_2O_5 coating. The highest energy, KE_{in}, is the backscattered energy from Ta atoms at the outer surface of the coating. This is related to the incident energy, E_{in}, and the kinematic recoil factor, K.[63] The kinematic factor is determined from the mass of
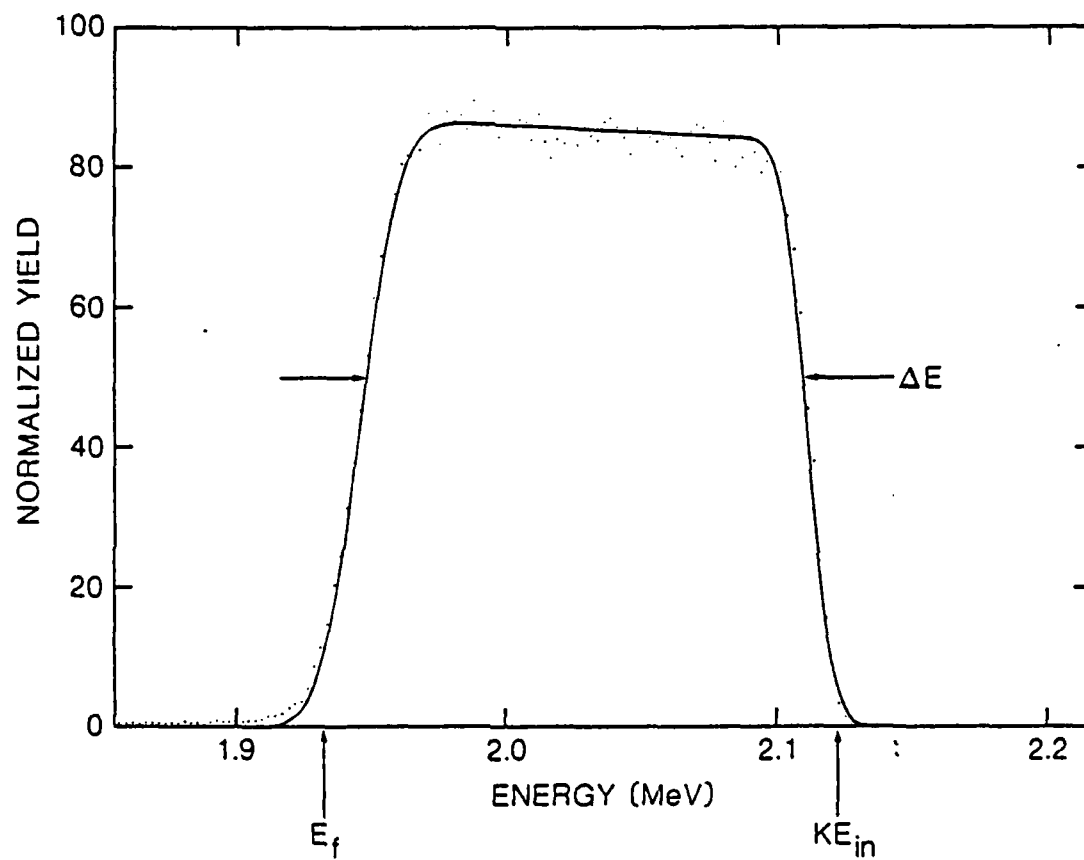
Figure VI-3. RBS spectrum for Ta in Ta_2O_5 coating.

the target atom (M), the mass of the incident ion (m) and the scattering angle (ϕ) using

$$K = [m\cos\phi + (M^2 - m^2\sin^2\phi)^{\frac{1}{2}}/m+M]^2. \qquad (VI-9)$$

It can be seen from equation (VI-9) that as the mass of the target atom increases the value of K increases and approaches unity. The scattered particles from deeper in the coating have lower energy because of the energy loss as the particles transverse through the coating. The energy, E_f represents scattering from the deepest part of the coating (at the substrate interface). The difference, ΔE, is the amount of energy loss by the particles on their round-trip through the coating.

The value of ΔE is proportional to coating thickness and stopping cross-section (often called stopping power).[63] The stopping power, ξ, is related to the energy loss per unit length (dE/dx), atomic mass of the target (M) and density (p), as follows:

$$\xi = [M/N_0 p](dE/dx), \qquad (VI-10)$$

where N_0 is Avogadro's number. It is the value of dE/dx which introduces the largest uncertainty in the determination of ξ. Values of dE/dx are usually measured for single element thin films in transmission. The measurement of dE/dx for Ta is relatively straightforward using a thin, solid Ta target. However, the measurement for oxygen is not as straight-forward. This is usually accomplished using a gas cell filled with oxygen in gaseous form. These results are compiled in empirical tables of stopping power.[133]

The stopping powers are assumed additive following Bragg's rule.[134] For example, the stopping power of SiO_2 is calculated as

$$\varepsilon_{SiO_2} = \varepsilon_{Si} + 2\varepsilon_O. \qquad\qquad (VI\text{-}11)$$

Likewise, the stopping power of Ta_2O_5 is calculated as

$$\varepsilon_{Ta_2O_5} = 2\varepsilon_{Ta} + 5\varepsilon_O. \qquad\qquad (VI\text{-}12)$$

However, the accuracy of Bragg's rule has been questioned for a number of compound materials, especially metal oxides.[134,135] Feng et.al.[134] measured RBS spectra for a number of compound materials. They reported that Bragg's rule was valid for metal alloys but not necessarily for Al_2O_3 and SiO_2. They reported 10-20% discrepancies between the experimentally measured stopping powers and those calculated using Bragg's rule. The oxygen stopping power introduced the largest uncertainty. Behrisch and Scherzer reported that Bragg's rule gave lower values for stopping powers of Ta_2O_5 than those obtained with measurements (~10% difference).[135] Thus, there is experimental evidence to doubt the direct application of Bragg's rule for the Ta_2O_5 measurements in this study.

It is recommended that another compositional analysis technique be applied to the coatings to provide corroboration of the RBS results obtained. Although ESCA and AES are surface analysis techniques which have small sampling depths, they could be used in conjunction with RBS to better determine correct film compositions. This work is continuing in collaboration with scientists at Los Alamos National Laboratory to determine more accurately the values of oxygen stopping power in Ta_2O_5.

VI.7 Fluorine Gas Tests

A number of coatings were examined for the effects of static exposure to fluorine gas. The coatings were tested at Los Alamos National Laboratory (LANL) by exposure to 0.5% F_2 in He gas mixture as described in Chapter II. To date the results from all tests at LANL have shown degradation in optical performance (transmittance) of almost all coatings exposed to fluorine gas. The one exception has been AlN/Al_2O_3 AR coatings on CaF_2 produced using reactive rf sputtering by W. Pawlewicz at Battelle Pacific Northwest Laboratory. A number of these coatings have shown little or no degradation after more than 1000 hours exposure. Although the coatings show promising fluorine gas resistance, the laser damage threshold values for these coatings have been low ($<$1 J cm^{-2}).[136] Other results from the fluorine gas tests at LANL have shown that the laser damage threshold values of coatings were significantly lower after exposure to fluorine gas. The laser damage threshold values were decreased by factors of 3-7 after exposure to 0.5% F_2 for 165 hours.

The dynamics of fluorine gas attack in optical coatings are not well understood. Some simple ideas on possible mechanisms can be developed from known results from etching studies. Fluorine etching of surfaces is often described as halogenation--the analog of oxidation of surfaces due to oxygen exposure. Both fluorine and oxygen are highly electronegative atoms. Thus they can be very reactive. Oxidation frequently produces an involatile oxide which remains on a surface. A similar surface inter-action with fluorine often yields a volatile product which is desorbed into the gas phase. Therefore, the halogenation process may continue indefinitely because the products are desorbed. A reaction sequence for the interaction of fluorine with a surface has been developed based on

experimental observations.[137] Small doses of F_2 produced a chemisorbed layer but no etching. A larger dose created a fluoride compound layer (2-6 monolayers thick) at the surface. A further increase in F_2 dose caused saturation and desorption (etching) of the fluoride compound.

It has been speculated that less porous coatings would be more resistant to fluorine gas attack. The reason for this speculation was that denser coatings would adsorb less water. When exposed to fluorine gas the tendency to form HF would be smaller because the hydrogen content in the coatings was negligible. There is evidence which supports the contention that IAD coatings are dense. The evidence includes larger values of refractive index and good optical stability upon exposure to humidity as observed in this study and reported by others.[29,30] This would indicate that IAD coatings should be less susceptible to F_2 attack. However, the results obtained from the fluorine tests in this study are inconclusive and somewhat contradictory.

For Ta_2O_5 coatings (Figure III-14), the coating bombarded during deposition with 300 eV O_2^+ at a current density of 20 μA cm^{-2} had the best resistance to degradation due to F_2. For Al_2O_3 coatings (Figure III-21), the coating deposited without bombardment exhibited no degradation after 670 hours of F_2 exposure. This coating is still under test. For SiO_2 coatings (Figure III-25), the coating deposited without bombardment exhibited minor degradation after 698 hours of F_2 exposure. This coating is still under test. For Al_2O_3/SiO_2 AR coatings (Figure V-9), the coating bombarded during deposition with 500 eV O_2^+ at a current density of 80 μA cm^{-2} exhibited the smallest amount of optical degradation (3% decrease in transmittance) after 47 hours of F_2 exposure. If the mechanism for fluorine degradation is the formation of HF due to the

presence of adsorbed water in the coatings, then these results do not support this scenario.

The results obtained in this study can be examined using the mechanisms developed from etching studies: adsorption of the etching species, product formation and product desorption (halogenation process). To this process a mechanism developed by Flamm and Donnelly[138] will be added. They attributed increased etch rates in ion-enhanced etching to enhanced chemical reaction rates. They suggested that the enhanced reaction rates of the incident fluorine gas was due to lattice damage in Si and SiO_2 produced by ion bombardment. It is possible that an outer 2-4 nm layer (ion penetration depth) of the IAD coatings had lattice damage. Recall the results of Müller's computations (section VI.3) where IAD ZrO_2 coatings were modeled as having an ~2 nm deep surface depletion region. If the mechanism for fluorine degradation is related to the Flamm and Donnelly process, then the results for Al_2O_3 and SiO_2 coatings appear to support this scenario. However, any analysis of fluorine attack at this time is speculative because of the limited number of coatings tested and the inconclusive trends exhibited by those that have been tested.

A few of the coatings were examined using a Nomarski microscope after the fluorine gas tests. The micrographs illustrate different damage morphologies exhibited in the fluorine-damaged coatings. It initially appeared that the nature of the damage initiation and evolution might be deduced from these micrographs. However, these micrographs are of coatings that have degraded to a "catastrophic" point. It is suggested that in the future, examination be accomplished at regular time intervals during fluorine exposure to ensure correct identification of

the damage initiation and evolution morphologies.

Figure VI-4 illustrates what appear to be damage initiation sites. These small sites might evolve into blister-like damage sites (~100 μm diameter) as illustrated in Figure VI-5. When examined under the microscope the blister-like damage sites appeared to go in random motion as the "skin" of the blisters flexed. This motion would occur whenever a new site was exposed to the microscope illumination source, and would stop after about a 10 sec exposure. This seems to imply that there is a small amount of gas trapped inside the "blister", and the motion was due to thermal expansion of this gas. The damage appears to further evolve into larger sites (~150 μm diameter) with a darkened crater (~40 μm diameter) in the center (Figure VI-6). This has the appearance of a volcano-type crater and implies that the damage site may actually "explode". Figure VI-7 illustrates a damage site where the coating material has actually delaminated from the substrate surface.

Figure VI-8 illustrates damage morphology that appears to be initiation sites surrounding an evolved "blister". The diameter of the "blister" is approximately 30 μm. The "blister" also appeared to go into random motion when exposed to the microscope illumination source as did the "blister" in Figure VI-5. The small initiation sites imply that the fluorine might permeate through microvoids and along boundaries into the coatings. Reactions of the fluorine with the coating material and/or substrate would create volatile products in the gaseous state. These products might be trapped inside a small volume of coating material and create the blisters. These blisters would increase in size as more fluoride products are created. Eventually the blisters would saturate and "explode".
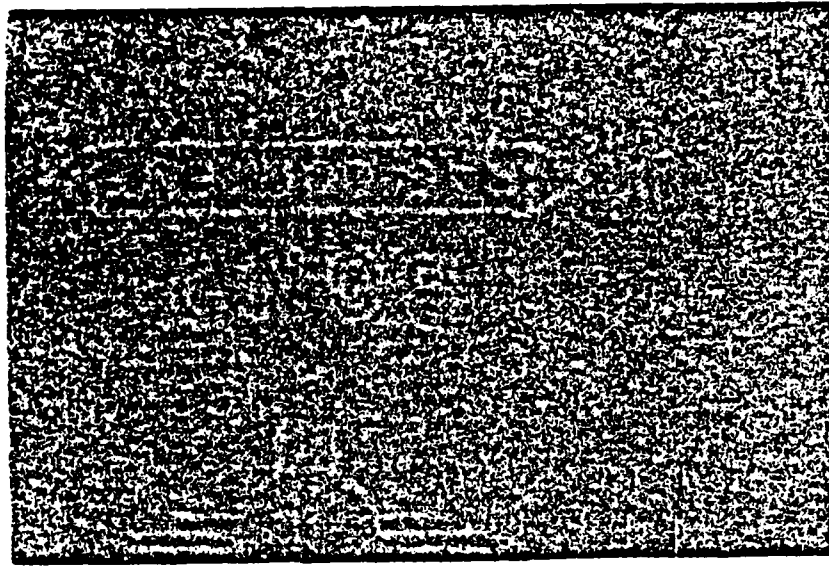
10 μm

Figure VI-4. Micrograph of fluorine damaged Al$_2$O$_3$/SiO$_2$ AR coating (40X).

10 µm

Figure VI-5. Micrograph of fluorine damaged Al_2O_3/SiO_2 AR coating (20X).
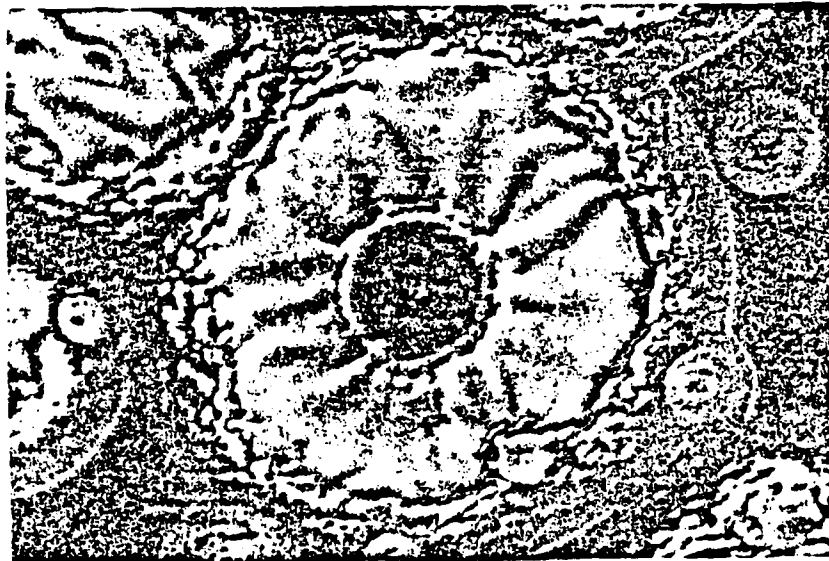
10 μm

Figure VI-6. Micrograph of fluorine damaged Al_2O_3/SiO_2 AR coating (20X); different site than in Figure VI-5.

10 μm

Figure VI-7. Micrograph of fluorine damaged Ta₂O₅ coating (20X); illustrates area where delamination of coating material has occurred.
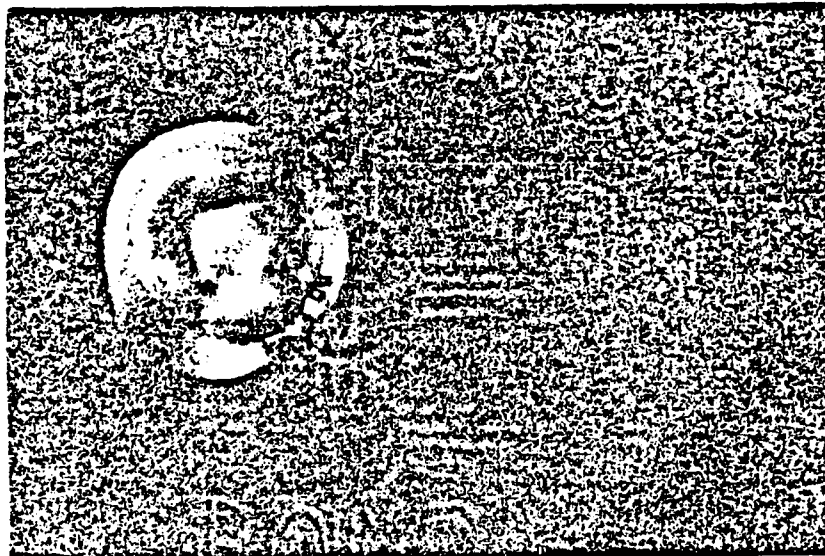
10 μm

Figure VI-8. Micrograph of fluorine damaged Ta$_2$O$_5$ coating (40X) illustrating "blister" site.

Chapter VII

SUMMARY

Ion assisted deposition (IAD) was used to produce Ta_2O_5, Al_2O_3, HfO_2 and SiO_2 single- and multi-layer coatings. This was the first systematic investigation of the effects of IAD on the properties of Ta_2O_5, Al_2O_3, HfO_2 and SiO_2 coatings. This study was the first attempt to examine the laser damage thresholds for anti-reflection coatings produced using IAD. This was the first study of the properties of IAD Al_2O_3, SiO_2 and MgF_2 coatings on heavy metal fluoride (HMF) glass substrates. The coatings were deposited by electron-beam evaporation with simultaneous O_2^+ bombardment. A Kaufman ion source was used to provide a monoenergetic, neutralized ion beam independent of the material evaporation process. The ion energy ranged from 200 to 1000 eV. The ion current density ranged from 0 to 200 $\mu A\ cm^{-2}$. Results are summarized in Table VII-1.

Oxygen ion bombardment during deposition produced Ta_2O_5 and Al_2O_3 coatings with increased values of refractive index. The increase in n was dependent on ion energy and current density. No increase in n was observed for IAD SiO_2 coatings. An increase in optical absorption was observed for IAD Ta_2O_5 coatings. The values of optical absorption increased for bombardment at increasing values of ion current density for a constant ion energy. For bombardment at a constant current density value, optical absorption was larger for larger values of ion energy. The increase in optical absorption was attributed to preferential sputtering of oxygen in the Ta_2O_5 molecule. Increases in optical absorption were not observed for Al_2O_3 and SiO_2 coatings except for

coatings bombarded at very high current densities. A simple model based on an elastic-collision energy transfer criterion was suggested to explain preferential sputtering effects in IAD oxide coatings. The effects on the optical constants of IAD coatings were found to be material dependent.

The optical scatter characteristics for IAD coatings were measured. The optical scatter for IAD coatings was lower than the scatter for unbombarded coatings. Improved environmental stability was obtained for IAD Ta_2O_5 coatings exposed to humidity testing. The humidity test results, as well as observations of increased values of refractive index and reduced optical scatter, are consistent with IAD coatings having increased values of packing density and thin film properties closer to the material in bulk form.

Ion bombardment-induced crystalline phase transitions were observed in IAD Ta_2O_5 coatings. The coatings were examined using Raman spectroscopy and the results were consistent with the temperature-ratio criterion developed by Naguib and Kelly. The values of film stress for IAD Ta_2O_5 coatings were measured. The film stress was compressive and increased for bombardment at increasing values of ion current density. These results were consistent with reported stress results for bombarded metal films in which ion incorporation correlated with increasing compressive film stress.

A limited number of coatings were exposed to fluorine gas tests. It appeared that IAD did not improve the resistance of single-layer Al_2O_3 and SiO_2 coatings to fluorine gas attack. A small improvement was observed in IAD Ta_2O_5 coatings. Further testing is required before any definite conclusions can be made about the effects of IAD on the fluorine

resistance of coatings.

Ion assisted deposition was successfully applied to deposit coatings at low temperature on HMF glass substrates. Heavy metal fluoride glasses are relatively soft and hygroscopic. The coatings deposited using IAD were hard, dense and improved the durability of the HMF glass substrates. The IAD coatings exhibited improved abrasion resistance over unbombarded coatings. The corrosion resistance of the HMF glass surfaces was significantly improved. As only a limited number of samples were investigated, further work is recommended to fully investigate the effects of using IAD to coat HMF glass substrates.

A number of Al_2O_3/SiO_2 and Ta_2O_5/SiO_2 anti-reflection (AR) coatings were laser damage tested at Los Alamos National Laboratory. It appears that the IAD coatings did not have higher laser-induced damage threshold (LIDT) values than the coatings deposited with no ion bombardment. The one exception was Al_2O_3/SiO_2 AR coatings bombarded with 300 eV O_2^+ at a current density of 10 μA cm^{-2}. Due to the limited number of coatings examined, further testing is required before any definite conclusions can be made.

As part of the laser damage study a number of IAD Al_2O_3/SiO_2 AR coatings were deposited using different filament materials in the ion source. A set of coatings were deposited using tungsten filaments in the ion source ("W coatings"). Another set of coatings were deposited using similar IAD conditions except tantalum filaments were used in the ion source ("Ta coatings"). The "Ta coatings" had LIDT values consistently larger than the "W coatings". The average value of the increase in LIDT values was 40%.

It is recommended that a systematic investigation of the effects of

IAD on the properties of low-temperature coatings be conducted. The results of such an investigation could be applied to coating substrates requiring specialized, controlled processing (e.g. HMF glasses). Another area recommended for examination is an extension of this study using very low-energy ions (60-200 eV). The purpose of such a study would be to observe the effects of low-energy ion bombardment on the optical properties and the environmental stability of coatings.

It is recommended that continued laser damage testing of IAD coatings be conducted. The results for single-layer coatings indicated that IAD coatings had increased values of n and improved environmental stability. These improvements in the properties of IAD coatings did not result in improved LIDT values for IAD AR coatings. The possibility of increased incorporation of contaminants due to the ion source might override improvements expected due to more dense coatings. The results from these continued laser damage tests, combined with results for low-energy IAD coatings, might aid in the understanding of the damage mechanism(s) in IAD coatings.

It is recommended that collaboration with Dr. Mueller be pursued to improve the model for ion assisted film growth. Also, this modeling effort should be expanded to include the development of comparable capabilities at other institutions. A final recommendation is made for continued support of coating diagnostics work. In particular, the information obtained in applying Rutherford backscattering spectroscopy (RBS) to Ta_2O_5 coatings should be applied to improve the accuracy of the technique in determining metal oxide film content. Corroboration of the RBS results with the results from Auger electron spectroscopy and/or electron spectroscopy for chemical analysis (ESCA) should be performed.

Table VII-1

IAD Summary Table

	Ta_2O_5	Al_2O_3	SiO_2	MgF_2
n	↑	↑	U	n/e
k	↑	U	U	n/e
optical scatter	↓	↓	↓	n/e
optical stability	I	n/e	I	n/e
crystal changes	Y	n/e	n/e	n/e
stress	↑	n/e	n/e	n/e
fluorine gas test	SI	NI	NI	n/e
abrasion resistance	n/e	n/e	I	I
laser damage	NI	U	U	n/e

↑ = increase

↓ = decrease

I = improvement

NI = no improvement

SI = slight improvement

U = unchanged

Y = yes, ion-induced

n/e = not evaluated

APPENDIX I

Refractive Index Calculation and Error Analysis

The values of refractive index (n) and extinction coefficient (k) for the single-layer coatings were determined from transmittance spectra measured using a spectrophotometer. The analysis was based on a method developed by Manifacier et.al.[43] to determine n, k and the thickness (t) of a weakly absorbing film on a non-absorbing substrate. A computer program (THINCO) was written to implement the procedure. The equations used to determine n, k and t were:

$$u=(T_{max}+T_{min})/2T_{max}T_{min} \qquad \text{(A.1-1)}$$

$$c=(T_{max}-T_{min})/2T_{max}T_{min} \qquad \text{(A.1-2)}$$

$$n=\tfrac{1}{2}([8n_sc+(n_s+1)^2]^{\frac{1}{2}}+[8n_sc+(n_s-1)^2]^{\frac{1}{2}}) \qquad \text{(A.1-3)}$$

$$t=(4[(n/\lambda_{max})-(n/\lambda_{min})])^{-1} \qquad \text{(A.1-4)}$$

$$\sigma=[(n_s^2-1)/8n_s]^2[n-n^{-1}]^2 \qquad \text{(A.1-5)}$$

$$a=(n+1)^3(n+n_s^2)/16n_sn^2 \qquad \text{(A.1-6)}$$

$$k=(\lambda/4\pi d)\ln([u+(u^2-c^2+\sigma)^{\frac{1}{2}}]/2a). \qquad \text{(A.1-7)}$$

The required inputs were:

T_{max} = maximum transmittance value

T_{min} = minimum transmittance value

n_s = substrate refractive index

λ_{max} = wavelength at which T_{max} occurred

λ_{min} = wavelength at which T_{min} occurred.

The relative errors in the resulting values of n were determined as follows. The relative errors for T_{max} and T_{min} were considered uncorrelated. The equation for n (A.1-3) was differentiated and equations A.1-1 and -2 were substituted into the result. The resulting relation was:

$$\Delta n/n = (\Delta T/T)[(T_{max}+T_{min})/(T_{max}-T_{min})]|f|^{-1} \quad (A.1-8)$$

where $\Delta T/T$ was the relative precision of the spectrophotometer measurements and

$$f = -2[(n^2-n_s)(n^2+n_s)]/(n^2-1)(n^2-n_s^2). \quad (A.1-9)$$

REFERENCES

1. K. H. Guenther and H. K. Pulker, "Electron microscopic investigation of cross sections of optical thin films," Appl. Opt. 15, 2992, (1976).

2. K. H. Guenther, "Experimental observation and computer simulation of the microstructure of vapor deposited thin films," Nat. Bur. Stand. (US) Spec. Publ. 688, 393 (1983).

3. H. A. Macleod, "Microstructure of optical thin films," Proc. Soc. Photo-Opt. Instrum. Eng. 325, 21 (1982).

4. For examples, see the extensive literature in "Laser Induced Damage in Optical Materials," Nat. Bur. Stand. (US) Spec. Publ.

5. T. W. Walker, A. H. Guenther and P. E. Nielsen, "Pulsed laser-induced damage to thin-film optical coatings - Part I: Experimental," IEEE J. Quant. Elect. QE-17, 2041 (1981).

6. H. A. Macleod and L. Bangjun, "Thin-film microstructure modeling," Proc. Soc. Photo-Opt. Instrum. Eng. 540, 150 (1985).

7. R. Messier, A. P. Giri and R. A. Roy, "Revised structure zone model for thin film physical structure," J. Vac. Sci. Technol. A2, 500 (1984).

8. A. G. Dirks and H. J. Leamy, "Columnar microstructure in vapor-deposited thin films," Thin Solid Films 47, 219 (1977).

9. B. A. Movchan and A. V. Demchishin, "Study cf structure and properties of thick vacuum condensates of nickel, titanium, tungsten, aluminum oxide and zirconium oxide," Phys. Met. Metallogr. 28, 83 (1969).

10. J. A. Thornton, "Influence of apparatus geometry and deposition conditions on the structure and topography of thick sputtered coatings," J. Vac. Sci. Technol. 11, 666 (1974).

11. D. M. Mattox and G. J. Kominiak, "Structure modification by ion bombardment during deposition," J. Vac. Sci. Technol. 9, 528 (1972).

12. W. T. Pawlewicz, R. Busch, D. D. Hays, P. M. Martin and N. Laegreid, "Reactively sputtered optical coatings for use at 1064 nm," Nat. Bur. Stand. (US) Spec. Publ. 568, 359 (1980).

13. T. M. Reith and P. J. Ficalora, "The reactive sputtering of tantalum oxide: Compositional uniformity, phases and transport mechanisms," J. Vac. Sci. Technol. A1, 1362 (1983).

14. J. R. Sites, P. Gilstrap and R. Rujkorakarn, "Ion beam sputter deposition of optical coatings," Nat. Bur. Stand. (US) Spec. Publ. 669, 243 (1982).

15. H. Demiryont, J. R. Sites and Kent Geib, "Effects of oxygen content on the optical properties of tantalum oxide films deposited by ion-beam sputtering," Appl. Opt. 24, 490 (1985).

16. L. M. Williams and D. W. Hess, "Structural properties of titanium dioxide films deposited in an rf glow discharge," J. Vac. Sci. Technol. A1, 1810 (1983).

17. M. J. Rand, "Plasma-promoted deposition of thin inorganic films," J. Vac. Sci. Technol. 16, 420 (1979).

18. J. Wong, T. M. Lu and S. Mekta, "Nozzle beam deposition of SiO_2 films," J. Vac. Sci. Technol. B3, 453 (1985).

19. J. Dudonis and L. Pranevicius, "Influence of ion bombardment on the properties of vacuum-evaporated thin films," Thin Solid Films 36, 117 (1976).

20. M. Marinov, "Effect of ion bombardment on the initial stages of thin film growth," Thin Solid Films 46, 267 (1977).

21. P. J. Martin, H. A. Macleod, R. P. Netterfield, C. G. Pacey and W. G. Sainty, "Ion-beam-assisted deposition of thin films," Appl. Opt. 22, 178 (1983).

22. W. C. Herrmann, Jr. and J. R. McNeil, "Ion beam applications for optical coating," Proc. Soc. Photo-Opt. Instrum. Eng. 325, 101 (1982).

23. A. E. Eltoukhy and J. E. Greene, "Diffusion enhancement due to low-energy ion bombardment during sputter etching and deposition," J. Appl. Phys. 51, 4444 (1980).

24. D. W. Hoffman and M. R. Gaerttner, "Modification of evaporated chromium by concurrent ion bombardment," J. Vac. Sci. Technol. 17, 425 (1980).

25. J. E. Greene and S. A. Barnett, "Ion-surface interactions during vapor phase crystal growth by sputtering, MBE and plasma-enhanced CVD: Applications to semiconductors," J. Vac. Sci. Technol. 21, 285 (1982).

26. I. Yamada and T. Takagi, "Vaporized-metal cluster formation and ionized-cluster deposition and epitaxy," Thin Solid Films 80, 105 (1981).

27. J. J. Cuomo, J. M. E. Harper, C. R. Guarnieri, D. S. Yee, L. J. Attanasio, J. Angilello, C. T. Wu and R. H. Hammond, "Modification of Nb film stress by low-energy ion bombardment during deposition," J. Vac. Sci. Technol. 20, 349 (1982).

28. T. Allen, "Properties of ion assisted deposited silica and titania films," Proc. Soc. Photo-Opt. Instrum. Eng. 325, 93 (1982).

29. P. J. Martin, R. P. Netterfield and W. G. Sainty, "Modification of the optical and structural properties of dielectric ZrO_2 films by ion-assisted deposition," J. Appl. Phys. 55, 235 (1984).

30. R. P. Netterfield, W. G. Sainty, P. J. Martin and S. H. Sie, "Properties of CeO_2 thin films prepared by oxygen-ion assisted deposition," Appl. Opt. 24, 2267 (1985).

31. J. R. McNeil, G. A. Al-Jumaily, K. C. Jungling and A. C. Barron, "Properties of TiO_2 and SiO_2 thin films deposited using ion assisted deposition," Appl. Opt. 24, 486 (1985).

32. J. R. McNeil, A. C. Barron, S. R. Wilson and W. C. Herrmann, Jr., "Ion-assisted deposition of optical thin films: low energy vs high energy bombardment," Appl. Opt. 23, 552 (1984).

33. G. A. Al-Jumaily, J. J. McNally, J. R. McNeil and W. C. Herrmann, Jr., "Effects of ion assisted deposition on optical scatter and surface microstructure of thin films," J. Vac. Sci. Technol. A3, 651 (1985).

34. G. A. Al-Jumaily, S. R. Wilson, J. J. McNally, K. C. Jungling and J. R. McNeil, "Reduction of optical scatter in coated metal surfaces," J. Vac. Sci. Technol. A5 (1986), in press.

35. G. A. Al-Jumaily, S. R. Wilson, J. J. McNally, J. R. McNeil, J. M. Bennett and H. H. Hurt, "Influence of metal films on the optical scatter and related microstructure of coated surfaces," Appl. Opt., to be published (1986).

36. H. R. Kaufman, "Technology of ion beam sources used in sputtering," J. Vac. Sci. Technol. 15, 272 (1978).

37. J. J. McNally, G. A. Al-Jumaily and J. R. McNeil, "Ion assisted deposition of Ta_2O_5 and Al_2O_3 thin films," J. Vac. Sci. Technol. A5 (1986), in press.

38. J. J. McNally, G. A. Al-Jumaily, S. R. Wilson and J. R. McNeil, "Ion-beam-assisted deposition of optical thin films - recent results," Proc. Soc. Photo-Opt. Instrum. Eng. 540, 479 (1985).

39. J. J. McNally, G. A. Al-Jumaily, J. R. McNeil and B. Bendow, "Ion assisted deposition of optical and protective coatings for heavy metal fluoride glass," Appl. Opt. 25, (1986), in press.

40. J. J. McNally, F. L. Williams, S. R. Wilson and J. R. McNeil, "Properties of IAD Al_2O_3/SiO_2 and Ta_2O_5/SiO_2 thin film AR structures," Nat. Bur. Stand. (US), to be published (1986).

41. G. A. Al-Jumaily, S. R. Wilson, A. C. Barron, J. R. McNeil and B. L. Doyle, "Contamination analysis of TiO_2 thin films deposited using ion assisted deposition," Nucl. Instr. and Meth. B7/8, 906 (1985).

42. A. F. Turner, notes from Short Course in Applied Thin Film Optics, Amer. Vac. Soc. Mtg. (1976).

43. J. C. Manifacier, J. Gasiot and J. P. Fillard, "A simple method for the determination of the optical constants n,k and the thickness of a weakly absorbing thin film," J. Phys. E9, 1002 (1976).

44. J. R. McNeil, L. J. Wei, G. A. Al-Jumaily, S. Shakir and J. McIver, "Surface Smoothing Effects of Thin Films?", Appl. Opt. 24, 480 (1985).

45. A. E. Ennos, "Stresses developed in optical film coatings", Appl. Opt. 5, 51, (1966).

46. G. J. Exarhos and P. L. Morse, "Raman studies of laser damaged single- and multi-layer optical coatings," Proc. SPIE 540, 460 (1985).

47. J. G. Beery, M. G. Hollander, C. J. Maggiore, A. Redondo and T. N. Taylor, "Ion beam characterization of multi-layer dielectric reflectors," Nat. Bur. Stand. (US) Spec. Publ., to be published (1986).

48. D. H. Hensler, J. D. Cuthbert, R. J. Martin and P. K. Tien, "Optical propagation in sheet and pattern generated films of Ta_2O_5," Appl. Opt. 10, 1037 (1971).

49. W. C. Herrmann, Jr., "E-beam deposition characteristics of reactively evaporated Ta_2O_5 for optical interference coatings," J. Vac. Sci. Technol. 18, 1303 (1981).

50. F. Rubio, J. M. Albella, J. Denis and J. M. Martinez-Duart, "Optical properties of reactively sputtered Ta_2O_5 films," J. Vac. Sci. Technol. 21, 1043 (1982). see also, F. Rubio, J. Denis. J. M. Albella and J. M. Martinez-Duart, "Sputtered Ta_2O_5 anti-reflection coatings for silicon solar cells," Thin Solid Films 90, 405 (1982).

51. H. Terui and M. Kobayashi, "Refractive-index-adjustable SiO_2 - Ta_2O_5 films for integrated optical circuits," Appl. Phys. Lett. 32, 666 (1978).

52. S. Schiller, U. Heisig, K. Steinfelder and J. Strumpfel, "Reactive d.c. sputtering with the magnetron-plasmatron for tantalum pentoxide and titanium dioxide films," Thin Solid Films 63, 369 (1979).

53. E. E. Khawaja and S. G. Tomlin, "The optical properties of thin films of tantalum pentoxide and zirconium dioxide," Thin Solid Films 30, 361 (1975).

54. Y. Nakagawa and Y. Gomi, "New piezoelectric Ta_2O_5 thin films", Appl. Phys. Lett. 46, 139 (1985).

55. The Oxide Handbook, edited by G. V. Samsonov, translated by R. K. Johnston, (IFI/Plenum, New York, 1982).

56. E. Taglauer, W. Heiland and R. J. MacDonald, "The study of sputtering effects in oxides and metal-adsorbed gas systems using combined analytical techniques," Surface Sci. $\underline{90}$, 661 (1979).

57. J. H. Thomas and S. Hofman, "Ion bombardment induced changes in SiO_2 surface composition studied by x-ray photoelectron spectropscopy," J. Vac. Sci. Technol. $\underline{A3}$, 1921 (1985).

58. P. Swab and R. E. Klinger, "Physical microstructure of evaporated titania-silica and zirconia-silica multilayer thin films," J. Opt. Soc. Am. $\underline{A2}$, P77 (1985). see also, T. H. Allen, "Optical materials deposited using ion beam sputtering," J. Opt. Soc. Am. $\underline{A2}$, P92 (1985).

59. H. M. Naguib and R. Kelly, "Criteria for bombardment-induced structural changes in non-metallic solids," Rad. Effects $\underline{25}$, 1 (1975).

60. D. K. Murti, R. Kelly, Z. L. Liau and J. M. Poate, "Structural and compositional changes in ion-bombarded Ta_2O_5," Surface Sci. $\underline{81}$, 571 (1979).

61. R. Kelly, "Phase changes in insulators produced by particle bombardment," Nucl. Instr. and Meth. $\underline{182/183}$, 351 (1981).

62. G. J. Exarhos, private communication.

63. W. K. Chu, J. W. Mayer, M. A. Nicolet, T. M. Buck, G. Amsel and F. Eisen, "Principles and applications of ion beam techniques for the analysis of solids and thin films," Thin Solid Films $\underline{17}$, 1 (1973).

64. R. E. Hibshman, Jr., private communication.

65. W. T. Pawlewicz, "Reactively sputtered amorphorus optical coatings for visible and near-infrared laser mirrors," Final Report, AFWL - TR-84-84, 12 (1984).

66. E. H. Hirsh and I. K. Varga, "Thin film annealing by ion bombardment," Thin Solid Films $\underline{69}$, 99 (1980).

67. J. A. Thornton and D. W. Hoffman, "Internal stresses in amorphous silicon films deposited by cylindrical magnetron sputtering using Ne, Ar, Kr, Xe, and Ar + H_2," J. Vac. Sci. Technol. $\underline{18}$, 203 (1981).

68. S. Foltyn, private communication.

69. D. Hoffman and D. Leibowitz, "Effect of substrate potential on Al_2O_3 films prepared by electron beam evaporation," J. Vac. Sci. Technol. 9, 326 (1972). See also D. Hoffman and D. Leibowitz, "Al_2O_3 films prepared by electron-beam evaporation of hot-pressed Al_2O_3 in oxygen ambient," J. Vac. Sci. Technol. 8, 107 (1971).

70. G. Hass, J. B. Heaney, H. Herzig, J. F. Osantowski and J. J. Triolo, "Reflectance and durability of Ag coated mirrors coated with thin layers of Al_2O_3 plus reactively deposited silicon oxide," Appl. Opt. 14, 2639 (1975).

71. R. Nowicki, "Properties of rf-sputtered Al_2O_3 films deposited by planar magnetron," J. Vac. Sci. Technol. 14, 127 (1977).

72. D. L. Lunt, "Development of rf-sputtered laser coatings at Burleigh Northwest," Nat. Bur. Stand. (US) Spec. Publ. 688, 287 (1985).

73. H. Sankur, "Properties of dielectric thin films formed by laser evaporation," Mat. Res. Soc. Symp. Proc. 29, 373 (1984).

74. K. A. Emery, P. K. Boyer, L. R. Thompson, R. Solanki, H. Zarnani and G. J. Collins, "Thin film deposition by UV laser photolysis," Proc. Soc. Photo-Opt. Instrum. Eng. 459, 9 (1984).

75. T. F. Deutsch, D. J. Silversmith and R. W. Mountain, "UV laser-initiated deposition of Al_2O_3 films: the effect of surface irradiation," Mat. Res. Soc. Symp. Proc. 29, 67 (1984).

76. H. Birey, "Anodization rate and augmentation factor of anodic aluminum oxide films," J. Appl. Phys. 50, 2906 (1979).

77. F. Rainer, W. Lowdermilk, D. Milam, C. Carniglia, T. Hart and T. Lichtenstein, "Materials for optical coatings in the ultraviolet," Appl. Opt. 24, 496 (1985).

78. B. Newman and D. Gill, "UV damage resistance of laser coatings," Nat. Bur. Stand. (US) Spec. Publ. 541, 190 (1979).

79. S. Foltyn and L. J. Jolin, "Alumina/silca multilayer coatings for excimer lasers," Laser Induced Damage in Optical Materials: 1983, Nat. Bur. Stand. (US) Spec. Publ. 688, 354 (1985).

80. P. B. Ghate, "Deposition techniques and microelectronics applications," in Deposition Technologies for Films and Coatings, edited by R. F. Bunshah (Noyes Publications, New Jersey, 1982).

81. R. Glang, in Handbook of Thin Film Technology, edited by L. I. Maissel and R. Glang (McGraw-Hill, New York, 1970).

82. K. A. Emery, L. R. Thompson, D. Bishop, H. Zarnani, P. K. Boyer, C.A. Moore, J. J. Rocca and G. J. Collins, "Beam-assisted CVD of microelectronics films," Mat. Res. Soc. Symp. Proc. 29, 81 (1984).

83. P. Baumeister and O. Arnon, "Use of hafnium dioxide in multilayer dielectric reflectors for the near UV," Appl. Opt. 16, 439 (1977).

84. O. A. Motovilov, "Narrow-band interference filters for the ultraviolet region of the spectrum," Optics and Spec. 22, 537 (1967).

85. D. Conlon and W. P. Doyle, "Absorption spectra of zirconium and hafnium dioxides," J. Chem. Phys. 42, 4315 (1965).

86. D. Smith, private communication.

87. D. P. Arndt et.al., "Multiple determination of the optical constants of thin-film coating material," Appl. Opt. 23, 3571 (1984).

88. M. Harris, H. A. Macleod, S. Ogura, E. Pelletier and B. Vidal, "The relationship between optical inhomogeneity and film structure," Thin Solid Films 57, 173 (1979).

89. M. G. Drexhage, B. Bendow, H. Lipson and C. T. Moynihan, "IR absorption in highly transparent glasses based on hafnium fluoride," Nat. Bur. Stand. (US) Spec. Publ. 620,94 (1981).

90. H. Poignant and D. C. Tran, "Viscosity and optical measurement on fluoride glasses", Electron. Lett. 18, 1044 (1982).

91. H. Poignant, "Dispersive and scattering properties of a ZrF_4 based glass," Electron. Lett. 17, 973 (1981).

92. D. C. Tran, G. H. Sigel, Jr., K. H. Levin, and R. J. Ginther, "Rayleigh scattering in ZrF_4 based glasses," Electron. Lett. 18, 1046 (1982).

93. J. Schroeder et.al., "Heavy metal fluoride glasses with low intrinsic rayleigh scattering," Electron. Lett. 20, 1044 (1984).

94. D. C. Tran, G. H. Sigel, B. Bendow, "Heavy metal fluoride glasses and fibers: A review," IEEE/OSA J. Lightwave Tech. 2, 566, 1984.

95. C. J. Simmons, S. A. Azali, J. H. Simmons, "Chemical durability studies of heavy metal fluoride glasses," Second Int. Symposium on Halide Glasses, Troy, NY, 1983.

96. T. Wydeven, "Plasma polymerized coating for polycarbonate: Single layer, abrasion resistant and antireflection," Appl. Opt. 16, 717 (1977).

97. T. Wydeven and R. M. Kubacki, "Antireflection coating prepared by plasma polymerization of perfluorobutene-2", Appl. Opt. 15, 132 (1976).

98. D. Milam, W. H. Lowdermilk, F. Rainer, J. Swain, C. K. Carniglia, T. T. Hart, "Influence of deposition parameters on laser-damage thresholds of silica-tantala AR coatings," Appl. Opt. 21, 3689 (1982).

99. C. K. Carniglia, "Oxide coatings for one micrometer laser fusion systems", Thin Solid Films 77, 225 (1981).

100. W. H. Lowdermilk and D. Milam, "Laser-induced surface and coating damage," IEEE J. Quant. Elect. QE-17, 1888 (1981).

101. S. R. Foltyn, L. J. Jolin and B. E. Newnam, "Progress in UV damage testing at Los Alamos," Nat. Bur. Stand. (US) Spec. Publ. 669, 266 (1983).

102. L. J. Jolin, private communication.

103. S. R. Foltyn, "Spotsize effects in laser damage testing," Nat. Bur. Stand. (US) Spec. Publ. 669, 368 (1983).

104. A. F. Stewart and A. H. Guenther, "Preliminary experimental results of spot size scaling in laser induced damage to optical coatings," Nat. Bur. Stand. (US) Spec. Publ. 638, 517 (1983).

105. S. R. Foltyn, B. E. Newnam and L. J. Jolin, "Laser damage results and analyses for UV reflectors under multiple-shot irradiation," Nat. Bur. Stand. (US) Spec. Publ. 638, 350 (1983).

106. J. M. E. Harper and R. J. Gambino, "Combined ion beam deposition and etching for thin film studies," J. Vac. Sci. Technol. 16, 1901 (1979).

107. J. M. E. Harper, J. J. Cuomo and H. R. Kaufman, "Technology and applications of broad-beam ion sources used in sputtering. Part II. Applications," J. Vac. Sci. Technol. 21, 737 (1982).

108. D. E. Aspnes and A. A. Studna, "An investigation of ion-bombarded and annealed surfaces of Ge by spectroscopic ellipsometry," Surf. Sci. 96, 294 (1980).

109. P. Sigmund, "Theory of sputtering, I. Sputtering yield of amorphous and polycrystalline targets," Phys. Rev. 184, 383 (1969).

110. G. Carter and D. G. Armour, "The interaction of low energy ion beams with surfaces," Thin Solid Films 80, 13 (1981).

111. T. Takagi, "Ion-surface interactions during thin film deposition," J. Vac. Sci. Technol. A2, 382 (1984).

112. R. Messier and J. Yehoda, "The geometry of thin film morphology," J. Appl. Phys., to be published (1986).

113. F. Seitz and J. S. Koehler, "Displacement of atoms during irradiation," Solid State Phys. 2, 305 (1956).

114. K. H. Müller, "Monte Carlo calculation for structural modifications in ion assisted thin film deposition due to thermal spikes," J. Vac. Sci. Technol. A4, 184 (1986).

115. K. H. Müller, "Monte Carlo calculation for ion assisted thin film deposition," J. Vac. Sci. Technol., to be published (1986).

116. J. P. Biersack and W. Eckstein, "Sputtering studies with the Monte Carlo program TRIM.SP," Appl. Phys. A34, 73 (1984).

117. K. H. Müller, "A model for ion assisted thin film densification," J. Appl. Phys., to be published (1986).

118. K. H. Muller, "Modelling ion-assisted deposition of CeO2 films," Appl. Phys. A, to be published (1986).

119. G. Betz and G. K. Wehner, "Sputtering of multicomponent materials," in Sputtering by Particle Bombardment: II, edited by R. Behrisch, Topics in Applied Physics, vol. 52 (Springer-Verlag, NY, 1982).

120. K. Kim, W. Baitinger, J. W. Amy and N. Winograd, "ESCA studies of metal-oxygen surfaces using argon and oxygen bombardment," J. Electron. Spectrosc. Relat. Phenom. 5, 351 (1984).

121. A. Turos, W. F. van der Weg, D. Sigurd and J. W. Mayer, "Change of surface composition of SiO2 layers during sputtering," J. Appl. Phys. 45, 2777 (1974).

122. S. Thomas, "AES-Ion Sputtering analysis and the surface composition of TiO2," Surf. Sci. 55, 754 (1976).

123. R. Holm and S. Storp, "ESCA studies on changes in surface composition under ion bombardment," Appl. Phys. 12, 101 (1977).

124. G. E. McGuire, "Effects of ion sputtering on semiconductor surfaces," Surf. Sci. 76, 130 (1978).

125. J. W. Coburn, "The influence of ion sputtering on the elemental analysis of solid surfaces," Thin Solid Films 64, 371 (1979).

126. P. H. Holloway and G. C. Nelson, "Preferential sputtering of Ta2O5 by argon ions," J. Vac. Sci. Technol. 16, 793 (1979).

127. J. H. Thomas and S. Hofmann, "Ion bombardment induced changes in SiO2 surface composition studied by x-ray photoelectron spectroscopy," J. Vac. Sci. Technol. A3, 1921 (1985). See also: S. Hofmann and J. H. Thomas, "An XPS study of the influence of ion sputtering on bonding in thermally grown SiO2," J. Vac. Sci. Technol. B1, 43 (1983).

128. S. S. Batsanov, "The concept of electronegativity. Conclusions and prospects," Russ. Chem. Rev. 37, 332 (1968).

129. H. F. Winters and P. Sigmund, "Sputtering of chemisorbed gas (nitrogen on tungsten) by low energy ions." J. Appl. Phys. 45, 4760 (1974).

130. Ch. Steinbrüchel, "On the sputtering yield of molecular ions," J. Vac. Sci. Technol. A3, 1913 (1985).

131. G. J. Exarhos, "High temperature Raman studies of phase transitions in thin film dielectrics," Mat. Res. Soc. Symp. Proc. 48,. 461 (1985).

132. R. Kelly, "The varieties of surface alterations: structural, topographical, electronic and compositional," in Ion Bombardment Modification of Surfaces, edited by O. Auciello and R. Kelly (Elsevier, New York, 1984).

133. J. F. Ziegler, Handbook of Stopping Cross-Sections of Energetic Ions in All Elements (Pergamon, New York, 1980).

134. J. S. Y. Feng, W. K. Chu and M. A. Nicolet, "Bragg's Rule study in binary metal alloys and metal oxides for MeV He^+ ions," Thin Solid Films 19, 227 (1973).

135. R. Behrisch and B. M. U. Scherzer, "Rutherford backscattering as a tool to determine electronic stopping powers in solids," Thin Solid Films 19, 247 (1973).

136. S. Foltyn, private communication.

137. H. F. Winters, J. W. Coburn and T. J. Chuang, "Surface processes in plasma-assisted etching environment," J. Vac. Sci. Technol. B1, 469 (1983).

138. D. L. Flamm and V. M. Donnelly, Plasma. Chem. Plasma Process. 1, 317 (1981).

END

DTIC

9 - 86